國立交通大學

電子工程學系 電子研究所

博士論文

利用大氣常壓電漿輔助化學氣相沉積製備氧化鋅系透明電極與氧化鋅/銦鎵鋅氧薄膜電晶體應用之特性研究

Study on Characterizations of ZnO-Based Transparent Electrodes and ZnO/IGZO Thin-Film Transistors Prepared by AP-PECVD

研究生：黃菘宏

指導教授：張國明　教授

吳建宏　教授

中華民國一〇一年八月

利用大氣常壓電漿輔助化學氣相沉積製備氧化鋅系透明電極與氧化鋅/銦鎵鋅氧薄膜電晶體應用之特性研究

Study on Characterizations of ZnO-Based Transparent Electrodes and ZnO/IGZO Thin-Film Transistors Prepared by AP-PECVD

研究生：黃菘宏　　Student：Sung-Hung Huang

指導教授：張國明　　Advisors：Kow-Ming Chang

吳建宏　　Chien-Hung Wu

國立交通大學

電子工程學系 電子研究所

博士論文

A Dissertation
Submitted to Department of Electronics Engineering and
Institute of Electronics
College of Electrical and Computer Engineering
National Chiao Tung University
in partial Fulfillment of the Requirements
for the Degree of
Doctor of Philosophy
in
Electronics Engineering

August 2012
Hsinchu, Taiwan, Republic of China

中華民國一〇一年八月

利用大氣常壓電漿輔助化學氣相沉積製備氧化鋅系透明電極與氧化鋅/銦鎵鋅氧薄膜電晶體應用之特性研究

研究生：黃菘宏 **指導教授：張國明 博士**

吳建宏 博士

國立交通大學

電子工程學系暨電子研究所

摘要

隨著光電領域的蓬勃發展，透明導電膜的需求量急速上升，商業化銦錫氧化物具有良好的光電特性，然而銦是稀有金屬且具毒性，新的替代材料開發是必需的，氧化鋅具有低成長溫度、低成本、鋅的蘊含量豐富且不具毒性等優點而受到很大的關注，而氧化鋅當作薄膜電晶體的主動層亦具有很大的發展潛力由於可增加開口率、低光敏感度以及可做為透明電路上應用，在另一方面，近年來非晶銦鎵鋅氧化物被廣泛的研究，主要由於其良好的均勻性及高的遷移率具有很大的發展性於大尺寸主動矩陣平面顯示器以及主動矩陣有機發光二極體應用。

本論文旨在新製程技術開發透明氧化物半導體，藉由新穎式大氣壓電漿輔助化學氣相沉積開發氧化鋅系透明電極以及氧化鋅/銦鎵鋅氧化物薄膜電晶體，利用較無環境危害水溶液式硝酸金屬鹽類的前驅物，可直接在大氣環境下沉積，而非真空大氣壓電漿技術具有、低溫、低成本、適合大面積化等競爭優勢，可期望於未來商業化應用。

首先，我們探討不同製程參數包括載氣流量、電漿噴嘴與基板的距離、基板溫度、不同摻雜鎵的百分比對於氧化鋅摻雜鎵薄膜特性影響，若在電漿區域通入過多的前驅物將導致大量的氣態附著性差的成核粒子產生，電漿噴嘴與基板的距離若太高會增加可以氣態成核的時間導致薄膜特性劣化，當基板溫度升高對於薄膜結晶特性並沒明顯改變，在 100°C 時得到較好特性，反而在基板溫度升高時電阻率升高，由於周圍的空氣的在高溫時氧吸附造成，而當摻雜 8 原子百分比的鎵時有最低電阻率並具有(002)優先取向，在基板溫度 100°C 下，電阻率可達到

$7.8\times10^{-4}\,\Omega\cdot\mathrm{cm}$，在可見光範圍穿透率大於 80%。而在氧化鋅摻雜銦方面，在基板溫度 200°C 得到較低的電阻率，當銦的摻雜濃度增加時表面形成尖錐狀增加表面粗糙度，摻雜 8 at.%的銦時有最低電阻率，在基板溫度 200°C 下，電阻率可達到 $1.8\times10^{-3}\,\Omega\cdot\mathrm{cm}$，此低溫製程且具有良好的特性的氧化鋅摻雜鎵與氧化鋅摻雜銦薄膜具有潛力於商業化應用。

其次，我們探討在基板溫度 100°C 下成長氧化鋅並探討主動層厚度以及氧氣對於薄膜電晶體特性影響，透過使用壓縮空氣當做載氣以及探討電漿氣體裡摻入氧氣，可以有效修補缺陷並得到較佳的切換特性，降低主動層厚度亦改善了電晶體特性由於降低了源極與汲極之間的漏電路徑，但太薄可能由於薄膜島狀不連續結構導致較低的遷移率，主動層約在 35~60nm 時可得到較佳的特性，最後在電漿氣體裡摻入 0.69%氧氣，可以得到遷移率 2.38cm^2/V-s、開關電流比達 4.63×10^9，此低溫成長的氧化鋅適合於軟性電子應用。

最後，我們先探討熱退火溫度 200-500°C 對於銦鎵鋅氧化物薄膜電晶體影響，再將高介電係數氧化鋁(Al_2O_3)應用於銦鎵鋅氧化物薄膜電晶體，結果顯示經由熱退火處理銦鎵鋅氧化物薄膜電晶體特性有效的提升，在 300°C 有良好的切換特性，經過 500°C 退火亦呈現類非晶態，經過熱退火製程在 500°C 有最好的特性，臨限電壓 6.74V、次臨界擺幅 1.54V/dec、遷移率可達到 10.31cm^2/V-s、開關電流比達到 3.28×10^8，使用高介電常數氧化鋁可以有效降低等效氧化層厚度(EOT)來達成提升電流密度及降低臨界電壓，結合氧化鋁製作銦鎵鋅氧化物薄膜電晶體具有低臨限電壓 0.71V、低次臨界擺幅 276mV/dec、優良的遷移率 8.39cm^2/V-s、高電流開關比 1×10^8，此利用非真空大氣壓電漿技術沉積的銦鎵鋅氧化物具有良好的元件特性且將可應用於大尺吋的平面顯示器以及驅動有機發光二極體。

Study on Characterizations of ZnO-Based Transparent Electrodes and ZnO/IGZO Thin-Film Transistors Prepared by AP-PECVD

Student: S. H. Huang **Advisors: Dr. Kow-Ming Chang**
Dr. Chien-Hung Wu

Department of Electronics Engineering

& Institute of Electronics

National Chiao Tung University

Abstract

The demand for transparent conductive oxide (TCO) is rising rapidly because of the booming field of optoelectronics. The commercial indium tin oxide (ITO) has excellent optical and electrical properties. However, indium is a rare and toxic metal. As a result, development of new alternative materials is necessary. Zinc oxide (ZnO) has attracted much attention due to low growth temperature, low cost, abundance and nontoxicity. Furthermore, ZnO thin film transistors (TFTs) have a great interest due to the potential in increase of the pixel aspect ratio, insensitivity to visible light, and application for transparent circuit. On the other hand, amorphous indium gallium zinc oxide (a-IGZO) is extensively studied and has great development in large-size active matrix liquid crystal displays (AMLCD) and active matrix organic light-emitting diode (AMOLED) applications because of its good uniformity and high mobility.

In this thesis, new process technology is developed to deposit transparent oxide semiconductors (TOSs). Novel atmospheric pressure plasma enhanced chemical vapor deposition oxide (AP-PECVD) is proposed to fabricate ZnO-based transparent electrodes and ZnO/IGZO thin film transistors. Also, water-based metal salt solution, which is an eco-friendly precursor, is adopted, and the thin film can be deposited in atmospheric environment. The non-vacuum AP-PECVD offers several competitive advantages, such as low temperature process, low cost and suitable for large area application. It is expected for commercial applications in the future.

First, we study on the different process parameters including carrier gas flow

rate, gap distance between plasma nozzle and the substrate, substrate temperature and the different gallium doping concentrations. Excessive precursor in the plasma region will lead to nucleation particles with poor adhesion. The longer distance increases the time to form gas phase nucleation particles resulting in a degradation of crystallinity. As substrate temperature increases, the cystallinity doesn't change obviously. The 100^{o}C samples exhibits a better performance, and the higher substrate temperature shows a higher resistivity. It is may be due to the adsorption of oxygen from the surrounding air which reduces the carrier concentration and mobility. Gallium-doped ZnO (GZO) has the lowest resistivity via 8 at.% doping possessing a (002) preferred orientation. The low resistivity of GZO thin film is 7.8×10^{-4} $\Omega\cdot$cm and the transmittance in the visual region is more than 80% at a substrate temperature of 100^{o}C. Indium-doped ZnO (IZO) has the lowest resistivity via 8 at.% at a substrate temperature of 200^{o}C. When the doping concentration becomes higher, the surface shows obviously needlelike geometry. As a result, the high indium content shows a rougher surface. The lowest resistivity of IZO is 1.8×10^{-3} $\Omega\cdot$cm at a substrate temperature of 200^{o}C. These good characteristics of GZO and IZO with low temperature process have high potential for commercial applications.

Next, ZnO active layer is deposited at a low substrate temperature of 100^{o}C. The effect of channel thicknesses and oxygen species on the characteristics of ZnO TFTs is studied. Using compressed dry air (CDA) as a carrier gas as well as incorporating oxygen gas in the plasma gas can effectively repair the defects, and excellent switching properties is achieved. Reducing the thickness can increase the channel resistance and reduce the undesired current flow between source and drain resulting in improvement of TFT properties. The too thin channel layer might lead to a low mobility due to discontinuous island structure. The channel layer with a thickness of 35~60nm can obtain a better performance. By incorporating 0.69% O_2 into plasma gas, a field-effect mobility of 2.38 cm^2/Vs and an I_{on}/I_{off} current ratio of 4.63×10^{9} are obtained. This ZnO with low-temperature process is suitable for flexible applications.

Finally, we investigate on the effect thermal annealing temperature 200-500^{o}C on the IGZO TFTs, and then the high-k dielectric aluminum oxide (Al_2O_3) is integrated in IGZO TFTs. The results shows switching characteristics is effectively improved the by thermal annealing. After post annealing in higher than 300 ^{o}C, the devices show clear switching properties. The defects can be repaired effectively by post annealing. After poster annealing, IGZO thin film shows an amorphous-like phase, and no obvious crystallization is observed even at 500 ^{o}C. IGZO TFT annealed at 500^{o}C in N_2 shows excellent electrical characteristics including a V_T of 6.74 V, a subthreshold swing of 1.54V/dec, a high mobility of 10.31cm^2/V-s and a large I_{on}/I_{off} ratio of

3.28×10^8. Using the high-k dielectric Al_2O_3 can effectively reduce the equivalent oxide thickness (EOT) to achieve a high drive current and a low threshold voltage. The PE-ALD Al_2O_3/IGZO TFT demonstrated excellent electrical characteristics, including a low V_T of 0.71 V, small subthreshold swing of 276 mV/dec, a mobility of 8.39 cm^2/V-s, and a large I_{on}/I_{off} ratio of 1×10^8. The IGZO TFTs deposited by non-vacuum APPECVD are suitable for large-size flat panel displays and driving OLED.

Acknowledgement

在交大的碩博士六年生涯裡，經歷了許多事情也讓我成長許多，有太多人讓我心存感激及感謝。首先，特別感謝指導教授張國明老師以及吳建宏老師，感謝老師們的指導、教誨與鼓勵，不僅在學術上研究上的指導，並培養出學生獨立思考以解決問題的能力，對於人生規畫及待人處世上亦讓我受益良多，使我能順利完成博士學位。還要感謝工研院機械所許文通副組長以及張加強經理提供大氣電漿設備以及在研究資源上幫忙協助，張經理在開發新製程技術有前瞻的視野及創造力，讓我啟發很多，感謝張經理在研究及生活上的提攜與照顧。諸位口試委員的指導與建議，也在此謹申謝意。

謝謝工研院機械所吳清吉研究員以及徐瑞美博士給予研究上的建議，感謝哲蔚、智翔在實驗上幫助以及提供的想法與經驗，謝謝劉志宏博士、楊國輝博士、蔡陳德研究員、陳志明研究員、鄭文欽研究員、楊德輝研究員、吳文獻研究員、偕睿仁研究員、蘇濬賢研究員、張瀛方研究員、劉世偉研究員、吳勝斌研究員、蕭明英助理、謝文宗研究員和M600的許沁如研究員、陳怡君研究員，還有一起在工研院打拼的柏慶、育成以及致緯學弟，再次感謝機械所M200電漿應用技術部全體同仁，在工研院的這幾年來從你們那邊獲取很多大氣電漿開發經驗，能你們一起共事是我的榮幸。

感謝我帶的學弟妹，憶雯學妹、偉強學弟、家威學弟、煒力學弟、偉韓學弟，有你們一起跟學長做實驗以及執行研究計畫，減輕了學長的負擔，可以忍受學長的碎碎念，以及學長心情不好時亦會帶學長去散心，學長點滴在心，有你們在實驗上的幫忙以及協助，讓我得以完成這個博士論文，在此也特別感謝堃濠學弟、彥凱學弟在工研院一起打拼的日子以及平常的照顧。

感謝實驗室的各位學長、學姐、同學、學弟、學妹，謝謝柏寧學長，建宏學長、士軒學長在研究實驗上的建議與意見，碩士班時蘇俊榮學長、阿茂學長在實驗及實驗機台的教學以及講解，一起打拼同學詩帆、庭嘉、彥忠、明頤、昇宇、聚翔，也謝謝鄧一中學長、賴瓊惠學姊，趙高毅學長、郭俊銘學長、林俊銘學長、林稔杰學長、張知天學長、陳巨峰學長、許信祐學長，感謝學長研究上的建議指導，也感謝其他實驗室的學長，張明峯學長、李振銘學長、蘇迺超學長、鄭淳護學長、林哲緯學長、王泰瑞學長提供寶貴的經驗及意見。

謝謝國家奈米實驗室(NDL)、交大奈米中心(NFC)及奈米科技中心提供良好的

研究設備與充足的資源，感謝國家奈米實驗室姚潔宜小姐，交大奈米中心葉雙德先生、林聖欽先生、黃國華先生、陳聯珠小姐、陳明麗小姐、何惟美小姐、許俊生先生、胡進章先生、陳悅婷小姐，倪月珍小姐..等，奈米科技中心賴良一先生、交大貴儀黃繡吟小姐，由衷感謝葉雙德先生在做人處事像我的父母一樣，叮嚀我以及教育我，每次去找他總是能跟我說個不停，林聖欽先生以及黃國華先生在實驗上的大力協助以及平常照顧，讓我們在實驗資源上減輕很大的負擔，以及雷射圖形產生器和黃光室工讀服務的機會。

謝謝生輔組曾信雄先生、蔡燕茹小姐、陳湘琇小姐、住服組林淡輝阿姨、謝謝你們讓我有工讀的機會，以及在生活輔導組時的照顧與關懷，還有教官室馬毓君教官。

謝謝新竹保護動物協會大家，DVA、阿萍、惠琳、Angel、旅貓、姥姥、自立、偉銘、玉靜、金田媽、名媛、Rachel、加菲、燕子，喜歡小動物志同道合的人，在這裡我看到了許多東西也學到許多東西，各位有愛心的大家 你們服務的熱忱以及那顆愛動物的心，還有那些可愛的貓兒跟狗兒深植我心。

還有謝謝大學同學，毓廷、倫倫、旻霖、青宇及伯俊美食專家趴趴走，讓我在研究所的生涯添加了一些色彩，以及大學同學兼室友冠迪，當下大雨時我在奈米中心時沒雨傘時帶來雨傘，以及論文上的建議，還有室友家駿幫我修改英文以及給我一些珍貴的意見，還有室友家群、曄仁謝謝你們的陪伴。

最後感謝實驗戰友陸冠文，好朋友岷臻帶我們到台南玩、好朋友坤億，剪頭髮的青青姐，還有碧芬妹妹，再次感謝求學過程中幫助忙及陪伴過我的人，謝謝三民國小同學們、礁溪國中同學們、宜蘭高中同學們、長庚大學的同學們、交大的同學們。

其他若有漏掉的請自己填上姓名

感謝________

最後，我願將這份榮耀呈現給我父母親-黃炎爐先生、王秀津女士，

以及我的哥哥耀德、弟弟菘志，還有礁溪鄉姓黃邱的大家。

Contents

Chapter 1 Introduction

Chapter 2 Characterizations of Gallium-Doped Zinc Oxide Films Prepared by AP-PECVD System

Chapter 3 Characterizations of Indium-Doped Zinc Oxide Films Prepared by AP-PECVD System

Chapter 4 The Effect of Channel Thicknesses and Oxygen Species on the Characteristics of ZnO TFTs Prepared by APPECVD system

Chapter 5 The Impacts of Thermal Annealing on the Properties of IGZO TFT Prepared by AP-PECVD

Chapter 6 Characterizations of IGZO TFT Prepared by AP-PECVD Using PE-ALD Al_2O_3 Gate Dielectric

Table Captions

Chapter 1 Introduction

Chapter 3 Characterizations of Indium-Doped Zinc Oxide Films Prepared by AP-PECVD System

Chapter 4 The Effect of Channel Thicknesses and Oxygen Species on the Characteristics of ZnO TFTs Prepared by APPECVD system

Chapter 5 The Impacts of Thermal Annealing on the Properties of IGZO TFT Prepared by AP-PECVD

Chapter 6 Characterizations of IGZO TFT Prepared by AP-PECVD Using PE-ALD Al_2O_3 Gate Dielectric

Figure Captions

Chapter 1 Introduction

Chapter 2 Characterizations of Gallium-Doped Zinc Oxide Films Prepared by AP-PECVD System

Chapter 3 Characterizations of Indium-Doped Zinc Oxide Films Prepared by AP-PECVD System

Chapter 4 The Effect of Channel Thicknesses and Oxygen Species on the Characteristics of ZnO TFTs Prepared by AP-PECVD system

Chapter 5 The Impacts of Thermal Annealing on the Properties of IGZO TFT Prepared by AP-PECVD

Chapter 6 Characterizations of IGZO TFT Prepared by AP-PECVD Using PE-ALD Al_2O_3 Gate Dielectric

Chapter 1

Introduction

1.1 Overview of Transparent Conductive Oxide

Transparent Conductive Oxide (TCO) films has attracted considerable attention due to a wide range of application, such as flat panel display (FPD), touch panels, solar cells, lighting emitting diodes (LED) and other optoelectronic devices [1.1]-[1.4]. Figure 1-1 shows the various applications of TCOs. Nowadays, TCO thin films have been the indispensable component to opto-electrical products. Typically, TCO films must possess a high optical transmittance of more than 80% in the visible region, a low electrical resistivity of less than $1x10^{-3}$ Ω · cm and stability in various environments. ZnO, In_2O_3 and SnO_2-based TCOs have been extensively studied in recent few years, because they exhibit high optical transparency and high conductivity that can be control of the non-stoichiometry and doping level [1.5]. Indium tin oxide (ITO) has dominant the TCO market for pass 20 years due to their high transmittance in the visible range and low electrical resistivity. The commercial ITO has been widely used, such as common electrode as well as pixel electrode in FPD application and sensing electrode in touch panels. Recently, smart phone and large-area size display boost the requirement of TCO. However, indium is high cost and scarce resources. A stable supply of ITO will become a critical issue in the future due to expanding market for optoelectronic devices. As a result, the development of decreasing the usage of indium or an alternative material to ITO films is necessary. In the last few years, ZnO has attracted much attention as a TCO material because of the higher abundance compared to the other TCO materials (about a factor of 1000 more abundant than indium as shown in Table 1.1 [1.6]). Furthermore, ZnO also have good stability in a silane (SiH_4) plasma discharge, which is used for preparation of a-Si:H thin film solar cell [1.6]. ZnO is wide band gap (Eg =3.35eV) II-VI semiconductor with hexagonal structure. Un-doped ZnO thin films have n type properties due to intrinsic defects, but un-doped ZnO films have poor thermal stability. In order to increase the conductivity and stability of ZnO films, group-Ⅲ elements (Al, Ga, In) can be used as substitutional dopant for Zn site. ZnO-based thin films can be prepared on several substrates in a number of ways: pulse laser deposition [1.7]-[1.8], ion plating [1.9], RF/DC magnetic sputtering [1.10]-[1.11], metalorganic chemical vapor deposition [1.12], spray pyrolysis [1.13], sol-gel [1.14]-[1.15] and atomic layer deposition [1.16]. Most ZnO-based thin films are deposited using conventional vacuum techniques because vacuum-processed devices exhibit excellent performance and reliability than non-vacuum process. However a non-vacuum process offers competitive advantages, such as low cost, high throughput, and excellent suitability for large-area applications.

1.2 Overview of Transparent Oxide Semiconductor Based Thin Film Transistors

Amorphous silicon (a-Si) and low-temperature poly-silicon thin film transistors (LTPS TFTs) dominate the active matrix technologies in the flat-panel display industry over the last ten years. However, these silicon-based TFTs have several limitations such as photosensitivity, light degradation, and opacity, etc. Oxide semiconductors are very interesting materials because they combine simultaneously high/low conductivity with high visual transparency via non-stoichiometry and doping level. Oxide-based semiconductors, such as ZnO [1.17]-[1.18], ZTO [1.9]-[1.20], IZO [1.21]-[1.22] and IGZO [1.23]-[1.25] have been reported for the active channel layer. These oxide-based thin film transistors offer good electrical properties and high transparency. Recently, interest has arisen in the possibility of fabricating active electronic devices from transparent oxide semiconductor, because these oxide semiconductors enable the manufacture of transparent circuit, called “transparent electronics’’. Transparent electronics are nowadays an emerging technology for the next generation of optoelectronic devices.

Zinc oxide thin-film transistors (ZnO TFTs) have high potential in the active matrix liquid crystal display (AMLCD) due to non-toxic property, low cost, high mobility, low growth temperature and wide bandgap. Because of low growth temperature, devices can be fabricated on inexpensive plastic substrate for flexible electronics applications. The wide bandgap of 3.35eV, which is transparent in the visible region, can also be employed to a channel layer for the transparent TFT (TTFT) application. ZnO TFT offers possibility of increased pixel aspect ratio and intrinsic advantage of insensitivity to visible light. Hence, the ZnO is a good candidate for the transparent electronics.

On the other hand, the transparent amorphous oxide semiconductors (TAOS) have attracted much attention due to high mobility and good uniformity for large-area applications. The ternary oxide system of In_2O_3, Ga_2O_3 and ZnO (IGZO) has presented promising performance for TFT channel layer due to superior performance compared with conventional Si-based TFT. Figure 1-2 shows the electron pathway carrier transport path in conventional covalent semiconductor and ionic oxide semiconductor [1.26]. The conduction band of IGZO is composed of metal s-orbitals and carrier transport is almost not affected by the chemical bond distortion. As a result, IGZO thin film shows a high mobility even in amorphous phase. Figure 1-3 depicts amorphous formation region and the electron mobilities and concentrations evaluated from the Hall effects for the amorphous thin films in the IGZO system [1.27]. It is clear that the mobility is primary determined by the fraction of In_2O_3 content and the highest value of 40 cm^2/V-s is obtained around the samples containing the maximum In_2O_3 fraction. The IGZO is currently promising AOS materials for mass production with low-temperature process and excellent performance. Several prototype displays using IGZO TFT have been demonstrated as shown in Fig. 1-4 [1.28]

1.3 Background of Atmospheric pressure plasma

Nowadays, the plasma technology is an indispensable technique in various material processes. The advantages of plasma are well known, and the plasma can be well-controlled to generate the high concentration of reactive species that can enhance etching and deposition rate. The most of plasma facilities was operated under vacuum ambient. However, vacuum systems are expensive and maintenance cost is high. Atmospheric pressure plasmas overcome the drawbacks of vacuum operation. Atmospheric pressure plasma is used in a variety of materials processes, such as surface modification, etching, and thin film deposition [1.29]-[1.31]. Conventional plasma source includes transferred arcs, plasma torches, corona discharge, dielectric barrier discharges and plasma jet as shown in Figure 1-5 [1.32]. Arc and torch are high gas temperature and not suitable for low-temperature application. A disadvantage of corona discharge and dielectric barrier discharges is that the plasmas are not uniform throughout the volume. On the other hand, non-thermal atmospheric pressure plasma jets are playing an important role in atmospheric pressure plasma technology.

The non-thermal plasma jet doesn't be spatially confined by electrodes and is compatible with low process temperature. In this dissertation, non-thermal atmospheric pressure plasma jet (APPJ) was proposed to fabricate ZnO-based TCOs and ZnO/IGZO TFTs.

1.4 Motivation

Recently, APPJ is attracted much attention because this kind of plasma does not require a complicated vacuum system. Non-vacuum system could reduces the cost of processing and enlarge the size limit. Moreover, APPJ is also a low temperature process. The temperature of plasma could be lower than 200^{o}C which could reduce the thermal damage of substrate and even be applied for plastic substrate. In the past, oxide semiconductor was usually fabricated in vacuum system, such as sputtering and evaporation, and MOCVD which would limit the size of substrate and increase the cost of equipment. In this thesis, a novel and innovative APPJ system (also called AP-PECVD system) is proposed to develop TCO and ZnO/IGZO TFTs. Furthermore, an environmentally friendly water-based solution precursor was used.

In order to overcome the shortage of indium, more and more conductive metal oxide materials have been studied such as AZO, GZO, and IZO because of its low cost, high transparency, and favorable conductivity. In this study, APPJ would be utilized to develop GZO and IZO thin film on glass substrate.

On the other hand, for the applications of ZnO TFTs in the flat-panel displays, the off current must be low. The carrier concentration of un-doped ZnO thin films results from the intrinsic defects. Higher carrier concentration generates the external scattering and unexpected leakage current. As a result, the background electron carrier concentration must be reduced while ZnO was used as a channel layer. In order to reduce the intrinsic defects, the oxygen species were incorporated during deposition. Also, to reduce the leakage current of source to drain current flow, thinner channel layer have been proposed by reducing the conductivity of channel layer.

Moreover, post annealing is usually performed to improve the performance of TFT. As a result, IGZO TFT was developed by APPJ and effect of annealing temperature on the properties of IGZO TFT was discussed. Furthermore, the high-k Al_2O_3 is a promising gate dielectric because of its low leakage current and excellent compatibility with the IGZO thin film. The plasma-enhanced ALD (PE-ALD) method was assumed to increase reactivity, reduce impurities, widen the process window, and increase the film density compared with conventional ALD. Thus, integration with PE-ALD Al_2O_3 was expected to achieve a higher performance IGZO TFT.

1.5 Thesis Organization

The organization of this thesis is separated in to seven chapters and organized as follows.

In the first chapter of this dissertation, we briefly give an introduction of the TCOs, oxide-based TFTs and atmospheric-pressure plasma. In the chapter 2 and chapter 3, we use AP-PECVD to deposit GZO and IZO thin films. The structural, optical and electrical properties were discussed. In the chapter 4, we use AP-PECVD to fabricate ZnO TFT at low temperature, and the effect of channel thickness and oxygen species is studied. In the chapter 5, we use AP-PECVD to fabricate IGZO TFTs and discuss the annealing temperature on the characteristic of IGZO TFTs. In the chapter 6, high-k PE-ALD Al_2O_3 is integrated as a gate dielectric with IGZO TFTs. Finally, in the chapter 7, the results are summarized and organized. Future work will be presented based on the result of the thesis.

Table 1-1 Properties of ZnO, SnO_2 and In_2O_3 in comparison to that of silicon [1.6].

Property	In_2O_3	SnO_2	ZnO	Si
Mineral name	—	cassiterite	zincite	silicon
Average amount of the metal in the earth's crust (ppm)	0.1	40	132	2.58×10^5
Band gap E_g (300 K) (eV)	2.7 (indir) 3.75 (dir)	3.6 (dir)	3.4 (dir)	1.12 (indir) 4.18 (dir)
Pressure coefficient dE_g/dp (meV $kbar^{-1}$)			2.33	−1.41
Static dielectric constant ε_r	≈9	$\parallel c$: 9.6 $\perp c$: 13.5	$\parallel c$: 8.75 $\perp c$: 7.8	11.9
Effective electron mass m^*/m_e	0.35	$\parallel c$: 0.23 $\perp c$: 0.3	0.28	0.337
Non-parabolicity parameter α (eV^{-1})		0.96	0.29 1.04	0.27 0.5
Effective conduction band density of states (300 K) N_C (cm^{-3})	4.1×10^{18}	3.7×10^{18}	3.7×10^{18}	4.9×10^{18}
Extrinsic dopants	Sn, Ti, Zr, F, Cl, Sb, Ge, Zn, Pb, Si	Sb, (As, P) F, Cl	B, Al, Ga, In, Si, Ge, Sn, Y, Sc, Ti, Zr, Hf F, Cl	B, Al, Ga, In P, As, Sb
Other phases in the dopant–host system (heat of formation (eV))	$In_4Sn_3O_{12}$ SnO (2.9) SnO_2 (6.0) TiO_2 (9.8) ZrO_2 (11.2) GeO_2 (5.6) SiO_2 (8.8) ZnO (3.6) Sb_2O_3 (7.2) Sb_2O_5 (10.0)	As_2O_3 (6.7) As_2O_5 (9.5) Sb_2O_3 (7.2) Sb_2O_5 (10.0) P_2O_5 (15.6)	ZnO_2 B_2O_3 (6.6) Al_2O_3 (8.7) Ga_2O_3 (5.7) In_2O_3 (4.8) TiO_2 (9.8) Y_2O_3 (19.8) HfO_2 (11.8) ZrO_2 (11.2) $ZnAl_2O_4$ (21.4) $ZnGa_2O_4$ (15.3)	SiB_3 SiB_6 SiP SiAs $SiAs_2$
Crystal structure	cubic, bixbyite	tetragonal, rutile	hexagonal, wurtzite	cubic, diamond
Space group (number)	$I2_13$ (no199)	$P4_2mnm$ (no 136)	$P6_3mc$ (no 186)	Fd3m (no 227)
Lattice parameter(s) (nm)	a: 1.012	a: 0.474 c: 0.319	a: 0.325 c: 0.5207	a: 0.5431
Density ρ (g cm^{-3})	7.12	6.99	5.67	2.33
Thermal expansion α (300 K) (10^{-6} K^{-1})	6.7	$\parallel c$: 3.7 $\perp c$: 4.0	$\parallel c$: 2.92 $\perp c$: 4.75	2.59
Melting point (°C)	2190	>1900[a]	2240	1415
Melting point of the metal (°C)	157	232	420	1415
Heat of formation (eV)	9.7	6.0	3.6	—

[a] Decomposition into SnO and O_2 at 1500 °C.

i-Phone 4S (Apple) **i-Pad (Apple)**

Flat-panel display (ASUS) **E-paper (Eink)**

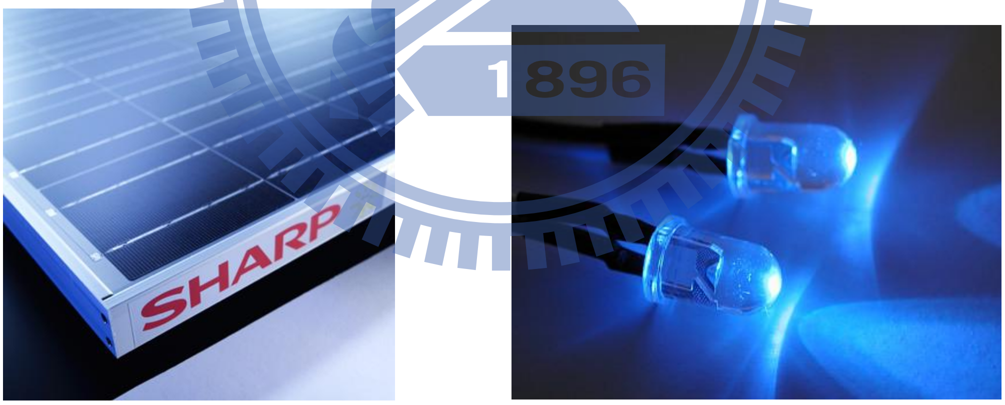

Solar cell (Sharp) **Light emitting diode**

Fig. 1-1 A variety of applications of transparent conductive oxide (TCO).

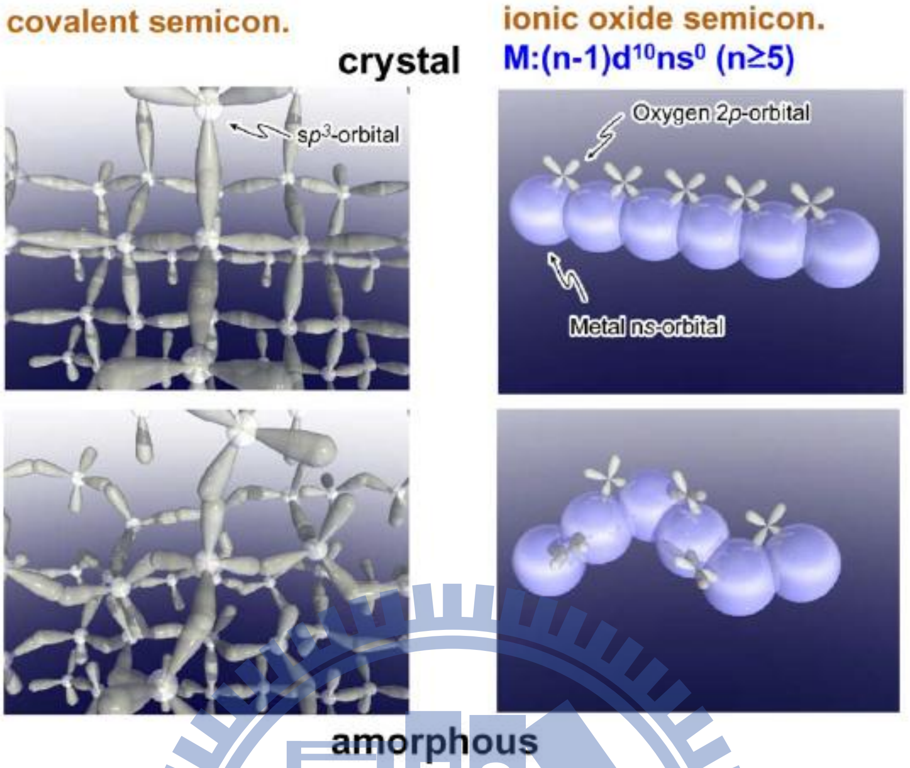

Fig. 1-2 Schematic orbital drawing of electron pathway (conduction band bottom) in conventional compound semiconductor and ionic oxide semiconductor [1.26].

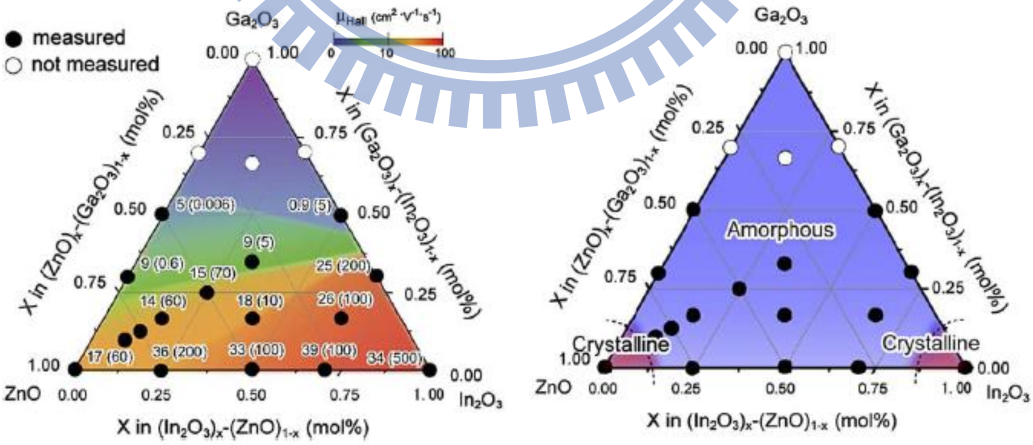

Fig. 1-3 The electron mobilities and concentrations evaluated from the Hall effects for the amorphous thin films (left) and the amorphous formation region (right) in the In_2O_3–Ga_2O_3–ZnO system [1.27].

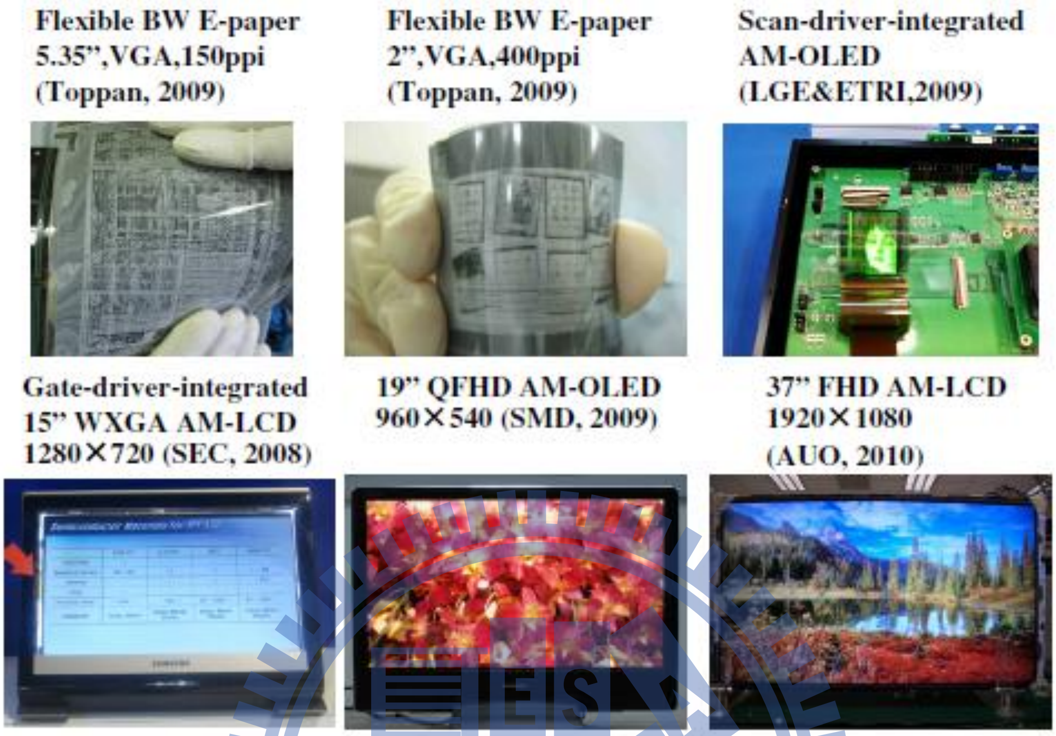

Flexible BW E-paper
5.35”,VGA,150ppi
(Toppan, 2009)

Flexible BW E-paper
2”,VGA,400ppi
(Toppan, 2009)

Scan-driver-integrated
AM-OLED
(LGE&ETRI,2009)

Gate-driver-integrated
15” WXGA AM-LCD
1280×720 (SEC, 2008)

19” QFHD AM-OLED
960×540 (SMD, 2009)

37” FHD AM-LCD
1920×1080
(AUO, 2010)

Fig. 1-4 Photographs of some prototype displays using AOS TFTs [1.28].

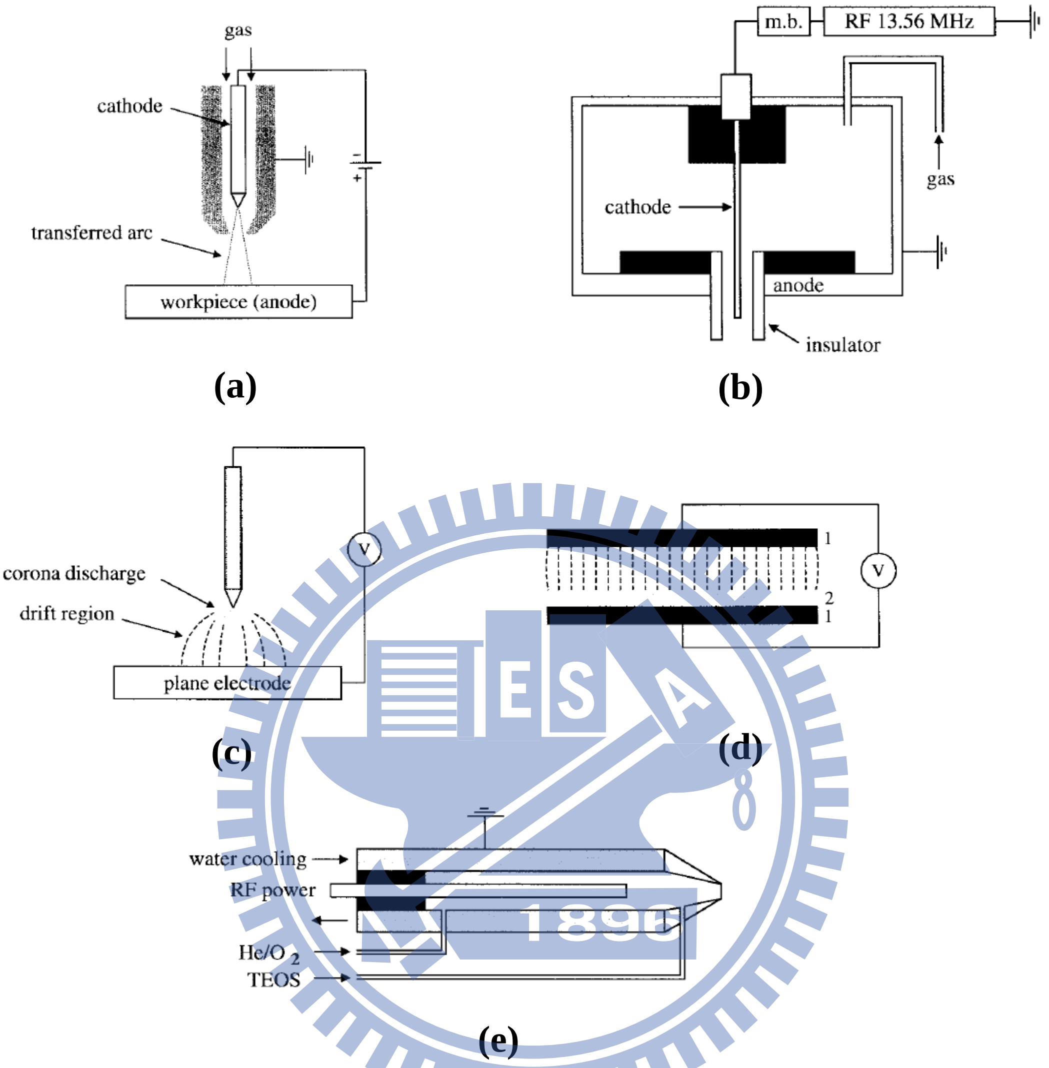

Fig. 1-5 Schematic of different kinds of plasma sources (a) Transferred arc (b) Cold plasma torch (c) Corona discharge (d) Dielectric barrier discharge (e) Plasma jet [1.32].

References

[1.1] X. Yu, J. Ma, F. Ji, Y. Wang, X. Zhang, C. Cheng, and H. Ma, "Preparation and properties of ZnO:Ga films prepared by r.f. magnetron sputtering at low temperature," *Applied Surface Science*, vol. 239, pp. 222-226, 2005.

[1.2] N. Yamamoto, H. Makino, T. Yamada, Y. Hirashima, H. Iwaoka, T. Ito, A. Ujihara, H. Hokari, H. Morita, and T. Yamamoto, "Heat Resistance of Ga-Doped ZnO Thin Films for Application as Transparent Electrodes in Liquid Crystal Displays," *Journal of The Electrochemical Society*, vol. 157, pp. J13-J20, 2010.

[1.3] M. Osada, T. Sakemi, and T. Yamamoto, "The effects of oxygen partial pressure on local structural properties for Ga-doped ZnO thin films," *Thin Solid Films*, vol. 494, pp. 38-41, 2006.

[1.4] J.-H. Lee and B.-O. Park, "Transparent conducting ZnO:Al, In and Sn thin films deposited by the sol-gel method," *Thin Solid Films*, vol. 426, pp. 94-99, 2003.

[1.5] D. H. Zhang and H. L. Ma, "Scattering mechanisms of charge carriers in transparent conducting oxide films," *Applied Physics A: Materials Science & Processing*, vol. 62, pp. 487-492, 1996.

[1.6] K. Ellmer, "Resistivity of polycrystalline zinc oxide films: current status and physical limit," *Journal of Physics D: Applied Physics*, vol. 34, p. 3097, 2001.

[1.7] S.-M. Park, T. Ikegami, K. Ebihara, and P.-K. Shin, "Structure and properties of transparent conductive doped ZnO films by pulsed laser deposition," *Applied Surface Science*, vol. 253, pp. 1522-1527, 2006.

[1.8] A. Suresh, P. Wellenius, A. Dhawan, and J. Muth, "Room temperature pulsed laser deposited indium gallium zinc oxide channel based transparent thin film transistors," *Applied Physics Letters*, vol. 90, pp. 123512-123512-3, 2007.

[1.9] T. Yamada, A. Miyake, S. Kishimoto, H. Makino, N. Yamamoto, and T. Yamamoto, "Low resistivity Ga-doped ZnO thin films of less than 100 nm thickness prepared by ion plating with direct current arc discharge," *Applied Physics Letters*, vol. 91, pp. 051915-051915-3, 2007.

[1.10] Q.-B. Ma, Z.-Z. Ye, H.-P. He, S.-H. Hu, J.-R. Wang, L.-P. Zhu, Y.-Z. Zhang, and B.-H. Zhao, "Structural, electrical, and optical properties of transparent conductive ZnO:Ga films prepared by DC reactive magnetron sputtering," *Journal of Crystal Growth*, vol. 304, pp. 64-68, 2007.

[1.11] K. H. Kim, K. C. Park, and D. Y. Ma, "Structural, electrical and optical properties of aluminum doped zinc oxide films prepared by radio frequency magnetron sputtering," *Journal of Applied Physics*, vol. 81, pp. 7764-7772, 1997.

[1.12] N. Oleynik, M. Adam, A. Krtschil, J. Bläsing, A. Dadgar, F. Bertram, D. Forster, A. Diez, A. Greiling, M. Seip, J. Christen, and A. Krost, "Metalorganic chemical vapor phase deposition of ZnO with different O-precursors," *Journal of Crystal Growth*, vol. 248, pp. 14-19, 2003.

[1.13] S. A. Studenikin, N. Golego, and M. Cocivera, "Optical and electrical properties of undoped ZnO films grown by spray pyrolysis of zinc nitrate solution," *Journal of Applied Physics*, vol. 83, pp. 2104-2111, 1998.

[1.14] J.-H. Lee, K.-H. Ko, and B.-O. Park, "Electrical and optical properties of ZnO transparent conducting films by the sol-gel method," *Journal of Crystal Growth*, vol. 247, pp. 119-125, 2003.

[1.15] K. Y. Cheong, N. Muti, and S. R. Ramanan, "Electrical and optical studies of ZnO:Ga thin films fabricated via the sol-gel technique," *Thin Solid Films*, vol. 410, pp. 142-146, 2002.

[1.16] D.-J. Lee, H.-M. Kim, J.-Y. Kwon, H. Choi, S.-H. Kim, and K.-B. Kim, "Structural and Electrical Properties of Atomic Layer Deposited Al-Doped ZnO Films," *Advanced Functional Materials*, pp. 1-8, 2010.

[1.17] G. Adamopoulos, A. Bashir, P. H. Wobkenberg, D. D. C. Bradley, and T. D. Anthopoulos, "Electronic properties of ZnO field-effect transistors fabricated by spray pyrolysis in ambient air," *Applied Physics Letters*, vol. 95, pp. 133507-3, 2009.

[1.18] H.-C. Cheng, C.-F. Chen, and C.-Y. Tsay, "Transparent ZnO thin film transistor fabricated by sol-gel and chemical bath deposition combination method," *Applied Physics Letters*, vol. 90, pp. 012113-3, 2007.

[1.19] C. Avis and J. Jang, "A High Performance Inkjet Printed Zinc Tin Oxide Transparent Thin-Film Transistor Manufactured at the Maximum Process Temperature of 300^{o}C and Its Stability Test," *Electrochemical and Solid-State Letters*, vol. 14, pp. J9-J11.

[1.20] S. K. Park, Y.-H. Kim, H.-S. Kim, and J.-I. Han, "High Performance Solution-Processed and Lithographically Patterned Zinc--Tin Oxide Thin-Film Transistors with Good Operational Stability," *Electrochemical and Solid-State Letters*, vol. 12, pp. H256-H258, 2009.

[1.21] Y.-L. Wang, F. Ren, W. Lim, D. P. Norton, S. J. Pearton, I. I. Kravchenko, and J. M. Zavada, "Room temperature deposited indium zinc oxide thin film transistors," *Applied Physics Letters*, vol. 90, p. 232103, 2007.

[1.22] C. Chang-Ken, H. Hsing-Hung, S. Jing-Jong, and W. Chung-Chih, "The Influence of Channel Compositions on the Electrical Properties of Solution-Processed Indium-Zinc Oxide Thin-Film Transistors," *Display Technology, Journal of,* vol. 5, pp. 509-514, 2009.

[1.23] L. Jae Sang, C. Seongpil, K. Sang-Mo, and L. Sang Yeol, "High-Performance a-IGZO TFT With ZrO2 Gate Dielectric Fabricated at Room Temperature," *Electron Device Letters, IEEE,* vol. 31, pp. 225-227, 2010.

[1.24] C. J. Chiu, S. P. Chang, and S. J. Chang, "High-Performance a-IGZO Thin-Film Transistor Using Ta2O5 Gate Dielectric," *Electron Device Letters, IEEE,* vol. 31, pp. 1245-1247, 2010.

[1.25] L. Linfeng and P. Junbiao, "High-Performance Indium-Gallium-Zinc Oxide Thin-Film Transistors Based on Anodic Aluminum Oxide," *Electron Devices, IEEE Transactions on,* vol. 58, pp. 1452-1455, 2011.

[1.26] K. Nomura, H. Ohta, A. Takagi, T. Kamiya, M. Hirano, and H. Hosono, "Room-temperature fabrication of transparent flexible thin-film transistors using amorphous oxide semiconductors," *Nature,* vol. 432, pp. 488-492, 2004.

[1.27] H. Hideo, "Ionic amorphous oxide semiconductors: Material design, carrier transport, and device application," *Journal of Non-Crystalline Solids,* vol. 352, pp. 851-858, 2006.

[1.28] T. Kamiya, K. Nomura, and H. Hosono, "Present status of amorphous In-Ga-Zn-O thin-film transistors," *Science and Technology of Advanced Materials,* vol. 11, p. 044305, 2010

[1.29] X. Yang and et al., "High stability of atmospheric pressure plasmas containing carbon tetrafluoride and sulfur hexafluoride," *Plasma Sources Science and Technology,* vol. 14, p. 412, 2005.

[1.30] G. R. Nowling and et al., "Remote plasma-enhanced chemical vapour deposition of silicon nitride at atmospheric pressure," *Plasma Sources Science and Technology,* vol. 11, p. 97, 2002.

[1.31] L. Chi-Hung and et al., "Surface characterization of the SiO x films prepared by a remote atmospheric pressure plasma jet," *Surface and Interface Analysis,* p. n/a, 2008.

[1.32] A. Schutze, J. Y. Jeong, S. E. Babayan, P. Jaeyoung, G. S. Selwyn, and R. F. Hicks, "The atmospheric-pressure plasma jet: a review and comparison to other plasma sources," *Plasma Science, IEEE Transactions on,* vol. 26, pp. 1685-1694, 1998.

Chapter 2

Characterizations of Gallium-Doped Zinc Oxide Films Prepared by AP-PECVD System

2.1 Introduction

Transparent conductive oxide (TCO) has attracted many researchers to study due to high demand for flat panel displays, touch panel, solar cells, and other optoelectronic devices [2.1]-[2.3]. Indium tin oxide (ITO) is currently the dominant TCO due to its excellent electrical and optical properties. For the large-size applications, such as flat panel display, the requirement for ITO using as the common electrode and pixel electrode will sharply increase. However, indium is a rare and toxic metal. As a result, development of substitute material is necessary. The ZnO-based thin films are promising material because of nontoxic, low cost and more stable in the hydrogen-containing plasma. Un-doped ZnO thin films are highly resistive; instead, ZnO thin films doping with group-III elements (Al, Ga, In) can increase the conductivity and stability. However, gallium is less reactive and more resistant to oxidation than aluminum and rather similar ionic radius to zinc [2.4]. These properties of gallium-doped ZnO (GZO) could have better process controllability and cause less lattice deformations. On the other hand, the GZO have demonstrated for the common electrodes of flat panel display [2.5]. Atmospheric pressure plasma is used in a variety of materials processes such as surface modification, etching, and thin film deposition [2.6]-[2.11]. Non-thermal atmospheric pressure plasma jets are playing an important role in atmospheric pressure plasma technology. The non-thermal plasma jet doesn’t be spatially confined by electrodes and is compatible with low process temperature [2.12].

ZnO:Ga (GZO) thin films can be prepared on several substrates in a number of ways: pulse laser deposition [2.13]-[2.14], ion plating [2.15], RF/DC magnetic sputtering [2.16]-[2.17], plasma-enhanced metalorganic chemical vapor deposition [2.18], atmospheric pressure plasma chemical vapor deposition [2.19], sol–gel [2.20] and spray pyrolysis [2.21], etc. Among the different techniques used for the growth of these layers, atmospheric pressure plasma jet (APPJ) technique have the advantages such as relatively low process temperature than conventional CVD , low cost and well suited for large-area applications since it does not need a vacuum chamber and associated pumping system.

This work proposed novel APPJ system, a plasma-enhanced chemical vapor deposition operated under atmospheric pressure (AP-PECVD), to deposit GZO thin film at low substrate temperature. Also, water-based metal salt solution, which is an eco-friendly precursor, was used. The electrical, structural and optical properties of

GZO thin films were studied.

2.2 Experimental procedure

Gallium doped zinc oxide thin films were grown on glass substrates (2.5 cm × 2.5 cm × 0.7 mm) by APPJ. Fig. 2-1(a) shows a schematic diagram of the experimental apparatus for APPJ. The deposition apparatus mainly is composed of a plasma jet, an ultrasonic generator, and a hot plate. The pulsed DC power supply and main gas (also called discharge gas) generate the downstream plasma. In order to deposit uniform gallium-doped ZnO thin film, the xy directional scan system was used. The position of plasma jet was fixed and the substrate was on the xy directional scan system. First, the gap distance between hot plate and plasma jet was set. Next, start point, endpoint and the pitch were set. Subsequently, the scan system moved start point to the end point, and the scan was repeated 10 times. The pitch controlled the overlap of the two paths of x direction. The scan rate of x direction was 20 mm/s, and the scan rate of y direction was 50mm/s. The pitch was set at 2mm and the scan path was shown in Fig. 2-1(b) For deposition of gallium-doped ZnO films, the zinc nitrate ($Zn(NO_3)_2$, 99% purity) and gallium nitrate ($Ga(NO_3)_2$, 99.99% purity) were used as the precursor without further purification. Pure deionized water was used as a solvent and the concentration of zinc nitrate in the deionized water was kept at 0.2 M. The precursor, mixed different zinc nitrate with gallium nitrate dissolved in deionized water, was prepared for different doping concentrations (Ga_{dop}) from 0 to 20 (Ga/Zn+Ga) at.%. Subsequently, the solution was ultrasonically atomized at 2.45 MHz into mist and then conveyed by carrier gas to the plasma region connected to a pulsed DC power supply at a repetition rate of 25kHz and voltage pulse of 15kV with a pulse width of 8μs. The nitrogen gas (N_2) was used as carrier gas and main gas. The N_2 gas flow rate of main gas was 35SLM. The carrier gas flow rate (CG) was varied from 300sccm to 600sccm, and gap distance (Gap) was varied from 5mm to 20mm. The substrate temperature (T_s) was controlled from 100^{o}C to 300^{o}C.

2.3 Results and discussion

Figure 2-2 shows the optical emission spectra of N_2 plasma and N_2 incorporated precursor. The spectra present Zn and Ga signal after incorporation of precursor. This can be deduced that the precursor was dissociated in the plasma region and relatively low process temperature can be expected. In this work, GZO thin films can deposited by AP-PECVD with a excellent properties at substrate temperature of 100^{o}C, which is much lower than the decomposing temperature of the zinc nitrate [2.22].

2.3.1 The Effect of Different Carrier Flow Rates on the Properties of Gallium-Doped ZnO Thin Films

The effect of the different carrier flow rates on the properties of GZO thin films was studied at Gap= 5mm, T_s= 100^{o}C and Ga_{dop}= 8at.%. Figure 2-3 shows SEM images of GZO deposited at different carrier gas flow rates. When the flow rate was larger than 450sccm, it can be obviously observed a number of particles. It is likely that increasing the concentration of precursor too much in the plasma region will result in more gas phase nucleation particles. These particles have poor adhesion and could generate the holes at the surface. Figure 2-4 depicts thickness and haze of GZO deposited at different carrier gas flow rates. The thickness initially rises with the flow rate, and then increase slowly. The haze factor increases with the flow rate resulting from the surface roughness and particles. From the Fig. 2-3 (c) and (d), the particles will result in loss of precursor to form thin film, so the thickness increase slowly. An appropriate increase in flow rate can increase the deposition rate. Furthermore, the particles also scatter the light and increase the haze factor. The carrier gas flow rate affects properties of the GZO thin films significantly. Carrier gas flow rate of 300 sccm has high deposition rate than 150sccm, and few particles than 450sccm as well as 600sccm.

2.3.2 The Effect of Different Gap Distances on the Properties of Gallium-Doped ZnO Thin Films

The effect of the different gap distances on the properties of GZO thin films was examined at CG=300sccm, T_s=100^{o}C and Ga_{dop}=8at.%. Figure 2-5 shows the SEM images of GZO deposited at different gap distances between the nozzle and substrate. As the gap distance increases, the surface shows more particles. Discontinue island structure is observed with a gap distance of 20mm. This may be due the fact that the longer distance increases the time to form gas phase nucleation particles. Another possible reason for this might be that a longer distance increases the probability of oxygen gas from surrounding to react with the dissociated precursor. Figure 2-6 depicts thickness and haze of GZO deposited at with different gap distances. A short distance is advantageous for preventing wasteful dispersion of dissociated precursor into surrounding atmosphere. Furthermore, the particles with a long gap distance will result in loss of precursor to form thin film. As a result, the thickness decreases with the increase of gap distance. The haze factors increase with the gap distance resulting from the surface roughness and particles. Figure 2-7 depicts GIXRD patterns of GZO deposited at different gap distances. Gap distance below 15mm indicates preferred c-axis of (002) peak. The longer gap distance causes the decline of crystallinity. Figure 2-8 shows the resistivity (ρ), carrier concentration (n), and Hall mobility (μ) of GZO deposited at different gap distances. A short gap distance shows a lower resistivity with a higher mobility and carrier concentration. Figure 2-9 shows transmission spectrum of GZO films with different gap distances. A longer gap presents a decline of transmittance due to the poor quality and those particles. However, with a gap distance up to 20mm, the resistivity sharply increases with a lower mobility and carrier concentration. With a small gap distance of 5mm, the better performance is achieved.

2.3.3 The Effect of Different Substrate Temperature on the Properties of Gallium-Doped ZnO Thin Films

The effect of the substrate temperature on the properties of GZO thin films was investigated at CG=300sccm, Gap=5mm and Ga_{dop}=8at.%. Figure 2-10 show the SEM of GZO deposited different substrate temperature. The surface becomes smoother with increase of substrate temperature, since surface mobility of adatom increases. Figure 2-11 depicts thickness and haze of GZO deposited at different substrate temperatures. The growth rate increase slightly with increase of T_s. The haze factor decreases with increase of T_s due to the smoother surface. Figure 2-12 presents the GIXRD patterns of GZO thin film deposited at different substrate temperature. All the samples shows a preferred (002) orientation. As T_s increases, the cystallinity doesn’t change obviously. This is deduced that the plasma supply the energy to form the film. Figure 2-13 the resistivity (ρ), carrier concentration (n), and Hall mobility (μ) of GZO deposited at different substrate temperatures. The higher substrate temperature shows a higher resistivity. It is may be due to the adsorption of oxygen from the air which reduces the carrier concentration and mobility. Figure 2-14 shows the transmission spectra of GZO thin film deposited at different substrate temperatures. The higher substrate temperature shows a higher transmittance.

2.3.4 The Effect of Gallium Doping Concentrations on the Properties of Gallium-Doped ZnO Thin Films

The effect of the gallium doping concentration on the properties of GZO thin films was investigated at CG=300sccm, Gap=5mm and $T_s=100^oC$. Figure 2-15 shows SEM (tilted angle) and the HRTEM (cross section) images of GZO thin film with 8at.% Ga doping. The GZO thin film exhibits a columnar structure. Fig. 2-16(a) presents the GIXRD patterns of undoped and different Ga-doped ZnO films deposited by APPJ at a substrate temperature of 100^oC. Ga-doped ZnO films demonstrate a high (002) preferential orientation; that is, the c-axis of the crystal lattice is normal to the plane of substrate. However, as the gallium concentration rise, the (002) diffraction peak intensity decrease and full width at half-maximum of (002) diffraction peak broaden resulting in degradation of crystallinity and smaller grain size. A graudually decreased in crystallinty is attributed to the increasing number of nucleation centers during incorporation of the Ga into ZnO. The position of (002) peak shifted to higher 2θ for the GZO films compared with that of undoped ZnO as shown Fig. 2-16(b). It is indicates the decrease of the c-axis lattice, because the ionic radius of Ga (0.62Å) is smaller than Zn (0.74 Å). Fig. 2-17 shows the resistivity (ρ), carrier concentration (n), and hall mobility (μ) of different Ga/(Zn+Ga) atomic ratios. Both the carrier concentration and hall mobility initially increase with gallium doping concentrations, but at high gallium doping, the carrier concentration and Hall mobility gradually decrease. When the doping concentration is low, gallium atoms effectively occupy the substitutional sites to generate free electrons resulting in the rise of carrier concentration. While the doping concentration is higher than 10 at.%, excess dopant atoms enter the interstitial sites to become ineffective dopant, and grain size decline due to increasing number of nucleation centers to cause more dopant segregate to grain boundary. These reasons resulting in the decrease of carrier concentration**.** As the doping concentration is inferior to 8 at.%, Hall mobility increases with increasing carrier density. This phenomenon can be explained by Seto model [2.23] that an increasing carrier concentration causes a lower and narrower potential barrier at grain boundary. Similar behavior had been published. The Hall mobility decreases at high doping concentrations because impurity scattering and more neutral defect [2.24]-[2.25]. The minimum resistivity of $7.8\times10^{-4}\ \Omega\cdot\mathrm{cm}$ was obtained in ZnO:Ga films deposited with 8 at.% gallium dopant at 100^{o}C. Fig. 2-18 depicts transmission spectrum of ZnO films with different Ga concentrations. The absorption edge shows a shift towards higher energy with the increase Ga concentration according to Burnstein-Moss effect [2.26], and this result was consistent with carrier concentration by Hall measurement. All films exhibited that average transmittance in visible region is more than 80%.

2.4 Conclusion

In summary, we successfully used APPECVD to fabricate GZO thin films. Gas phase nucleation reaction depends on the process condition of gap distance and carrier flow rate. The concentration of precursor in the plasma region must be well controlled. The abnormal phenomenon of degradation in electrical properties with increasing Ts is attributed to the adsorption of oxygen from air. Since the AP-PECVD operated under air, the effect of environment must be considered when deposited at high substrate temperature. A minimum resistivity was achieved via 8 at.% doping. The GZO thin film presents a resistivity of $7.8\times10^{-4}\ \Omega\cdot\mathrm{cm}$ and a transmittance of more than 80% at a low substrate temperature of 100^{o}C.

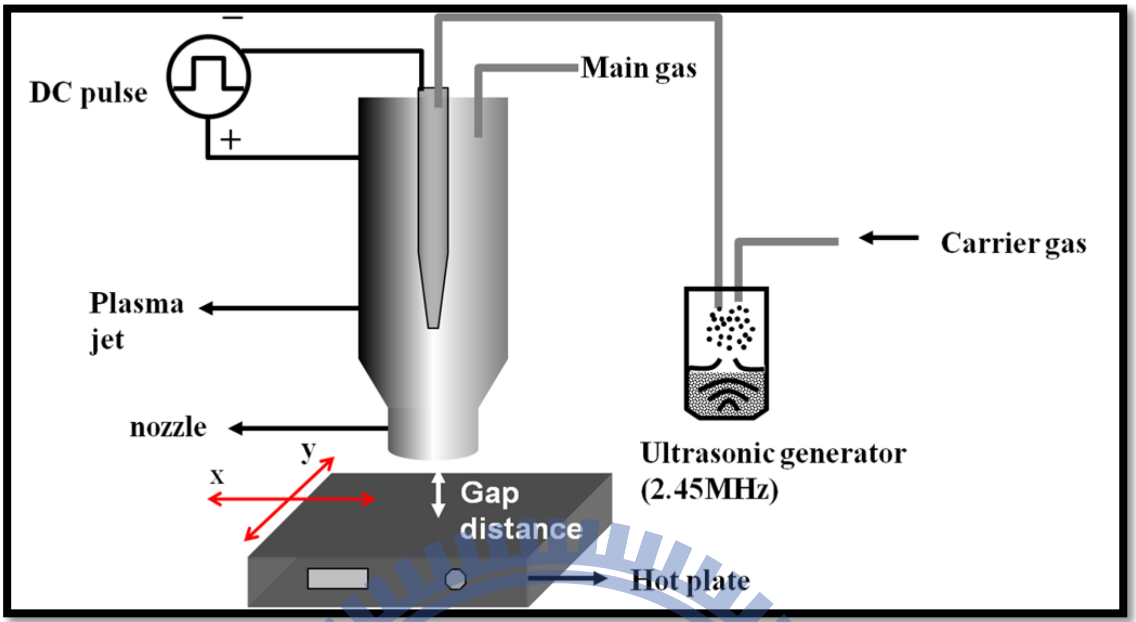

(a)

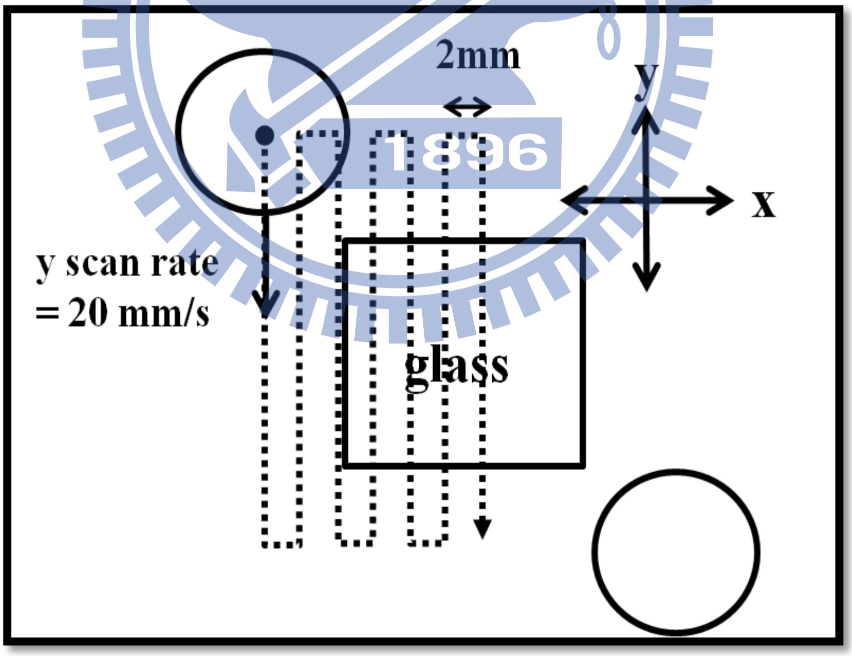

(b)

Fig. 2-1 Schematic diagram of the experimental apparatus (a) APPJ system (b) scan path.

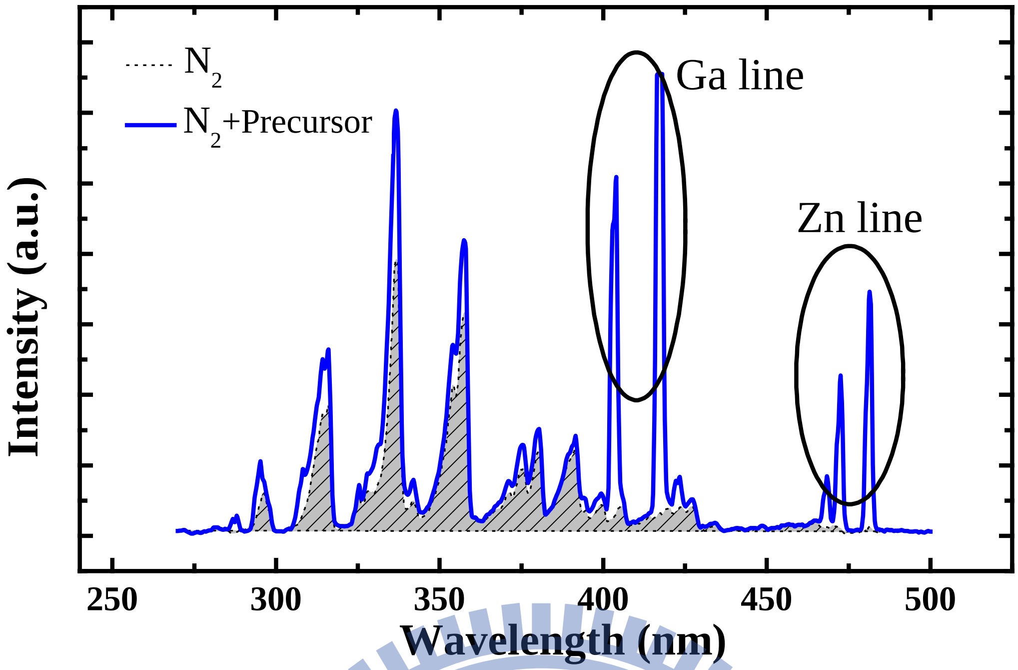

Fig. 2-2 Optical emission spectra of N_2 plasma and N_2 incorporated precursor.

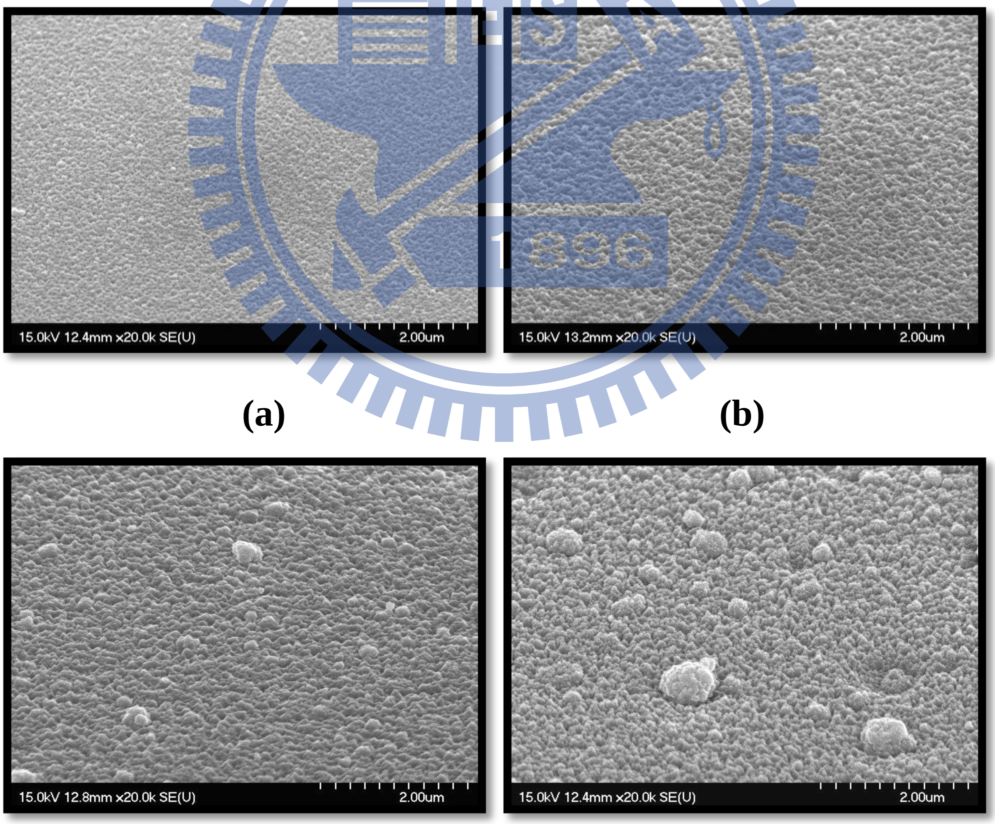

(a) (b)

(c) (d)

Fig. 2-3 SEM images (tilted angle) of GZO with different carrier gas flow rates.

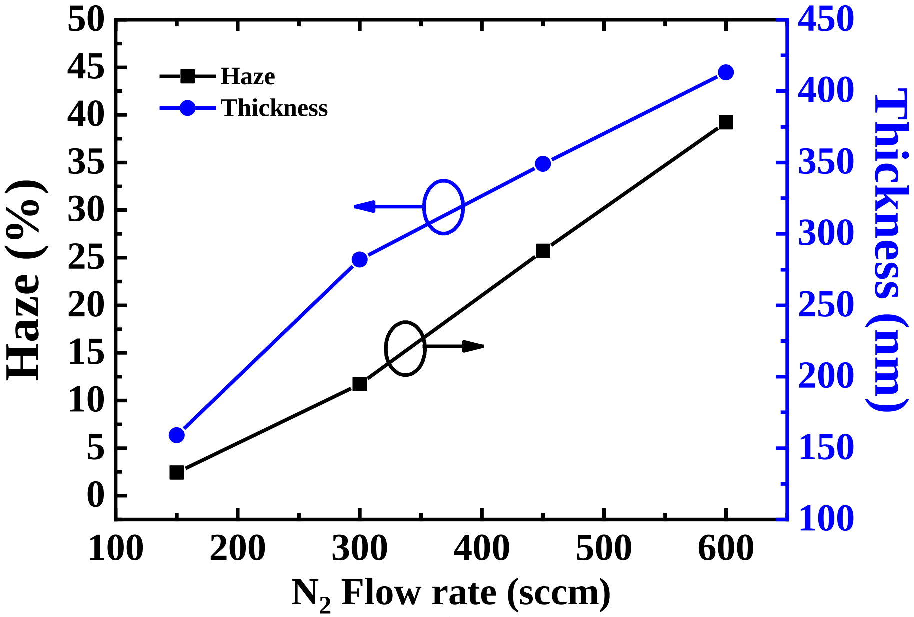

Fig. 2-4 Thickness and haze factor of GZO with different carrier gas flow rates.

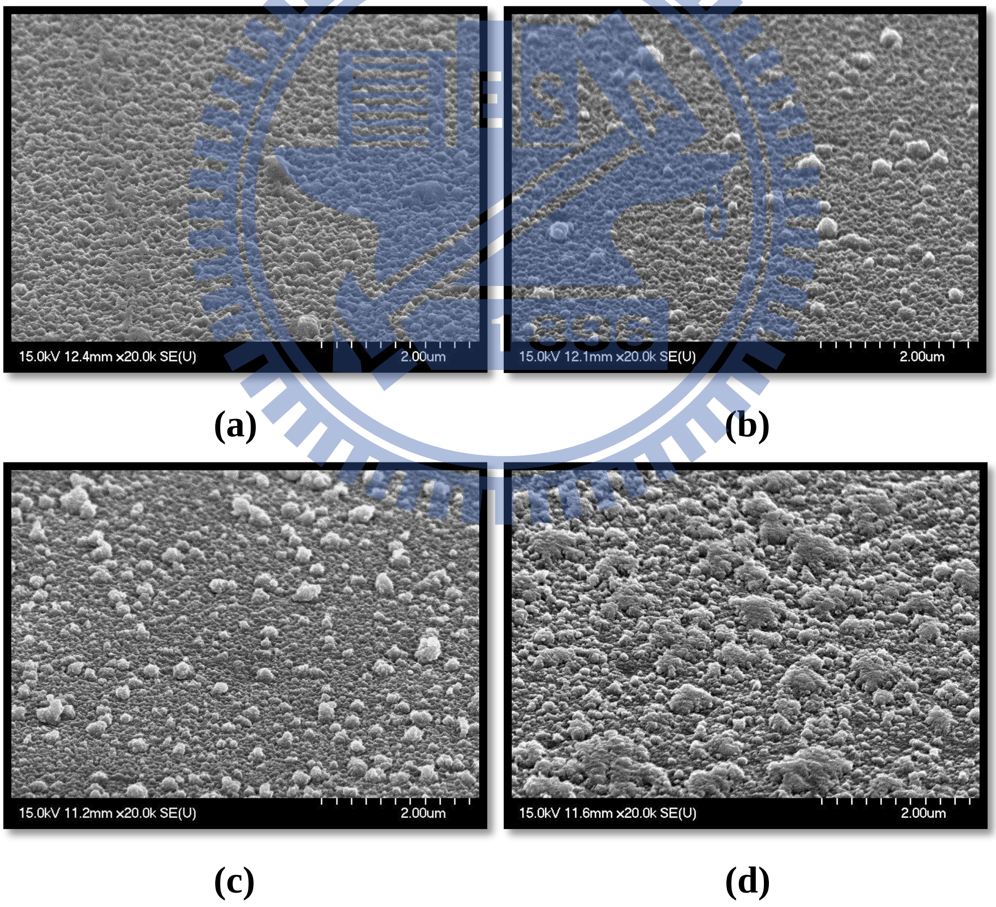

(a) (b)

(c) (d)

Fig. 2-5 SEM images (tilted angle) of GZO with different gap distances between the nozzle and substrate (a) 5mm (b) 10mm (c) 15mm (d) 20mm.

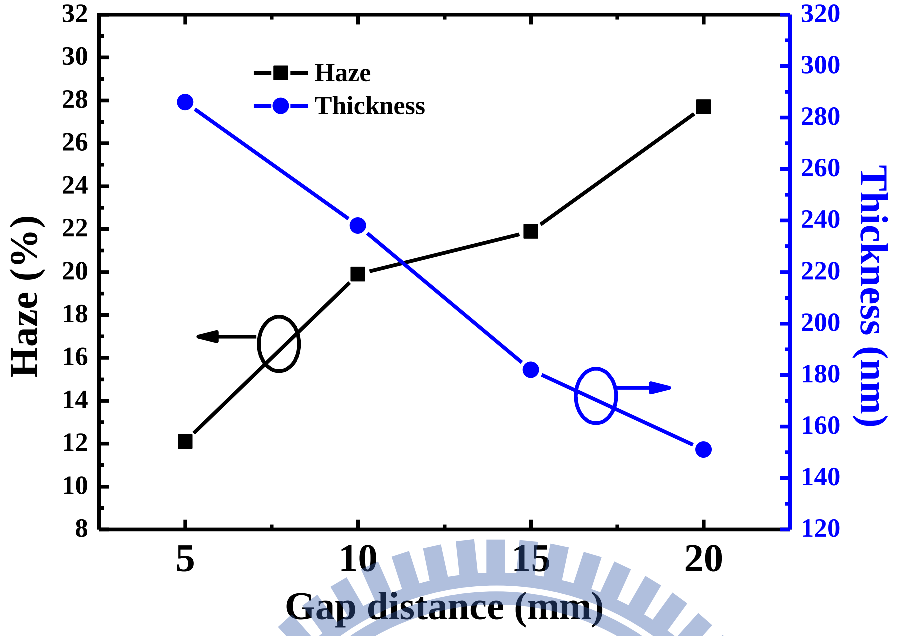

Fig. 2-6 Thickness and haze of GZO deposited at different gap distances.

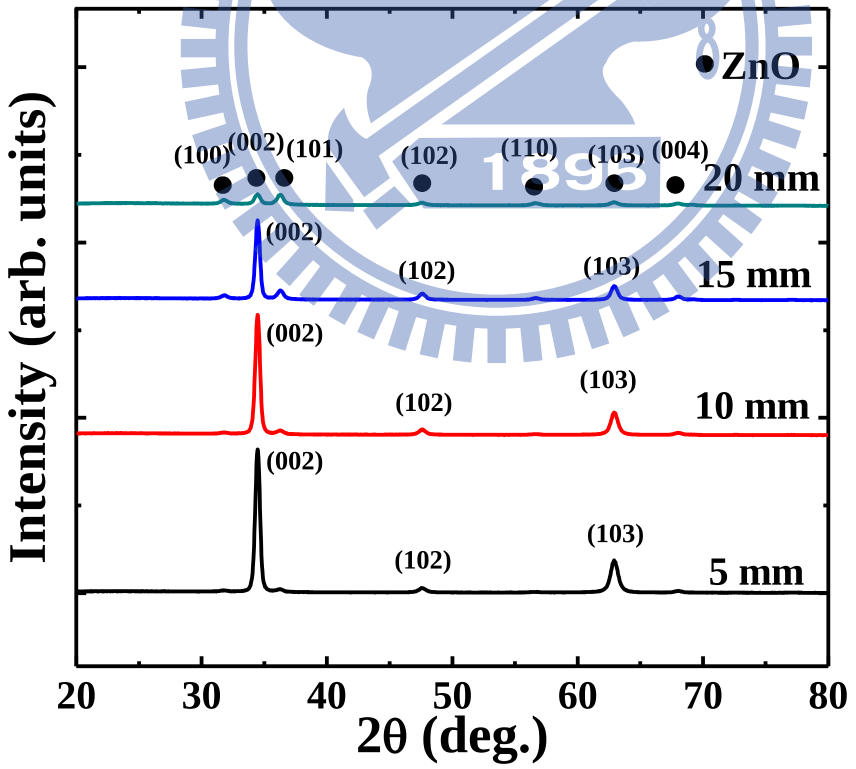

Fig. 2-7 GIXRD patterns of GZO deposited at different gap distances.

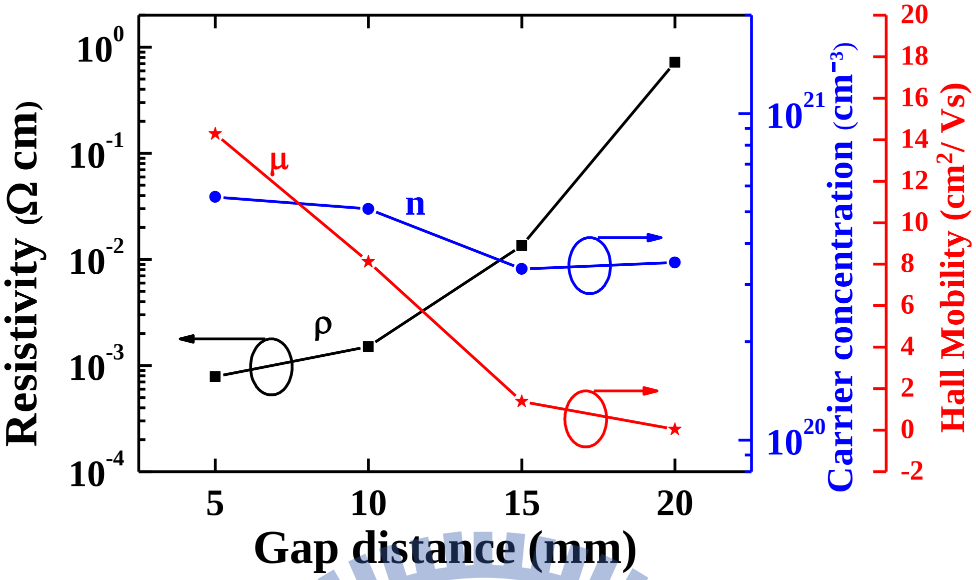

Fig. 2-8 The resistivity (ρ), carrier concentration (n), and Hall mobility (μ) of GZO thin films deposited at different gap distances.

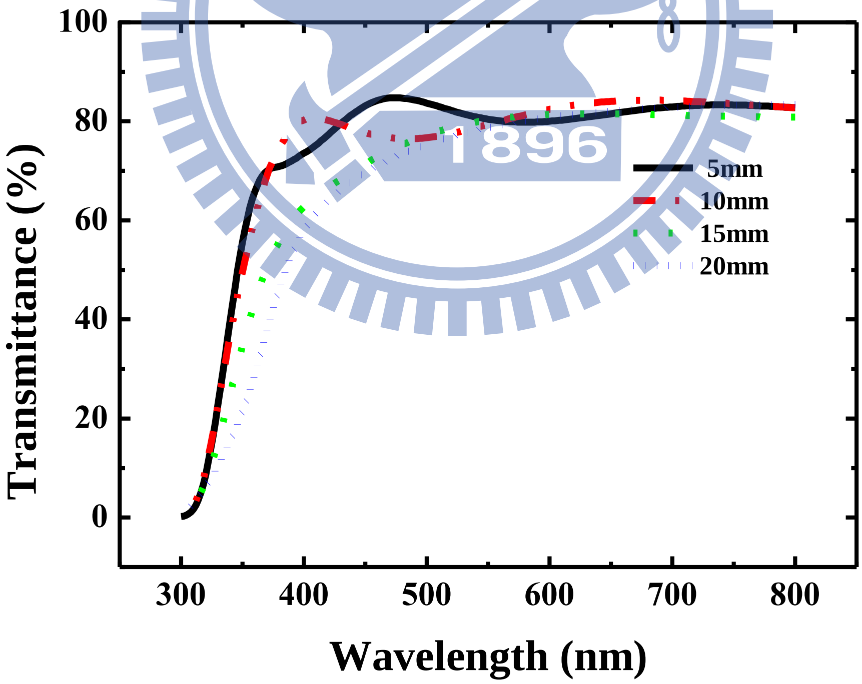

Fig. 2-9 Transmission spectrum of GZO films deposited different gap distances.

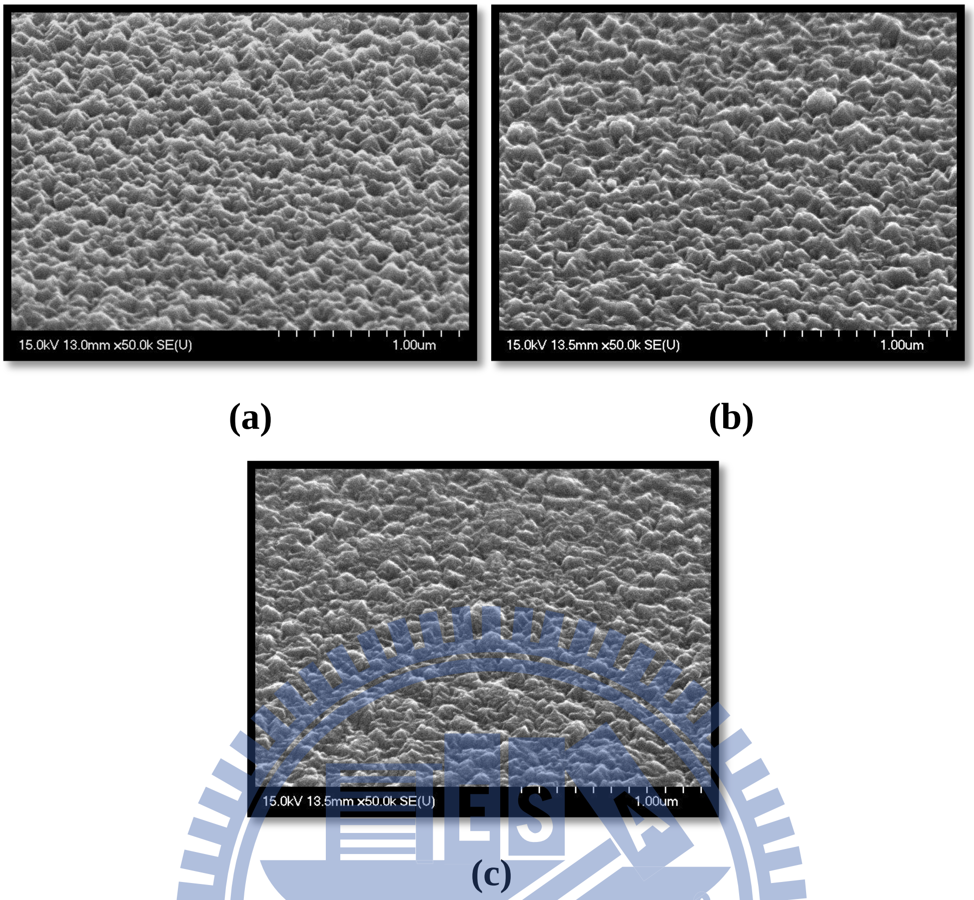

(a) (b)

(c)

Fig. 2-10 The SEM images of GZO deposited at different substrate temperatures.

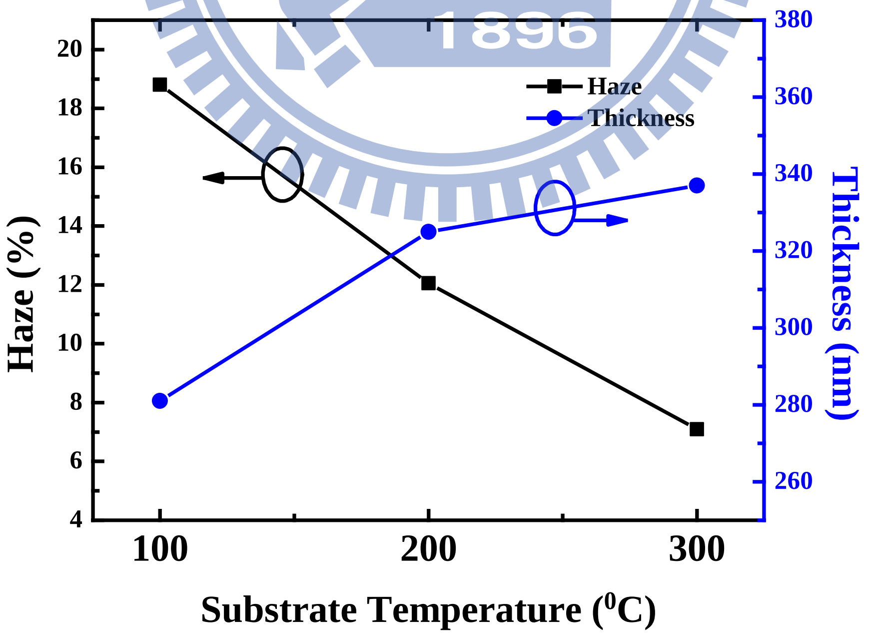

Fig. 2-11 Thickness and haze of GZO deposited at different substrate temperatures.

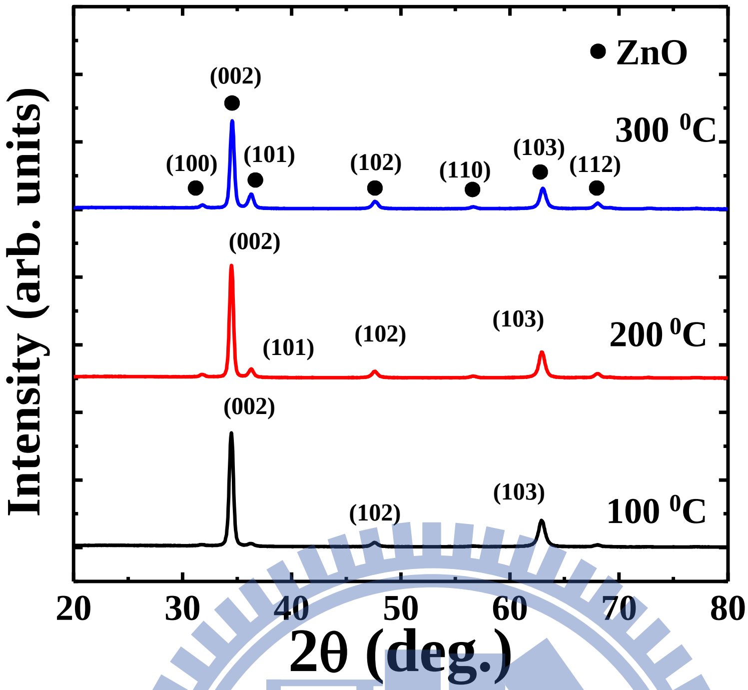

Fig. 2-12 The GIXRD patterns of GZO thin film deposited at different substrate temperatures.

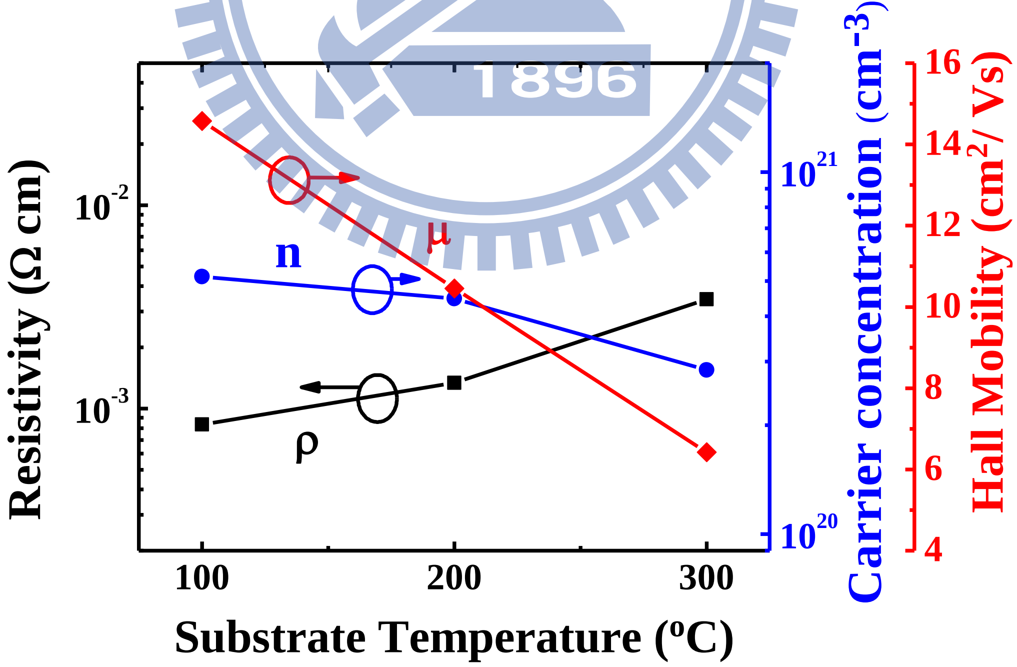

Fig. 2-13 The resistivity (ρ), carrier concentration (n), and Hall mobility (μ) of GZO deposited at different substrate temperatures.

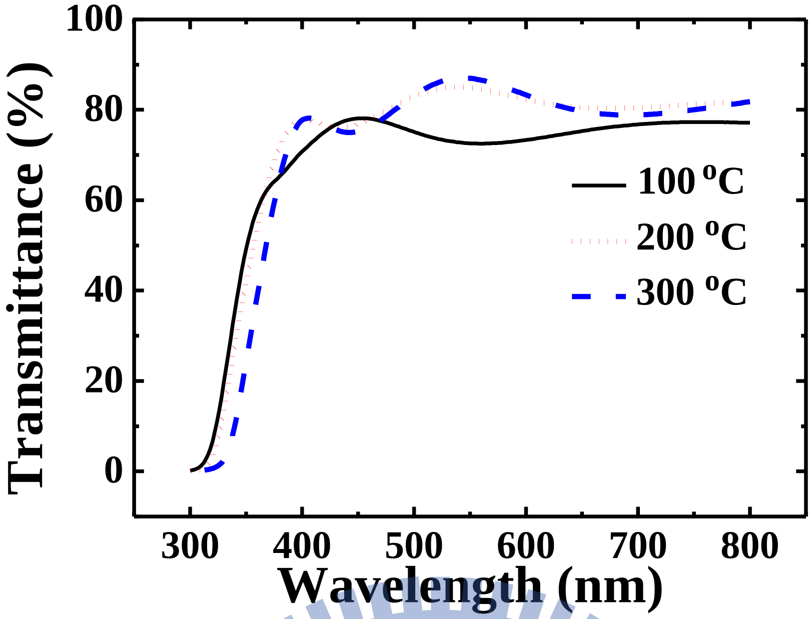

Fig. 2-14 Transmission spectra of GZO thin film deposited at different substrate temperatures.

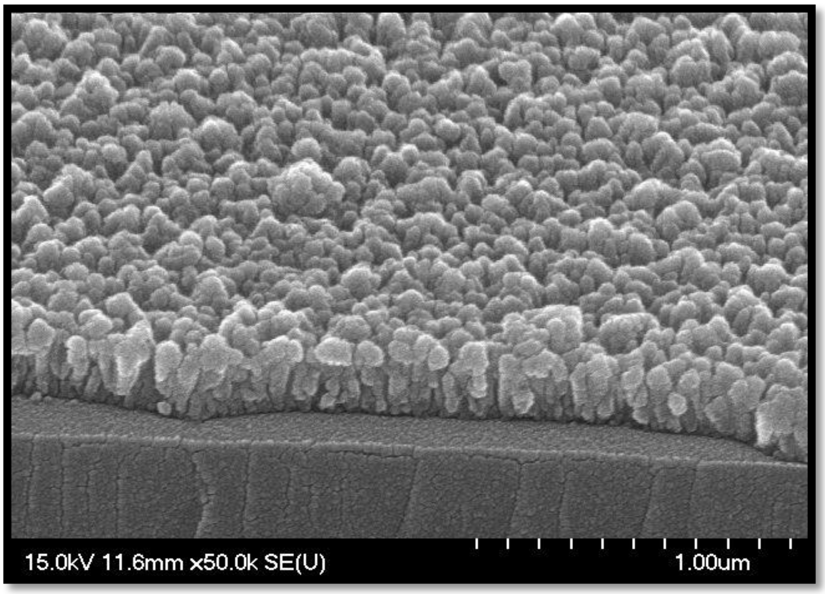

(a)

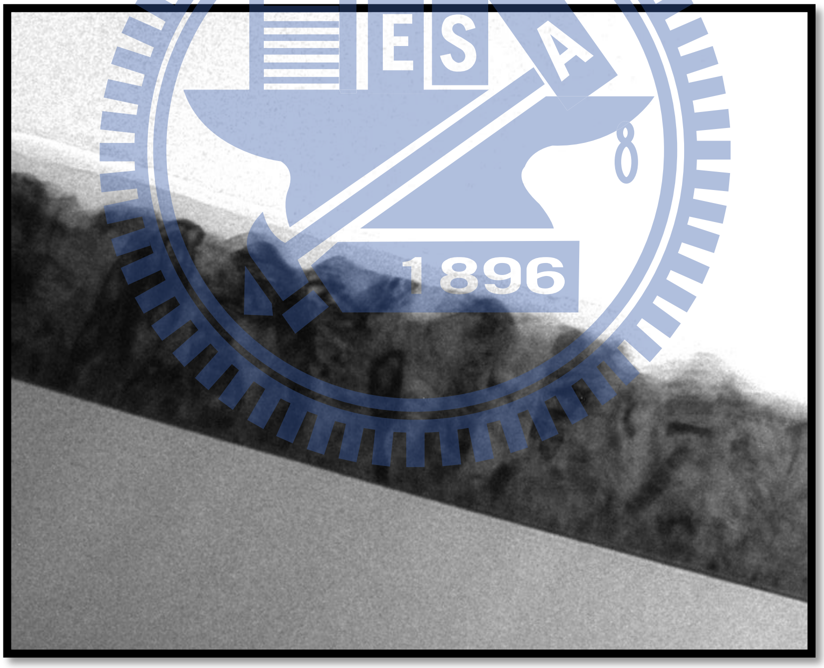

(b)

Fig. 2-15 SEM (tilted angle) and the HRTEM (cross section) images of GZO thin film with 8at% Ga doping (a) SEM (b) HRTEM.

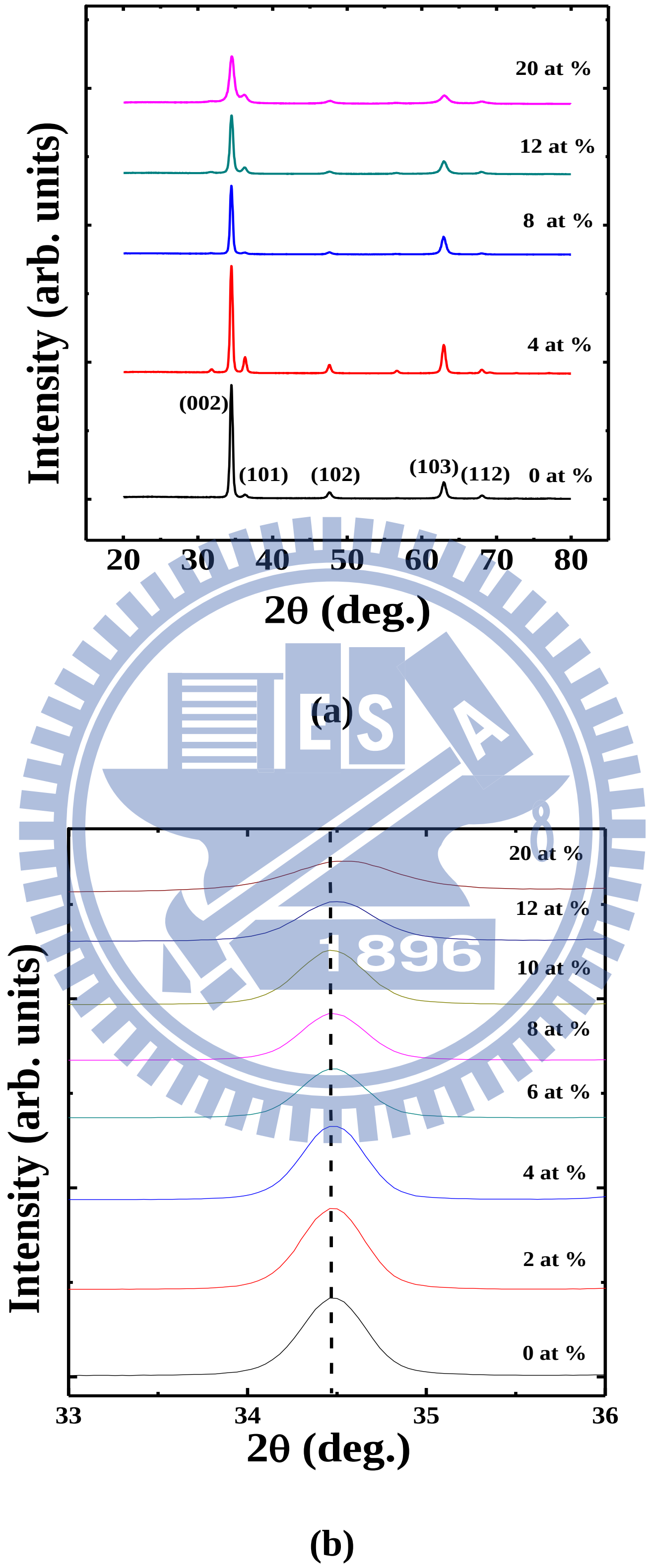

Fig. 2-16 The GIXRD patterns of undoped and different Ga-doped ZnO films deposited by APPJ at a substrate temperature of 100 °C.

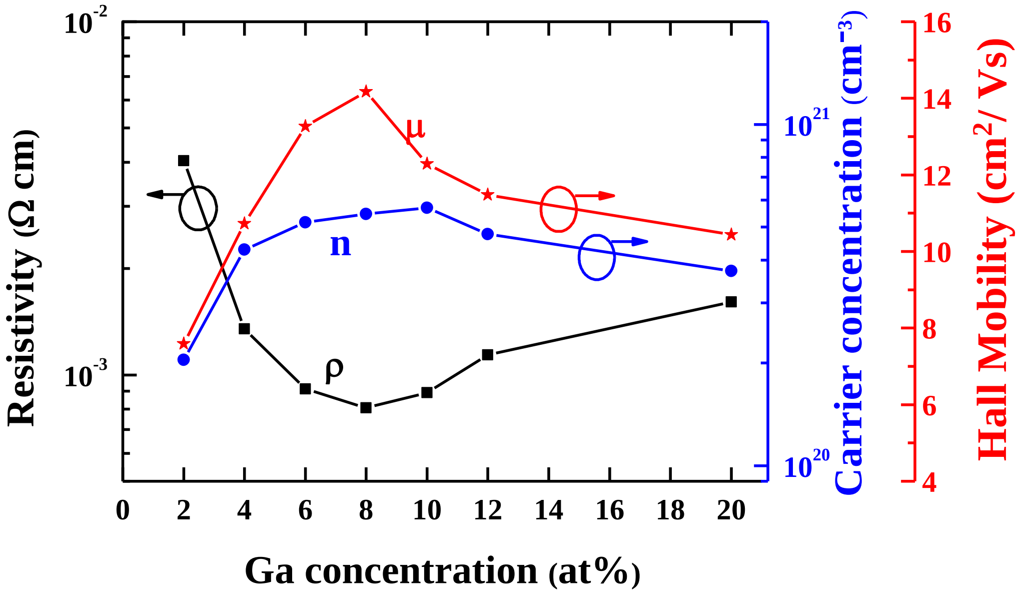

Fig. 2-17 The resistivity (ρ), carrier concentration (n), and hall mobility (μ) of GZO with different Ga/(Zn+Ga) atomic ratios.

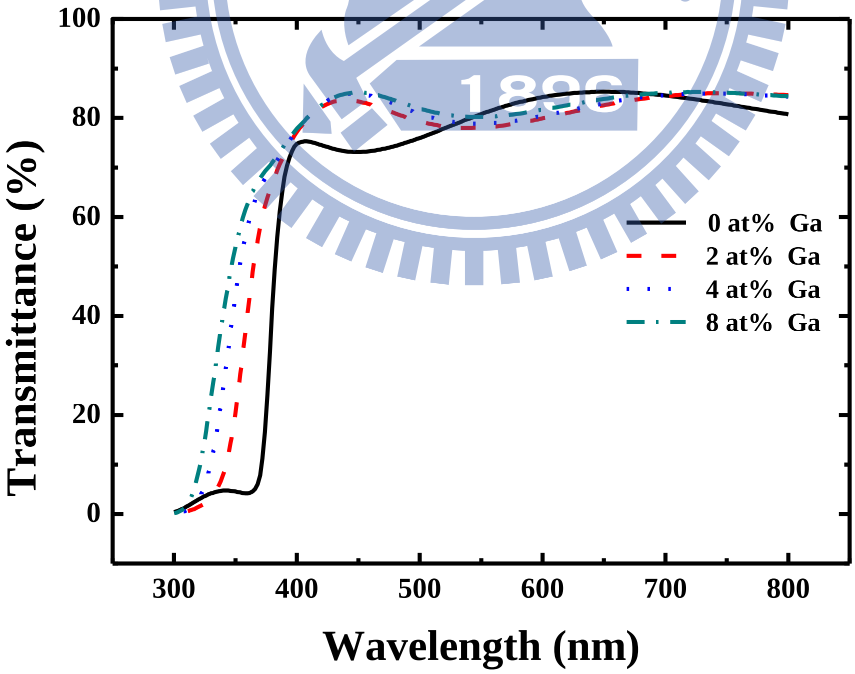

Fig. 2-18 Transmission spectrum of ZnO films with different Ga concentrations.

References

[2.1] D.-J. Lee, H.-M. Kim, J.-Y. Kwon, H. Choi, S.-H. Kim, and K.-B. Kim, "Structural and Electrical Properties of Atomic Layer Deposited Al-Doped ZnO Films," *Advanced Functional Materials,* pp. 1-8, 2010.

[2.2] J.-H. Lee, K.-H. Ko, and B.-O. Park, "Electrical and optical properties of ZnO transparent conducting films by the sol-gel method," *Journal of Crystal Growth,* vol. 247, pp. 119-125, 2003.

[2.3] J.-H. Lee and B.-O. Park, "Transparent conducting ZnO:Al, In and Sn thin films deposited by the sol-gel method," *Thin Solid Films,* vol. 426, pp. 94-99, 2003.

[2.4] B. D. Ahn, J. H. Kim, H. S. Kang, C. H. Lee, S. H. Oh, K. W. Kim, G.-e. Jang, and S. Y. Lee, "Thermally stable, highly conductive, and transparent Ga-doped ZnO thin films," *Thin Solid Films,* vol. 516, pp. 1382-1385, 2008.

[2.5] N. Yamamoto, H. Makino, T. Yamada, Y. Hirashima, H. Iwaoka, T. Ito, A. Ujihara, H. Hokari, H. Morita, and T. Yamamoto, "Heat Resistance of Ga-Doped ZnO Thin Films for Application as Transparent Electrodes in Liquid Crystal Displays," *Journal of The Electrochemical Society,* vol. 157, pp. J13-J20, 2010.

[2.6] K. Shin-ichi and et al., "Poly(methyl methacrylate) Films Deposited via Non-Equilibrium Atmospheric Pressure Plasma Polymerization Using Argon as Working Gas," *Plasma Processes and Polymers,* 2007.

[2.7] B. Philipp and et al., "Atmospheric Pressure Plasma Deposition of Adhesion Promotion Layers on Aluminium," *Plasma Processes and Polymers,* p. NA, 2009.

[2.8] H. Li, S. Wang, L. Zhao, and T. Ye, "Study on an Atmospheric Pressure Plasma Jet and its Application in Etching Photo-Resistant Materials," *Plasma Science and Technology,* vol. 6, p. 2481, 2004.

[2.9] M. H. Han, J. H. Noh, T. I. Lee, J. H. Choi, K. W. Park, H. S. Hwang, K. M. Song, and H. K. Baik, "High-Rate SiO_2 Deposition by Oxygen Cold Arc Plasma Jet at Atmospheric Pressure," *Plasma Processes and Polymers,* vol. 5, pp. 861-866, 2008.

[2.10] L. Chi-Hung and et al., "Surface characterization of the SiO x films prepared by a remote atmospheric pressure plasma jet," *Surface and Interface Analysis,* p. n/a, 2008.

[2.11] P.-E. Camille and et al., "Open Air Deposition of SiO2 Films by an Atmospheric Pressure Line-Shaped Plasma," *Plasma Processes and Polymers,* vol. 2, p. 407, 2005.

[2.12] L. Mounir and A. Tamer, "Arc-Free Atmospheric Pressure Cold Plasma Jets: A Review," *Plasma Processes and Polymers*, 2007.

[2.13] G. A. Hirata, J. McKittrick, J. Siqueiros, O. A. Lopez, T. Cheeks, O. Contreras, and J. Y. Yi, "High transmittance--low resistivity ZnO:Ga films by laser ablation," in *The 42nd national symposium of the American Vacuum Society*, Mineapolis, Minnesota (USA), 1996, pp. 791-794.

[2.14] S.-M. Park, T. Ikegami, K. Ebihara, and P.-K. Shin, "Structure and properties of transparent conductive doped ZnO films by pulsed laser deposition," *Applied Surface Science*, vol. 253, pp. 1522-1527, 2006.

[2.15] T. Yamada, A. Miyake, S. Kishimoto, H. Makino, N. Yamamoto, and T. Yamamoto, "Low resistivity Ga-doped ZnO thin films of less than 100 nm thickness prepared by ion plating with direct current arc discharge," *Applied Physics Letters*, vol. 91, pp. 051915-051915-3, 2007.

[2.16] X. Yu, J. Ma, F. Ji, Y. Wang, X. Zhang, C. Cheng, and H. Ma, "Preparation and properties of ZnO:Ga films prepared by r.f. magnetron sputtering at low temperature," *Applied Surface Science*, vol. 239, pp. 222-226, 2005.

[2.17] S. Kim, W. Lee, E.-H. Lee, S. Hwang, and C. Lee, "Dependence of the resistivity and the transmittance of sputter-deposited Ga-doped ZnO films on oxygen partial pressure and sputtering temperature," *Journal of Materials Science*, vol. 42, pp. 4845-4849, 2007.

[2.18] V. Khranovskyy, U. Grossner, O. Nilsen, V. Lazorenko, G. V. Lashkarev, B. G. Svensson, and R. Yakimova, "Structural and morphological properties of ZnO:Ga thin films," *Thin Solid Films*, vol. 515, pp. 472-476, 2006.

[2.19] J. Hu and R. G. Gordon, "Atmospheric pressure chemical vapor deposition of gallium doped zinc oxide thin films from diethyl zinc, water, and triethyl gallium," *Journal of Applied Physics*, vol. 72, pp. 5381-5392, 1992.

[2.20] K. Y. Cheong, N. Muti, and S. R. Ramanan, "Electrical and optical studies of ZnO:Ga thin films fabricated via the sol-gel technique," *Thin Solid Films*, vol. 410, pp. 142-146, 2002.

[2.21] A R Babar, P R Deshamukh, R J Deokate, D Haranath, C H Bhosale, and K. Y. Rajpure, "Gallium doping in transparent conductive ZnO thin films prepared by chemical spray pyrolysis," *Journal of Physics D: Applied Physics*, vol. 41, p. 135404, 2008.

[2.22] S. A. Studenikin, N. Golego, and M. Cocivera, "Optical and electrical properties of undoped ZnO films grown by spray pyrolysis of zinc nitrate solution," *Journal of Applied Physics*, vol. 83, pp. 2104-2111, 1998.

[2.23] J. Y. W. Seto, "The electrical properties of polycrystalline silicon films," *Journal of Applied Physics,* vol. 46, pp. 5247-5254, 1975.

[2.24] J. Steinhauser, S. Fay, N. Oliveira, E. Vallat-Sauvain, and C. Ballif, "Transition between grain boundary and intragrain scattering transport mechanisms in boron-doped zinc oxide thin films," *Applied Physics Letters,* vol. 90, pp. 142107-3, 2007.

[2.25] K. M. Chang, S. H. Huang, C. J. Wu, W. L. Lin, W. C. Chen, C. W. Chi, J. W. Lin, and C. C. Chang, "Transparent conductive indium-doped zinc oxide films prepared by atmospheric pressure plasma jet," *Thin Solid Films,* vol. 519, pp. 5114-5117, 2011.

Chapter 3

Characterizations of Indium-Doped Zinc Oxide Films Prepared by AP-PECVD System

3.1 Introduction

Atmospheric pressure plasma is used in a variety of materials processes, such as SiO_2 [3.1], TiO_2 [3.2], and ZnO thin films [3.3]. ZnO thin films have attracted much attention as the transparent conductive oxide due to their nontoxicity, low cost, and good stability in the hydrogen-containing plasma, which exists in the fabrication process of some optoelectronic devices. Un-doped ZnO thin films have n type properties due to intrinsic defects, but un-doped ZnO films have poor thermal stability. In order to increase the conductivity and stability of ZnO films, group-Ⅲ elements (Al, Ga, In) can be used as substitutional dopant for Zn site. Because indium has less reactivity and greater resistivity to oxidation than aluminum, indium has easier process controllability. ZnO-based thin films can be prepared on several substrates in a number of ways: pulse laser deposition [3.4]-[3.5], ion plating [3.6], RF magnetic sputtering [3.7], metalorganic chemical vapor deposition [3.8]. Among the different techniques used for the growth of these layers, atmospheric pressure plasma jet (APPJ) has many advantages, such as low cost and well suited for large-scale applications, since it does not need a vacuum chamber and associated pumping system. Zinc oxide thin films have been reported by using atmospheric pressure plasma technique [3.9]-[3.10]. However, to our knowledge, no complete investigation was reported for indium-doped ZnO thin films deposited by APPJ. In this study, we develop indium-doped ZnO by using APPJ and discuss the effect of different substrate temperatures and indium doping concentrations on the morphological, structural, electrical and optical properties of the films.

3.2 Experimental procedure

Indium doped zinc oxide thin films were grown on glass substrates (2.5 cm x 2.5 cm x 0.7 mm) by APPJ. For deposition of indium-doped ZnO films, the zinc nitrate ($Zn(NO_3)_2$,99% purity) and indium nitrate ($In(NO_3)_2$, 99.99% purity) were used as the precursor without further purification. Pure deionized water was used as a solvent and the concentration of zinc nitrate in the deionized water was kept at 0.2 M. The precursor, mixed different zinc nitrate with indium nitrate dissolved in deionized water, was prepared for different doping concentrations (In/Zn+In atomic ratios). Next, the solution was ultrasonically atomized at 2.45 MHz into mist and then conveyed by carrier gas to the plasma region. The nitrogen (N_2) was used as carrier gas and main gas. The flow rate of carrier gas was fixed at 300 sccm, while the flow rate of main gas was 35 SLM. The nozzle to substrate distance was 5mm. The power was set at 600 W. The various substrate temperatures from 100^{o}C to 300^{o}C with

In/Zn+In atomic ratio was 8at.%. On the other hand, different indium doping concentrations was deposited at substrate temperature of 200°C (optimized condition). In order to deposit uniform indium-doped ZnO thin film, the xy directional scan system was used. The position of plasma jet was fixed and the substrate was on the xy directional scan system. First, start point, endpoint and the pitch were set. Next, the scan system moved start point to the end point, and the scan was repeated 10 times. The pitch controlled the overlap of the two paths of x direction. The scan rate of x direction was 20 mm/s, and the scan rate of y direction was 50mm/s. The pitch was set at 2mm.

The morphological, structural, electrical and optical properties of the indium-doped ZnO films were characterized in this work. The crystallinity of the indium-doped ZnO thin films was investigated by using grazing incidence X-ray diffraction (GIXRD), and the thickness as well as the morphological property was determined by scanning electron microscopy (SEM), respectively. The roughness was determined by atomic force microscopy (AFM). Electrical properties were measured by using Hall measurement. Photoluminescence (PL) was used to measure optical properties and optical transmission through the films on the glass was measured in the wavelength range from 300nm to 800nm by using a UV-VIS-NIR spectrophotometer.

3.3 Results and discussion

3.3.1 The Effect of Different Substrate Temperatures on the Properties of Indium-Doped ZnO Thin Films

Figure 3-1 shows the SEM images (tilted angle) of different substrate temperatures and presents different morphological properties. The thicknesses of IZO thin film deposited at 100°C, 200°C and 300°C are 180nm, 270nm, and 286 nm, respectively. As the substrate temperature rises, the thickness increases, especially from 100°C to 200°C. Figure 3-2 shows the PL spectra of IZO thin films deposited at different substrate temperatures. The 100°C sample shows high deep level emission due to the presence of structure defects (ie. oxygen vacancies, oxygen interstitials, zinc vacancies, and zinc interstitials). Figure 3-3 shows the GIXRD pattern of IZO thin film. All the samples shows a preferred (002) orientation. The FWHM of IZO thin films deposited 100°C, 200°C and 300°C are 0.62°, 0.60° and 0.62°, respectively. The 200°C sample shows higher crystallinity than 100°C and 300°C. Since high substrate temperature can supply the energy of migration during deposition, the crystallinity can be improved by rise of temperature. During the deposition of IZO thin films fabricated by APPJ system, the surrounding is air. As the substrate temperature is 300 °C, some adsorbed oxygen from air may result in lattice distortion.

Figure 3-4 shows the hall measurement of different substrate temperatures. The minimum resistivity of $2.3\times10^{-3}\ \Omega\cdot\text{cm}$ is obtained at a substrate temperature of 200°C.

The carrier concentration increases with substrate temperature and decrease at 300^{o}C. This can be attributed to crystallinity and adsorbed oxygen. The mobility increases with substrate temperature. Figure 3-5 shows the transmission spectra in the visible range. The average transmittance is larger than 80% in the visible range. The BM shift is also observed. The bandgap can extract from the absorption edge. The bandgap of 100^{o}C, 200^{o}C and 300^{o}C are 3.45eV, 3.46eV and 3.41eV which are corresponded to the carrier concentration.

3.3.2 The Effect of Indium Doping Concentrations on the Properties of Indium-Doped ZnO Thin Films

SEM images of different indium doping concentrations and RMS roughness of AFM from 0 at.% to 10 at.% were shown in Fig. 3-6. When the doping concentration becomes higher, the surface shows obviously needlelike geometry. As a result, the high indium content shows a rougher surface. D.H. Kim et al. proposed that the IZO thin films deposited by RF magnetron sputter show the needlelike geometry. It is thought that the indium lies distributed randomly on the ZnO film, thus preventing an orderly arrangement [3.7]. Figure 3-7 presents the GIXRD patterns of different Indium-doped ZnO films deposited by APPJ at the substrate temperature of 200^{o}C. Indium-doped ZnO films demonstrate a high (002) preferential orientation, meaning that the c-axis of the crystal lattice is normal to the plane of substrate. As the indium concentration rises, the (002) diffraction peak intensity decreases and full width at half-maximum of (002) diffraction peak broaden resulting from degradation of crystallinity. Fig. 3-8 (a) shows a magnified GIXRD patterns of (002) peak. It is observed that the Braggs angle shift to lower angles with increasing indium doping concentrations. It is noted that the ionic radius of In (0.81Å) is larger than Zn (0.74 Å) [3.11]. Based on the Bragg's law, the Bragg angle shifts to lower angles, due to the larger lattice constant induced by In incorporation. The crystallite size along (002) direction is estimated according to $t = 0.9\lambda/B \cos\theta$, where λ is the x-ray wavelength, θ is the Bragg diffraction angle and B is full width at half maximum [3.12]. Figure 3-8 (b) shows that the un-doped films have lager crystallite size than the doped films, and the crystallite size tends to decrease as doing concentration increases. This may be due to the fact that indium prevents the orderly arrangement and increases number of nucleation centers. Figure 3-9 shows the resistivity (ρ), carrier concentration (n), and Hall mobility (μ) of different In/(Zn+In) atomic ratios. The minimum resistivity of $1.8\times10^{-3}\ \Omega\cdot\text{cm}$ was achieved at approximately 8 at.% indium doping. Both the carrier concentration and Hall mobility initially increase with indium doping concentrations； However, the carrier concentration gradually decreases beyond 8 at.%. When the doping concentration is low, indium atoms effectively occupy the substitutional sites to generate free electrons resulting in the rise of carrier concentration. While the doping concentration is higher than 8 at.%, the poor crystallinity may be responsible for the degraded carrier concentration. The structural defects can trap donors and free carriers result in the decrease of carrier concentration [3.13]. Also, the clustering or segregation of dopants may decrease the carrier concentration of TCO films with excess dopants [3.14]-[3.15]. Figure 3-10 depicts transmission spectrum of ZnO films with different indium concentrations. The inserted graph shows the magnified absorption band edge. All films exhibited that average transmittance in visible region is more than 80%. The absorption edge shows a shift towards shorter wavelength from 0 at.% to 8 at.%. It has been reported that the increase in the optical band gap with an increase in carrier concentration. This phenomenon is known as Burnstein-Moss effect [3.16]. The optical bandgap is estimated by extrapolating the square of absorption coefficient versus the photon energy curve [3.17]. The bandgap values of different indium doping are listed in Table 3-1. The optical bandgap initially tends to rise with indium doping concentration. It is seen that the optical bangap nearly saturates around 6 at.% to 10 at.%. Beyond 10 at.%, a decline of bandgap is observed at 12 at.%.

3.4 Conclusion

In summary, we have demonstrated that indium-doped ZnO films deposited on glass utilizing atmospheric pressure plasma jet. This technique is simple and inexpensive method. IZO thin film deposited at 100^{o}C shows a lager of structure defect due to the high DLE intensity. IZO thin film deposited at 300^{o}C presents the degradation of electrical properties which can be attributed to the absorption of oxygen. ZnO thin film deposited at an appropriate substrate temperature of 200^{o}C shows better properties. Furthermore, IZO thin films are polycrystalline with a preferred orientation along (002) plane and grain size tend to decrease as doping concentration increases. The SEM shows that the surface morphology is affected by indium doping. The films show needlelike geometry from 6 at.% to 10 at.% resulting in the rougher surface. The films prepared with 8at% indium-doped zinc oxide show a low resistivity of 1.8×10^{-3} Ω · cm, a carrier concentration of 2.69×10^{20}1/cm^{3}, a mobility of 12.86 cm^{2}/V-s, a band gap of 3.51eV and a transmittance of about 80% in the visible range.

Table 3-1 Optical bandgap of different indium doping concentrations.

	0 at%	2 at%	4 at%	6 at%	8 at%	10 at%	12 at%
Optical bandgap (eV)	3.28	3.41	3.49	3.51	3.51	3.51	3.47

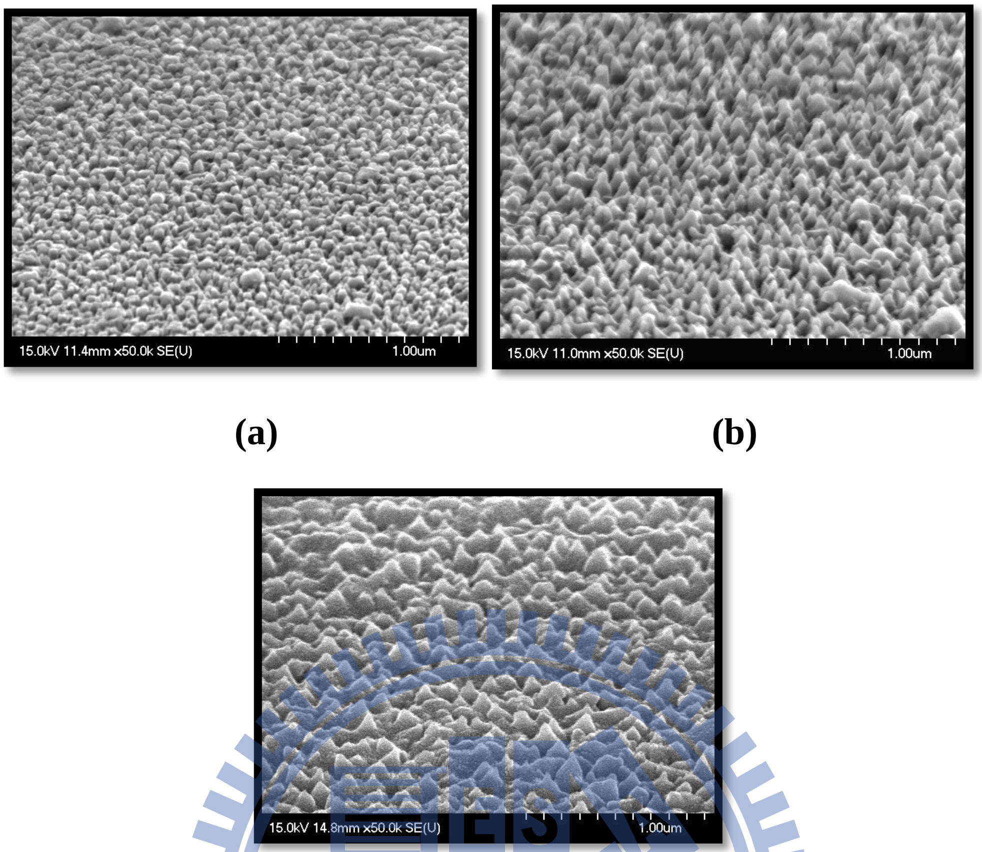

(a) (b)

(c)

Fig. 3-1 SEM images (tilted angle) of different substrate temperatures (a) 100^{o}C (b) 200^{o}C (c) 300^{o}C.

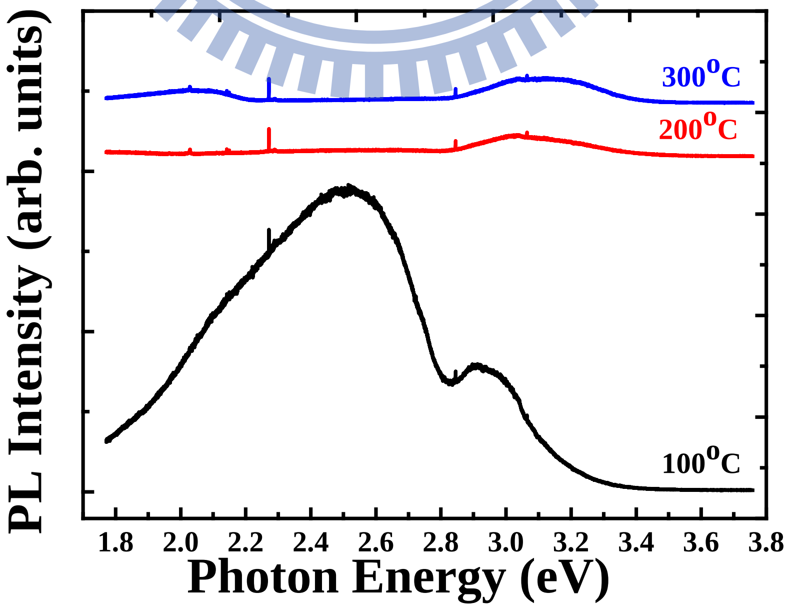

Fig. 3-2 PL spectra of IZO thin films deposited at different substrate temperatures.

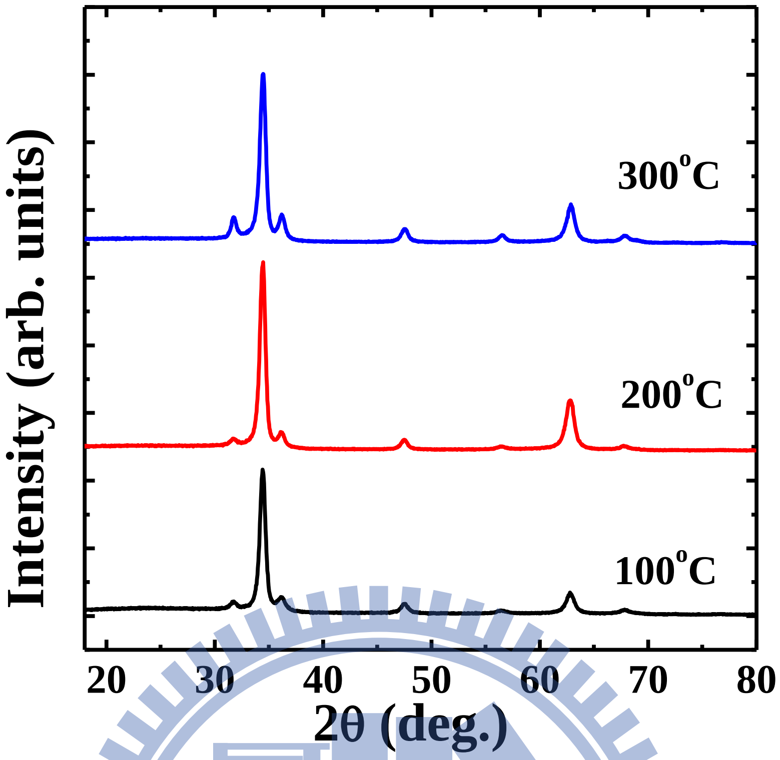

Fig. 3-3 The GIXRD pattern of IZO thin film at different substrate temperatures.

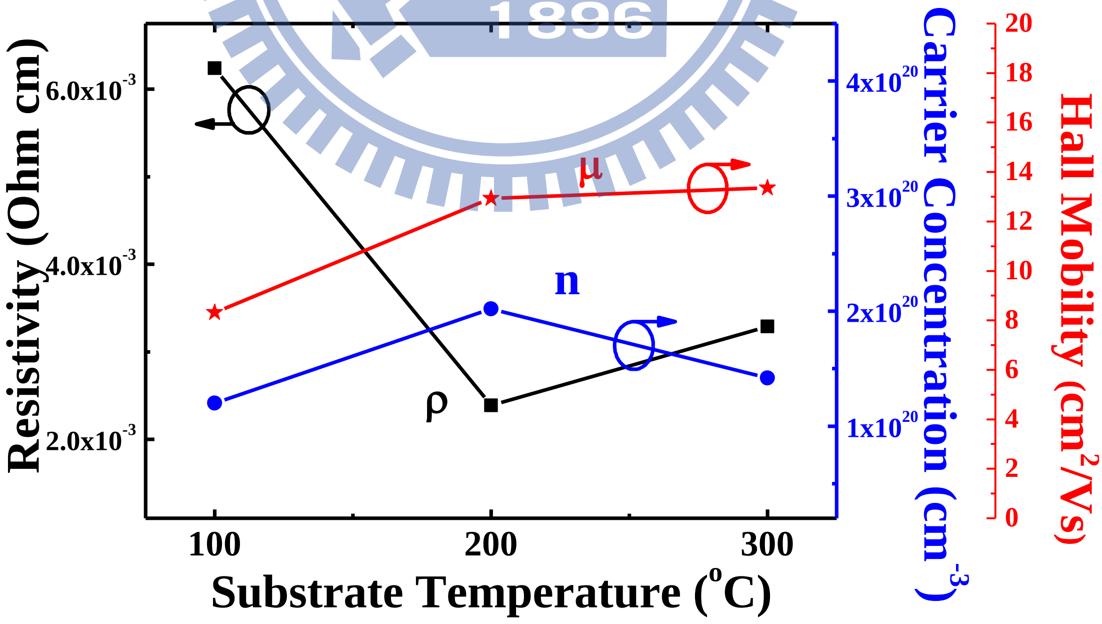

Fig. 3-4 Hall measurement of IZO thin film at different substrate temperatures.

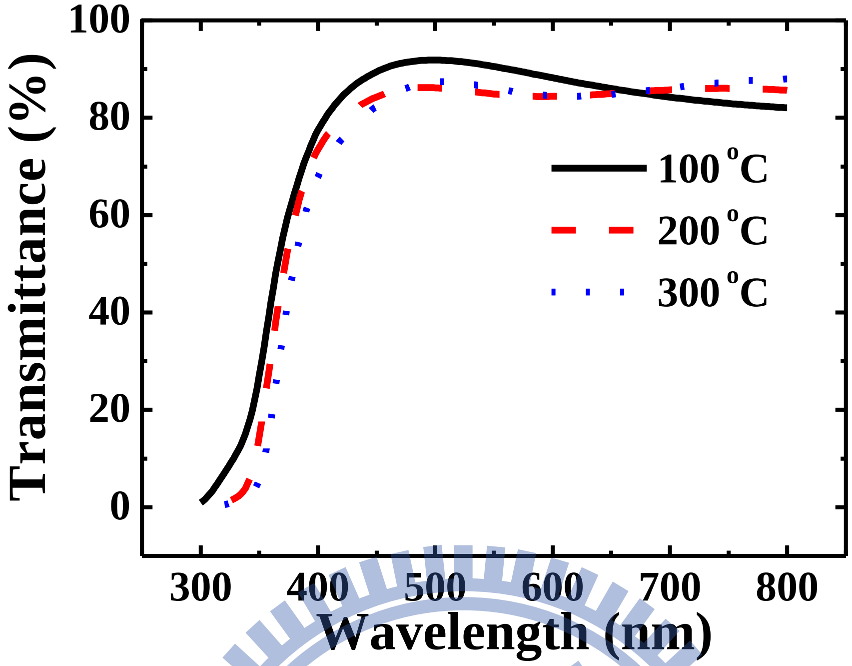

Fig. 3-5 The transmission spectra of IZO thin film in the visible range at different substrate temperatures.

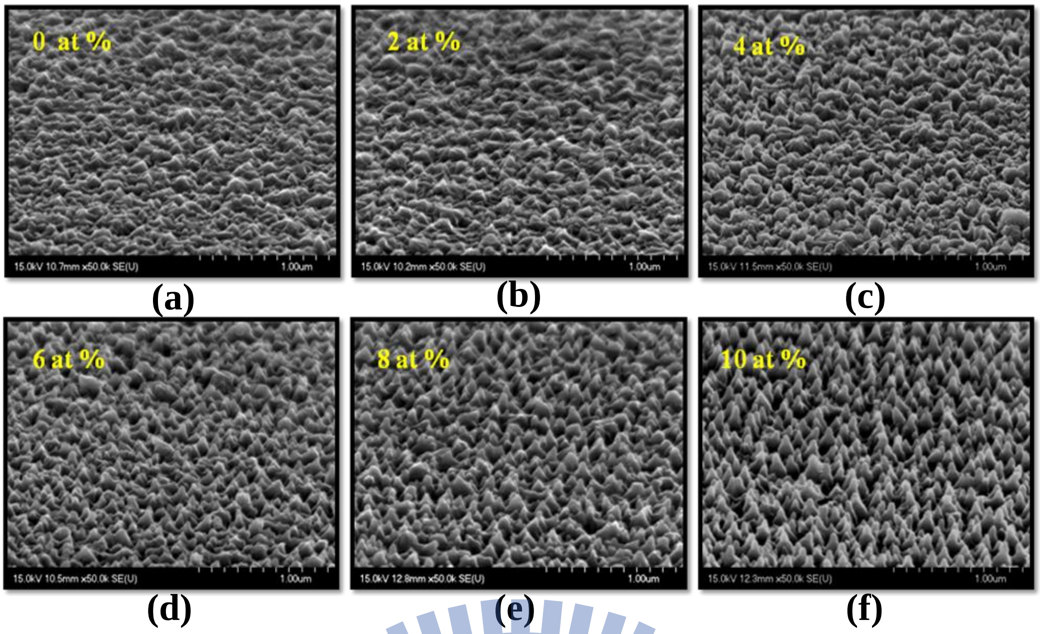

Fig. 3-6 SEM images (tilt angle) of different indium doping concentration from 0 at% to 10 at% (a) 0 at% (Rms=14.7nm)(b) 2 at% (Rms=12.7nm) (c) 4 at% (Rms=21.8nm) (d) 6 at% (Rms=28.5 nm) (e) 8 at% (Rms=28.5 nm) (f) 10 at% (Rms=34.8nm).

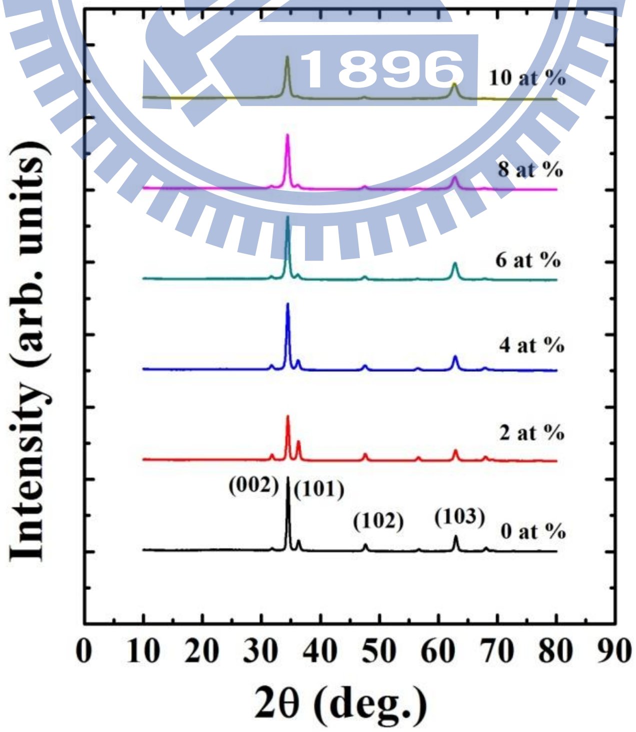

Fig. 3-7 GIXRD patterns of different Indium-doped ZnO films deposited by APPJ at substrate temperature of 200^{o}C.

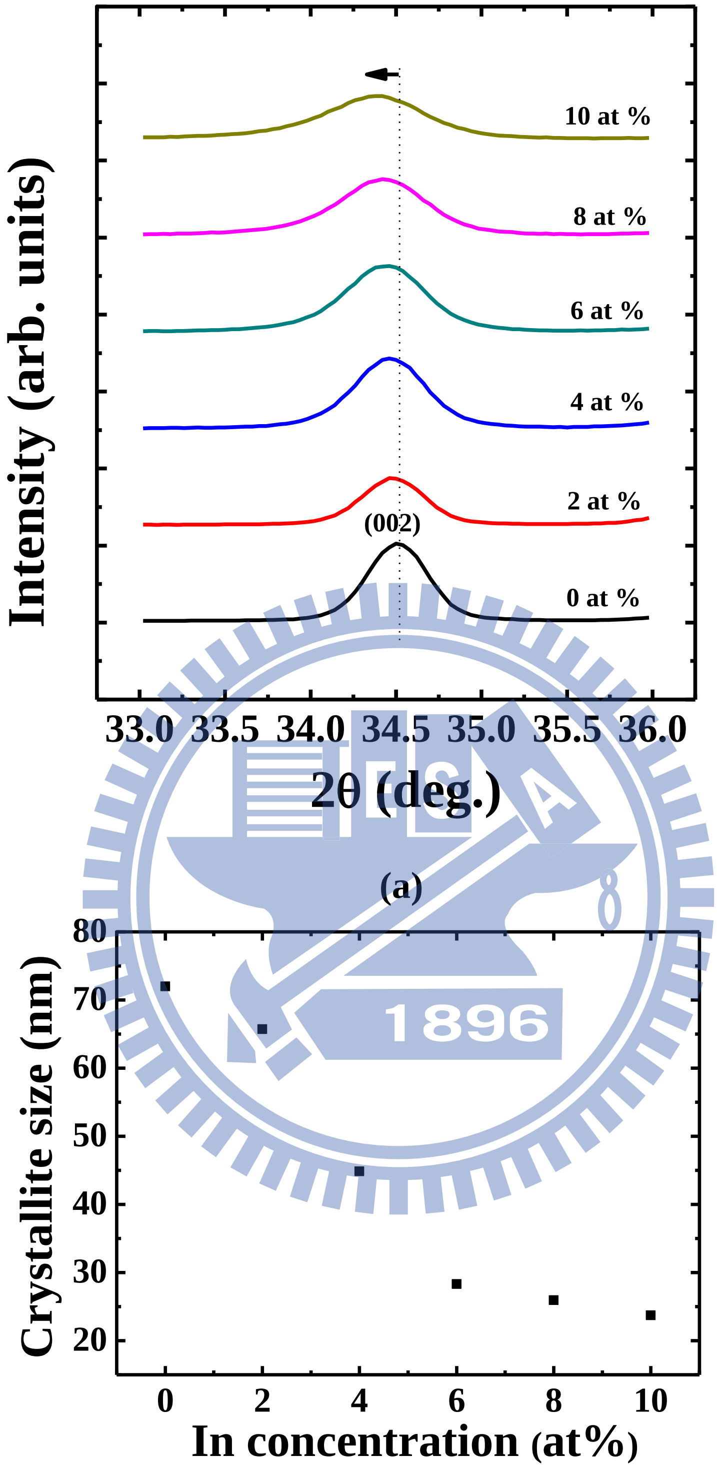

(a)

(b)

Fig. 3-8 (a) The magnified GIXRD patterns of (002) peak (b) crystalline size estimated along (002) peak with different indium doping concentration.

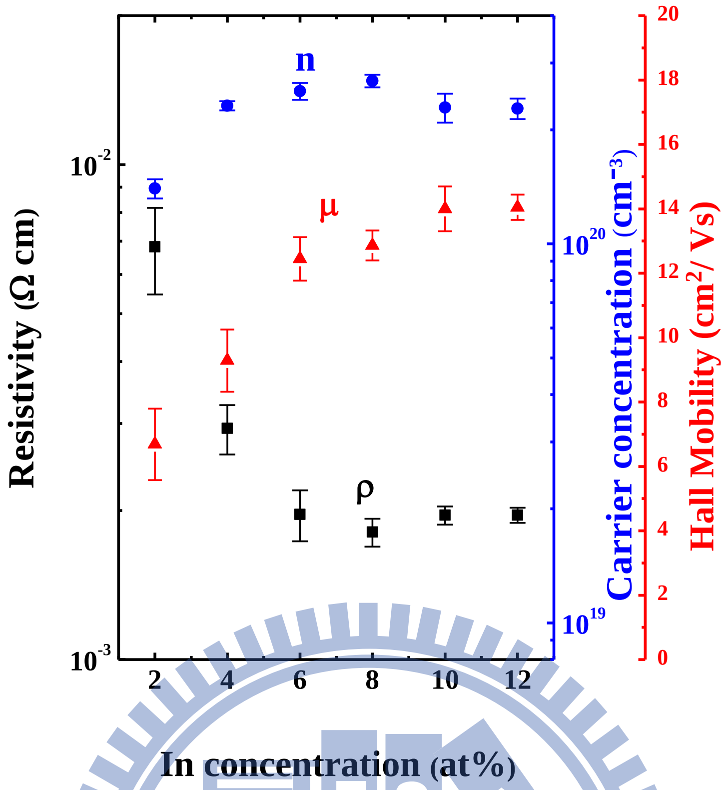

Fig. 3-9 The resistivity (ρ), carrier concentration (n), and Hall mobility (μ) of different In/(Zn+In) atomic ratios.

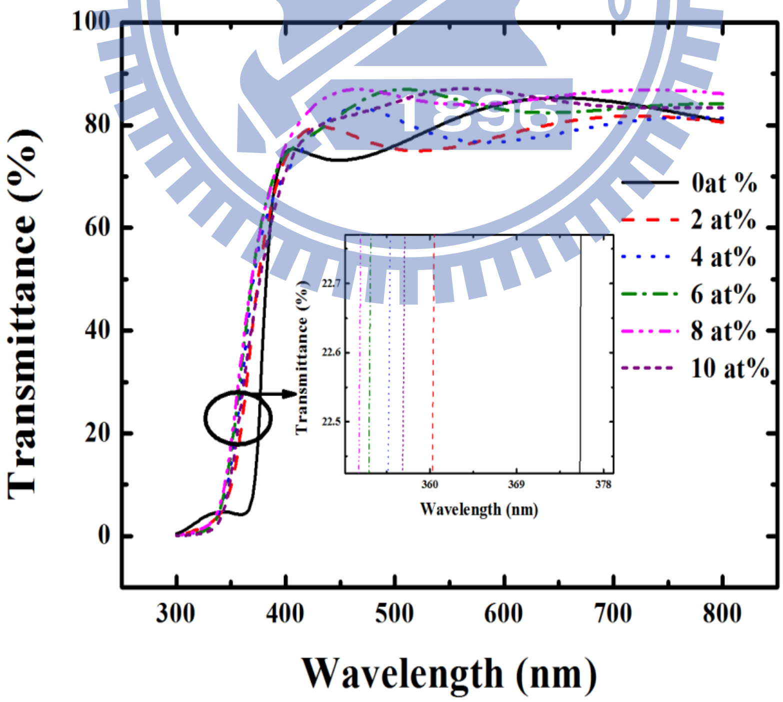

Fig. 3-10 Transmission spectrum of IZO films with different indium doping concentration.

References

[3.1] M. H. Han, J. H. Noh, T. I. Lee, J. H. Choi, K. W. Park, H. S. Hwang, K. M. Song, and H. K. Baik, "High-Rate SiO2 Deposition by Oxygen Cold Arc Plasma Jet at Atmospheric Pressure," *Plasma Processes and Polymers,* vol. 5, pp. 861-866, 2008.

[3.2] H.-K. Ha, M. Yoshimoto, H. Koinuma, B.-K. Moon, and H. Ishiwara, "Open air plasma chemical vapor deposition of highly dielectric amorphous TiO_2 films," *Applied Physics Letters,* vol. 68, pp. 2965-2967, 1996.

[3.3] K. Maruyama, I. Tsumagari, M. Kanezawa, Y. Gunji, M. Morita, M. Kogoma, and S. Okazaki, "Preparation of ZnO films from Zn^{2+} aqueous mist using atmospheric pressure glow plasma," *Journal of Materials Science Letters,* vol. 20, pp. 481-484, 28 February 2001 2001.

[3.4] K. Ramamoorthy, K. Kumar, R. Chandramohan, K. Sankaranarayanan, R. Saravanan, I. V. Kityk, and P. Ramasamy, "High optical quality IZO ($In_2Zn_2O_5$) thin films by PLD - A novel development for III-V opto-electronic devices," *Optics Communications,* vol. 262, pp. 91-96, 2006.

[3.5] V. Bhosle, A. Tiwari, and J. Narayan, "Electrical properties of transparent and conducting Ga doped ZnO," *Journal of Applied Physics,* vol. 100, p. 033713, 2006.

[3.6] T. Yamada, A. Miyake, S. Kishimoto, H. Makino, N. Yamamoto, and T. Yamamoto, "Low resistivity Ga-doped ZnO thin films of less than 100 nm thickness prepared by ion plating with direct current arc discharge," *Applied Physics Letters,* vol. 91, pp. 051915-051915-3, 2007.

[3.7] D. H. Kim, N. G. Cho, H. G. Kim, and W.-Y. Choi, "Structural and Electrical Properties of Indium Doped ZnO Thin Films Fabricated by RF Magnetron Sputtering," *Journal of The Electrochemical Society,* vol. 154, pp. H939-H943, 2007.

[3.8] I. Volintiru, M. Creatore, B. J. Kniknie, C. I. M. A. Spee, and M. C. M. v. d. Sanden, "Evolution of the electrical and structural properties during the growth of Al doped ZnO films by remote plasma-enhanced metalorganic chemical vapor deposition," *Journal of Applied Physics,* vol. 102, p. 043709, 2007.

[3.9] O. V. Penkov, H.-J. Lee, V. Y. Plaksin, R. Mansur, and J. H. Kim, "Deposition of the ZnO transparent electrodes at atmospheric pressure using a DC Arc Plasmatron," *Thin Solid Films,* vol. 518, pp. 6160-6162, 2010.

[3.10] Y. Suzaki, S. Ejima, T. Shikama, S. Azuma, O. Tanaka, T. Kajitani, and H. Koinuma, "Deposition of ZnO film using an open-air cold plasma generator," *Thin Solid Films*, vol. 506-507, pp. 155-158, 2006.

[3.11] M. P. Taylor, D. W. Readey, M. F. A. M. van Hest, C. W. Teplin, J. L. Alleman, M. S. Dabney, L. M. Gedvilas, B. M. Keyes, B. To, J. D. Perkins, and D. S. Ginley, "The Remarkable Thermal Stability of Amorphous In-Zn-O Transparent Conductors," *Advanced Functional Materials*, vol. 18, pp. 3169-3178, 2008.

[3.12] A. Mondal, N. Mukherjee, S. Kumar Bhar, and D. Banerjee, "An electrochemical technique to deposit thin films of PbTe," *Thin Solid Films*, vol. 515, pp. 1255-1259, 2006.

[3.13] P. K. Song, Y. Shigesato, M. Kamei, and I. Yasui, "Electrical and Structural Properties of Tin-Doped Indium Oxide Films Deposited by DC Sputtering at Room Temperature," *Japanese Journal of Applied Physics*, vol. 38, pp. pp. 2921-2927 1999.

[3.14] D. H. Lee, Y.-H. Song, H. H. Park, and S. S. Lee, "Hypertrophic cell treatment for apoptosis incucement by remote plasma," in *Plasma Science, 2010 Abstracts IEEE International Conference on*, 2010, pp. 1-1.

[3.15] K. H. Kim, K. C. Park, and D. Y. Ma, "Structural, electrical and optical properties of aluminum doped zinc oxide films prepared by radio frequency magnetron sputtering," *Journal of Applied Physics*, vol. 81, pp. 7764-7772, 1997.

[3.16] I. Hamberg, C. G. Granqvist, K. F. Berggren, B. E. Sernelius, and L. Engström, "Band-gap widening in heavily Sn-doped In2O3," *Physical Review B*, vol. 30, p. 3240, 1984.

[3.17] G. A. Hirata, J. McKittrick, J. Siqueiros, O. A. Lopez, T. Cheeks, O. Contreras, and J. Y. Yi, "High transmittance-low resistivity ZnO:Ga films by laser ablation," in *The 42nd national symposium of the American Vacuum Society*, Mineapolis, Minnesota (USA), 1996, pp. 791-794.

Chapter 4

The Effect of Channel Thicknesses and Oxygen Species on the Characteristics of ZnO TFTs Prepared by APPECVD system

4.1 Introduction

Amorphous silicon (a-Si) and polysilicon TFTs dominate the active matrix technologies in the flat-panel display industry over the last ten years. However, these silicon-based TFTs have several limitations such as photosensitivity, light degradation, and opacity, etc. Recently, transparent oxide semiconductors have been investigated as an active channel layer. Zinc oxide thin-film transistors (TFTs) have high potential in the active matrix liquid crystal display (AMLCD) due to non-toxic property, low cost, high mobility, low growth temperature and wide bandgap [4.1]-[4.3]. Because of low growth temperature, devices can be fabricated on inexpensive plastic substrate for flexible electronics applications. The wide bandgap of 3.35eV, which is transparent in the visible region, can also be employed to a channel layer for the transparent TFT (TTFT) application [4.4]-[4.5]. For the applications of ZnO TFTs in the flat-panel displays, the off current must be low. Large on-off ratio is preferred when used as switching device. The carrier concentration of un-doped ZnO thin films results from the intrinsic defects. Higher carrier concentration generates the external scattering and unexpected leakage current. As a result, the background electron carrier concentration must be reduced while ZnO was used as a channel layer. Also, to reduce the leakage current of source to drain current flow, thinner channel layer have been proposed by reducing the conductivity of channel layer [4.6]. In order to reduce the intrinsic defects, the compressed dry air (CDA, ~20% Oxygen gas) was also used as carrier gas to reduce the oxygen vacancies. Next, to improve the performance, the different channel thicknesses were discussed. Furthermore, the oxygen species was also incorporated into main gas.

The purpose of this chapter is to demonstrate the possibility to fabricate superior performance ZnO TFTs at low temperature by using atmospheric pressure plasma jet. In this chapter, we integrated ZnO as a channel layer by atmospheric pressure plasma jet and discussed the effects of oxygen species and channel thicknesses on the characteristics of ZnO TFTs.

4.2 Experimental Procedure

4.2.1 Device Fabricated with Different Carrier Gases and Channel Thicknesses

Zinc oxide thin films were grown on the glass substrates as well as high doping silicon substrate by atmospheric pressure plasma jet (APPJ). The high doping silicon wafer was used as gate electrode and thermally grown SiO_2 (110nm) on the silicon substrate was used as gate insulator. Then, ZnO thin films were deposited on SiO_2/Si by APPJ. For deposition of ZnO films, zinc nitrate ($Zn(NO_3)_2 \cdot 6H_2O$) dissolved in pure deionized water was used as the precursor. The concentration of zinc nitrate in the D.I. water was 0.2 M. Next, the aqueous solution was ultrasonically atomized at 2.45 MHz into mist and conveyed by carrier gas to the plasma region, which was connected to DC pulse power supply. The nitrogen (N_2) and compressed dry air (CDA) were used as carrier gases and the thickness of ZnO thin films were kept at 110 nm. The flow rate of both carrier gases was fixed at 300 sccm, while the flow rate of main gas was 35 SLM. The channel thickness was varied by scanning 1 times to 15 times while CDA used as carrier gas. The distance between nozzle and substrate was set as 5 mm. The power and substrate temperature fixed at 630 W and 100^{o}C, respectively. The pattern on ZnO thin film was obtained by conventional photolithography and wet etching using the HCl:H_2O (1:200). Finally, 100nm thick Al source/drain (S/D) layers were patterned by lift-off technique. A schematic cross view of the fabricated TFT is shown in Fig.4-1. The optical, structural, and electrical properties of the ZnO films were characterized. The crystallinity of the ZnO thin films was investigated by using grazing incidence X-ray diffraction (GIXRD). The thickness of the film as well as morphology was determined by scanning electron microscopy (SEM) and atomic force microscopy (AFM). Optical transmittance through the sample of ZnO/glass was measured in the wavelength range from 300nm to 800nm by using a UV-VIS-NIR spectrophotometer. Device characteristics, including transfer and output curves, were measured by semiconductor parameter analyzer (HP4156C).

4.2.2 Device Fabricated with Incorporation of Oxygen Species into Main Gas

Starting with n^+ silicon (100) wafer used as gate electrode, thermally grown SiO_2 (110nm) at 1050°C on the silicon substrate was adopted as gate insulator. Next, 50-nm ZnO thin films were deposited on SiO_2/Si by APPJ. The water-based solution, zinc nitrate ($Zn(NO_3)_2 \cdot 6H_2O$) dissolved in pure deionized water, was used as precursor. The nitrogen was used as plasma gas and the flow rate of plasma gas was 35 SLM. Different oxygen partial pressures were incorporated into plasma gas (N_2) in the percentage of 0%-1% (O_2/N_2+O_2). The power and substrate temperature were set at 630 W and 100°C, respectively. In order to analyze the transmittance, ZnO was also deposited on glass substrate. The pattern on ZnO channel layer was formed by conventional photolithography and wet etching using the $HCl:H_2O$ (1:200). Finally, 100nm thick Al source/drain (S/D) layers were patterned by lift-off technique.

The optical, structural, and electrical properties of the ZnO films at different oxygen partial oxygen were characterized. The crystallinity of the ZnO thin films was investigated by using grazing incidence X-ray diffraction (GIXRD). The morphology was determined by scanning electron microscopy (SEM). Photoluminescence (PL) was used to measure optical properties. Optical transmittance through the sample of ZnO/glass was measured in the wavelength range from 300nm to 800nm by using a UV-VIS-NIR spectrophotometer. Electrical properties were measured by semiconductor parameter analyzer (HP4156C).

4.3 Results and discussion

4.3.1 The Effect of Different Carrier Gases and Channel Thicknesses on the Characteristics of ZnO TFTs

Figure 4-2 shows the grazing incident X-ray patterns of 110-nm-thick ZnO films prepared with different carrier gases at a substrate temperature of 100°C by APPJ. From the figure it is seen that ZnO films exhibit hexagonal crystal structure with a preferential growth along (002) plane both in N_2 and CDA samples. The N_2 sample has higher intensity of the (002) plane than CDA, but CDA sample show the higher (100) and (101) peaks than N_2. The may be due to the fact that the gas phase nucleation particle increases when CDA is used as a carrier gas. Since the oxygen is high reactivity, it reacts with precursor in the gas phase leading to the random particle. Nevertheless, the FWHM of (002) peak in N_2 (0.46°) is similar to CDA (0.45°). Figure 4-3 shows AFM images of ZnO thin films with different carrier gas. CDA sample shows a smaller grain size than N_2.The reactive oxygen species maybe result in more nucleation sites. Figure 4-4 shows the optical transmission spectra of ZnO films deposited on glass with different carrier gases. The average transmittance of N_2 sample is slightly larger than CDA. The possible reason for this may be the scattering light by gas phase nucleation particles. The average optical transmittance of N_2 and CDA samples in the visible range is more than 80%. Figure 4-5 represents transfer characteristics of 110-nm-thick channel ZnO TFTs with different carrier gases. The channel length and width are 100 μm and 1000 μm. From the figure of N_2 sample, it can be observed that high leakage current and the poor I_{on}/I_{off} current ratio. However, ZnO TFT with CDA as carrier gas improves the off-leakage current about 3 orders of magnitude than N_2 sample. It is likely that oxygen species are efficient to repair the oxygen vacancies. The I_{on}/I_{off} ratio of N_2 sample and CDA sample were 1.6×10^2 and 2.59×10^5, respectively. Figure 4-6 represents $I_{DS}^{1/2}$ versus V_{GS}. The field effect mobility (μ_{FE}) and V_t were extracted using the following current equation.

$$I_D = (W/2L)\, Ci\mu_{FE}\, (V_{GS} - V_T)^2 \tag{4.1}$$

where Ci is the capacitance per unit area of the gate insulator and V_T is the threshold voltage. The μ_{FE} of N_2 sample and CDA sample were 2.3 $cm^2V^{-1}s^{-1}$ and 4.9 $cm^2V^{-1}s^{-1}$. The CDA sample has lower mobility than N_2. From AFM images, CDA sample with smaller grain size will result in more grain boundary scattering. Furthermore, it has been reported that external oxygen was absorbed in the grain boundaries and this oxygen trapped free electrons. Although using CDA as a carrier gas repair oxygen vacancies, smaller grain size and some adsorbed oxygen in the grain boundaries maybe results in the slight decline of mobility. The threshold voltage of N_2 sample and CDA sample were 16.6 V and 31.5 V respectively, showing that the ZnO-TFT operates the enhancement mode .The result also indicates that CDA sample has the smaller electron carrier concentration than N_2 sample. The background carrier concentration can effectively decrease using CDA as a carrier gas. Output characteristics (ID-VD) of ZnO TFT are shown in Fig. 4-7. It is observed that I_D of N_2 sample increase with V_{DS} at saturation region. Since the N_2 sample has higher carrier concentration, the channel region is not totally depleted, and the undepleted region contributes the external current. However, the CDA sample shows a hard saturation. This indicates that the ZnO channel is fully depletion and this behavior is desired for circuit application because of a lager output resistance [4.7]. Transfer characteristics of ZnO TFT with different channel thicknesses are shown in Fig 4-8. The off-leakage current of 110-nm-thick (10times) and 165-nm-thick (15times) channel ZnO TFTs are 3.82×10^{-9}A and 5.42×10^{-9} A, respectively. The undesired source to drain leakage current flow has less dependence with gate voltage. By reducing the channel thickness, the channel resistance increases result in the low leakage current. When the thickness reduces to 55 nm (5times), the leakage current significantly reduces. The leakage current of 3times sample reaches a minimum value of 1.84×10^{-11} A. The 1time sample shows low drain current because the thin ZnO film maybe result in a discontinue structure. Figure 4-9 shows Output characteristics (IDVD) of ZnO TFT with different channel thicknesses. All the samples operate in enhancement mode, and the 55-nm-thick sample shows a higher saturation current. The mobility of 55 nm sample is higher compared with 110 nm and 165 nm. This may be due to the less series resistance. Table 4-1 summarizes the electrical properties of field effect mobility, threshold voltage, subthreshold swing, and I_{on}/I_{off} ratio with different channel thicknesses. The 3times and 5times show a better performance.

4.3.2 The Effect of Incorporated Oxygen Species into Main Gas on the Characteristics of ZnO TFTs

Figure 4-10 shows the grazing incident X-ray patterns of ZnO films with different oxygen partial pressures by APPJ. ZnO thin films exhibit a predominant (002) diffraction peak with small (100) and (101) peaks, indicating a preferential growth along (002) plane. When the oxygen species are incorporated into plasma gas, the intensity of the (002) slightly decreases, and the intensity of (100) as well as (101) peaks increase. This may be due to the fact that the gas phase nucleation particle increases with increasing oxygen partial pressure. Since the oxygen is high reactivity, it reacts with precursor in the gas phase leading to the random particle. Figure 4-11 shows SEM images of ZnO thin film with different oxygen partial pressures. With increasing oxygen partial pressure, the gas phase nucleation particle increases and ZnO thin films show a rough surface. The 1% O_2 sample shows amount of gas phase nucleation particles. These particles could affect carrier transport and contact property. Figure 4-12 shows optical transmission spectra of ZnO thin film deposited on glass. A hump is observed at wavelength of 350nm. This is attributed to the finite absorption and a thin ZnO thickness. The average transmittance in the visible region is more than 80%. The 1% shows a slightly lower transmittance. Figure 4-13 shows a UV emission peak at 3.25eV. The UV emission was attributed to the near bandgap transition. The intensity of the UV emission peak increases when oxygen was incorporated into plasma gas. Generally, it is believed that the UV emission comes from stoichiometry of the ZnO with less oxygen vacancies [4.8]. Figure 4-14 represents transfer characteristics of ZnO TFT with different oxygen ratios. From the curve of 0% O_2 sample, it can be observed that high leakage current and the low I_{on}/I_{off} ratio. However, ZnO TFT incorporated oxygen species obviously improves the leakage current. This can be deduced the oxygen vacancy density was efficiently reduced. The 1% O_2 sample shows degradation of electrical properties than 0.69% resulting from the particles with extra oxygen species. Table 4-2 summarizes the electrical properties of the ZnO TFTs. The I_{on}/I_{off} current ratio is improved about six orders of magnitude by incorporating 0.69% O_2 compared with the 0% O_2 sample. The mobility was slightly degraded with increasing oxygen ratios. This may be due to the fact that gas phase nucleation is formed external scattering center. The 0.69% O_2 sample shows the lowest SS and the highest I_{on}/I_{off} current ratio.

4.4 Conclusion

In summary, ZnO films deposited by APPJ were successfully integrated as a channel layer. The ZnO thin films exhibit a preferred (002) orientation and the average transmittance of ZnO thin films deposited on glass are more than 80%. During deposition, using CDA as carrier gas can effectively reduce oxygen vacancies and improve the I_{on}/I_{off} current ratio from 1.6×10^2 to 2.59×10^5. Reducing the thickness can increase the channel resistance and reduce the undesired current flow. Using CDA as a carrier gas and reducing the channel thickness to 55nm, a subthreshold swing of 3.75V/decade, a field-effect mobility of 3.49 cm^2/Vs and an I_{on}/I_{off} current ratio of 4.08×10^7 were obtained.

With increasing oxygen partial pressure, the gas phase nucleation particle increases and ZnO thin films show a rough surface. PL spectra show that the oxygen vacancies could be repaired effectively by incorporating oxygen into plasma gas. By incorporating 0.69% O_2 into plasma gas, a threshold voltage of 26.7 V, a subthreshold swing of 3.89 V/decade, a field-effect mobility of 2.38 cm^2/Vs and an I_{on}/I_{off} current ratio of $4.63x10^9$ were obtained.

Table 4-1 The electrical properties of different channel thicknesses.

	1times	3times	5times	10times	15times	20times
V_t (V)	**24**	**35.6**	**33.8**	**31.5**	**31.1**	**28.7**
SS (V/dec.)	**2.87**	**4**	**3.75**	**6.33**	**6.25**	**6.21**
Mobility (cm^2/V-s)	**0.05**	**3.13**	**3.49**	**2.33**	**2.33**	**3.78**
I_{on}/I_{off} ratio	**$5.56x10^5$**	**$5.92x10^7$**	**$4.08x10^7$**	**$7.06x10^5$**	**$3.34x10^5$**	**$8.4x10^4$**

Table 4-2 The electrical properties of different oxygen ratios.

	0% O_2	0.34% O_2	0.69% O_2	1% O_2
Vt (V)	**15.9**	**24.9**	**26.7**	**26.4**
SS (V/dec.)	**14.67**	**5.74**	**3.89**	**4.78**
Mobility (cm^2/V-s)	**2.75**	**2.67**	**2.38**	**2.33**
I_{on}/I_{off} ratio	**$2.71x10^3$**	**$4.15x10^7$**	**$4.63x10^9$**	**$8.48x10^7$**

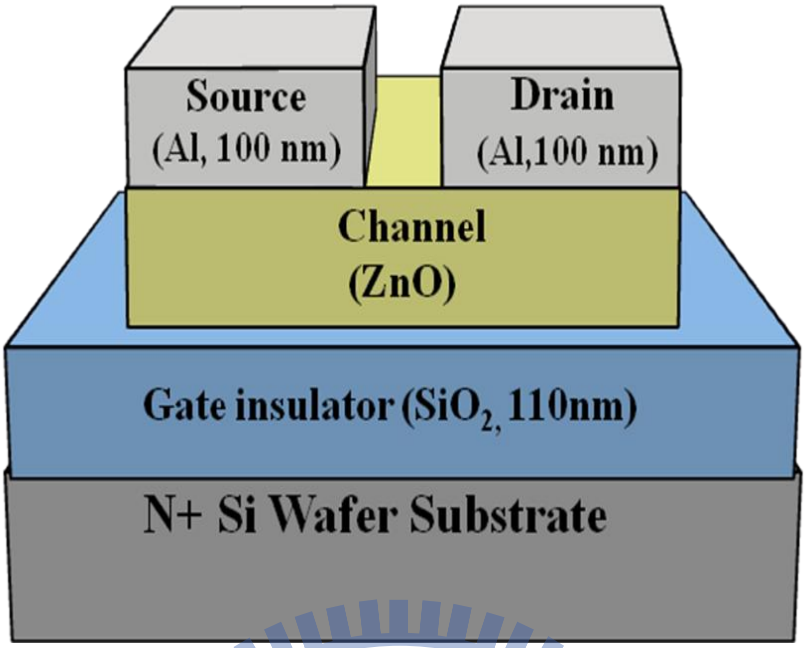

Fig. 4-1 Schematic structure of the bottom-gate TFT test structure.

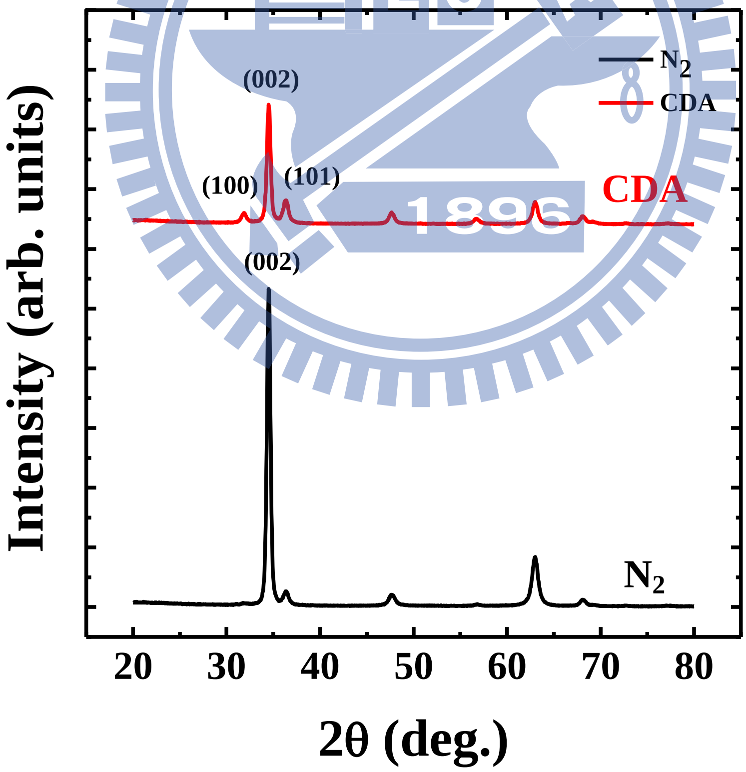

Fig. 4-2 Grazing incident X-ray patterns of ZnO films prepared with different carrier gases.

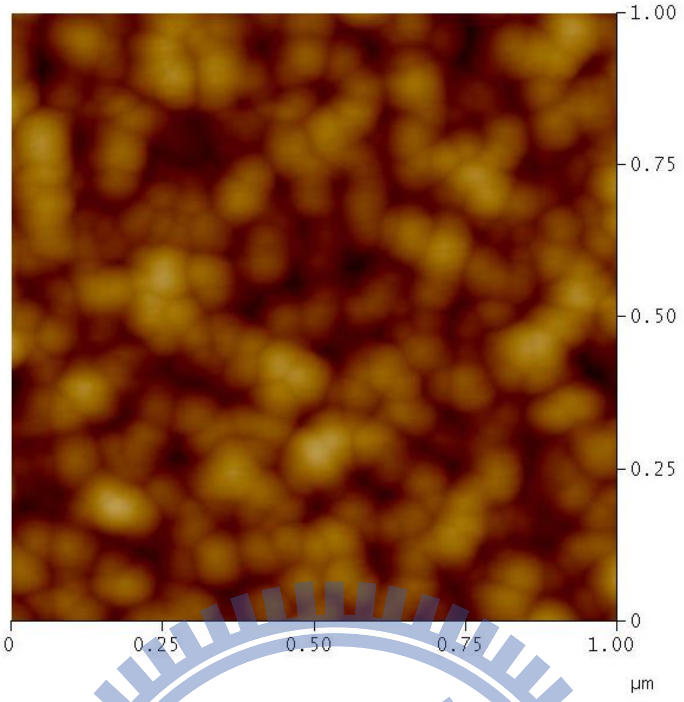

(a)

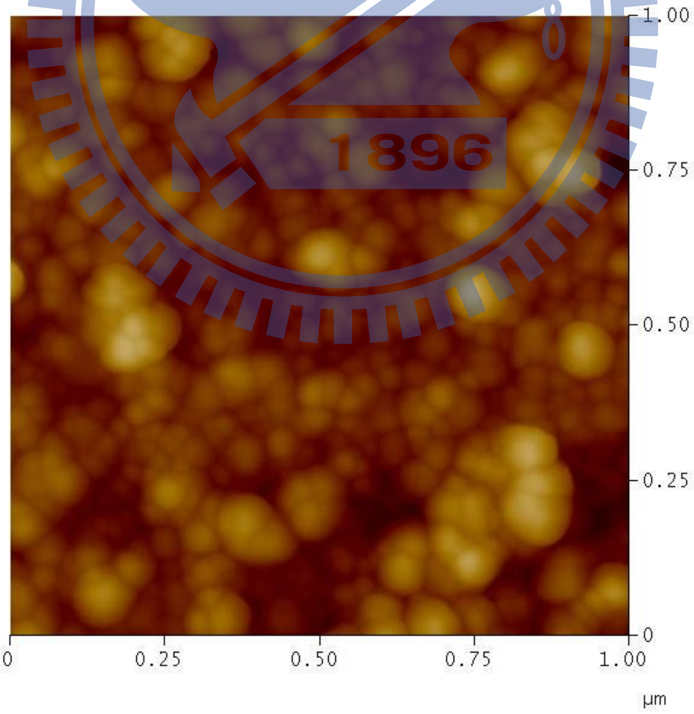

(b)

Fig. 4-3 AFM images of ZnO thin films with different carrier gas (a) N_2 (b) CDA.

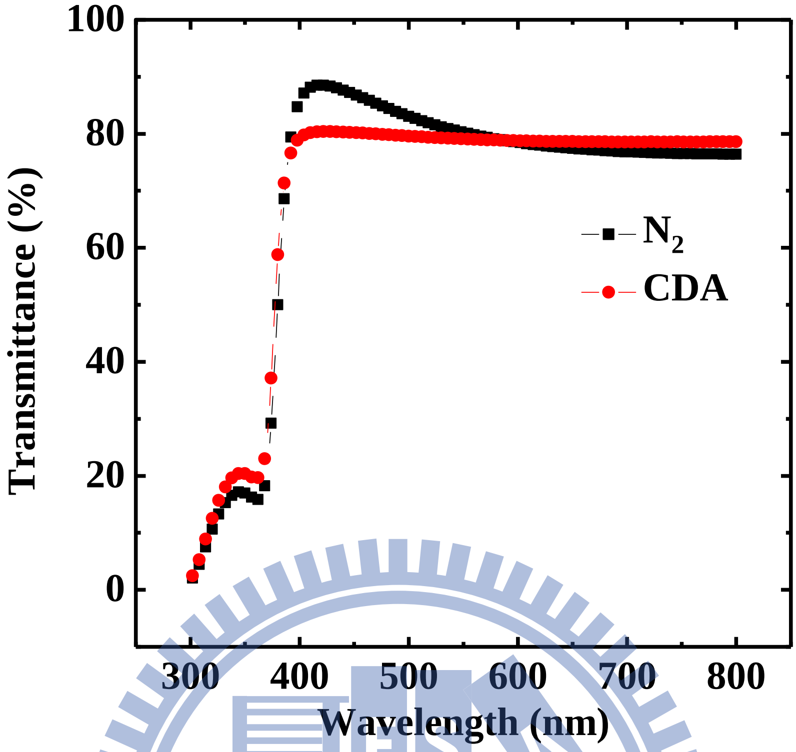

Fig. 4-4 The optical transmission spectra of ZnO films deposited on glass with different carrier gases.

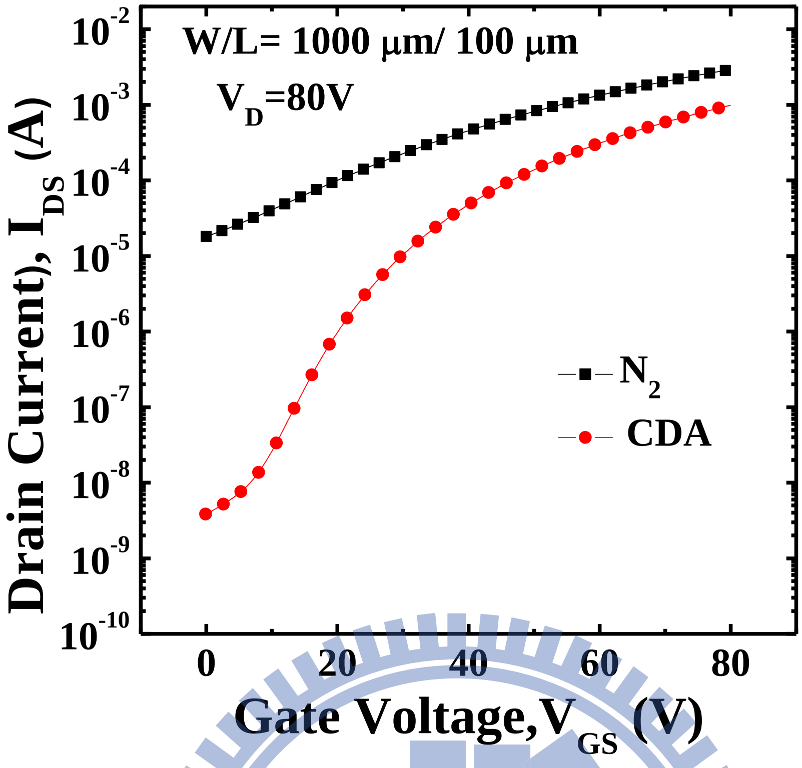

Fig. 4-5 Transfer characteristics of ZnO TFT with different carrier gases.

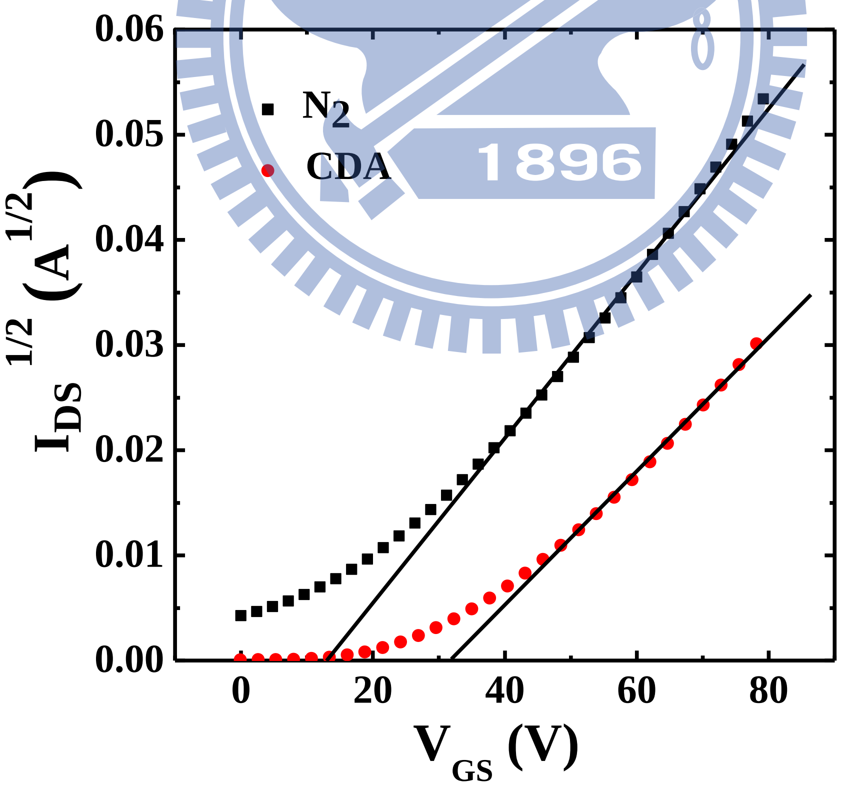

Fig. 4-6 $I_{DS}^{1/2}$ versus V_{GS} at V_D of 80V, used to calculate the threshold voltage and saturation mobility.

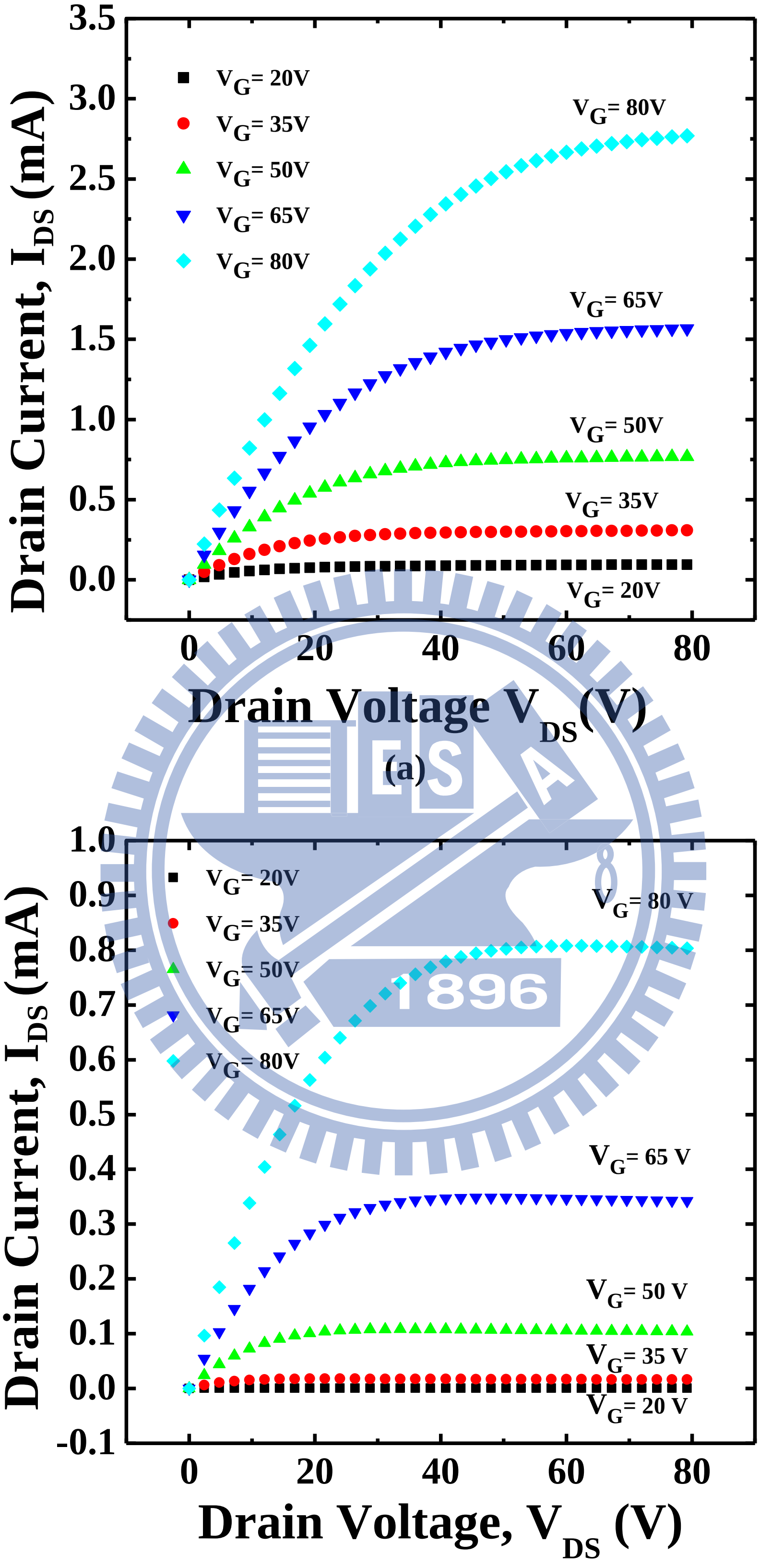

(a)

(b)

Fig. 4-7 Output characteristics (IDVD) of ZnO TFT with different carrier gas (a) N_2 (b) CDA.

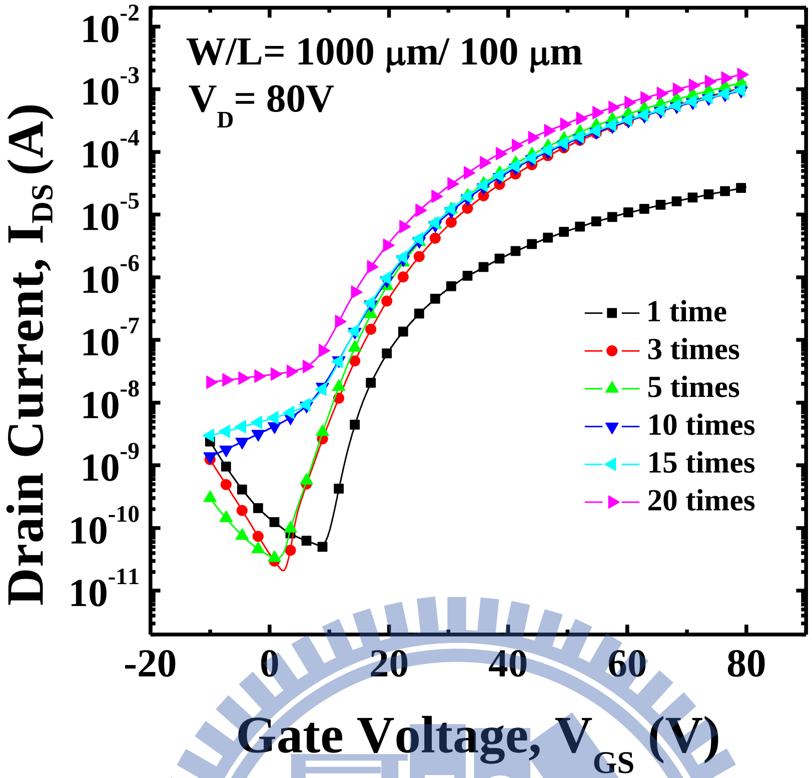

Fig. 4-8 Transfer characteristics of ZnO TFT with different channel thicknesses.

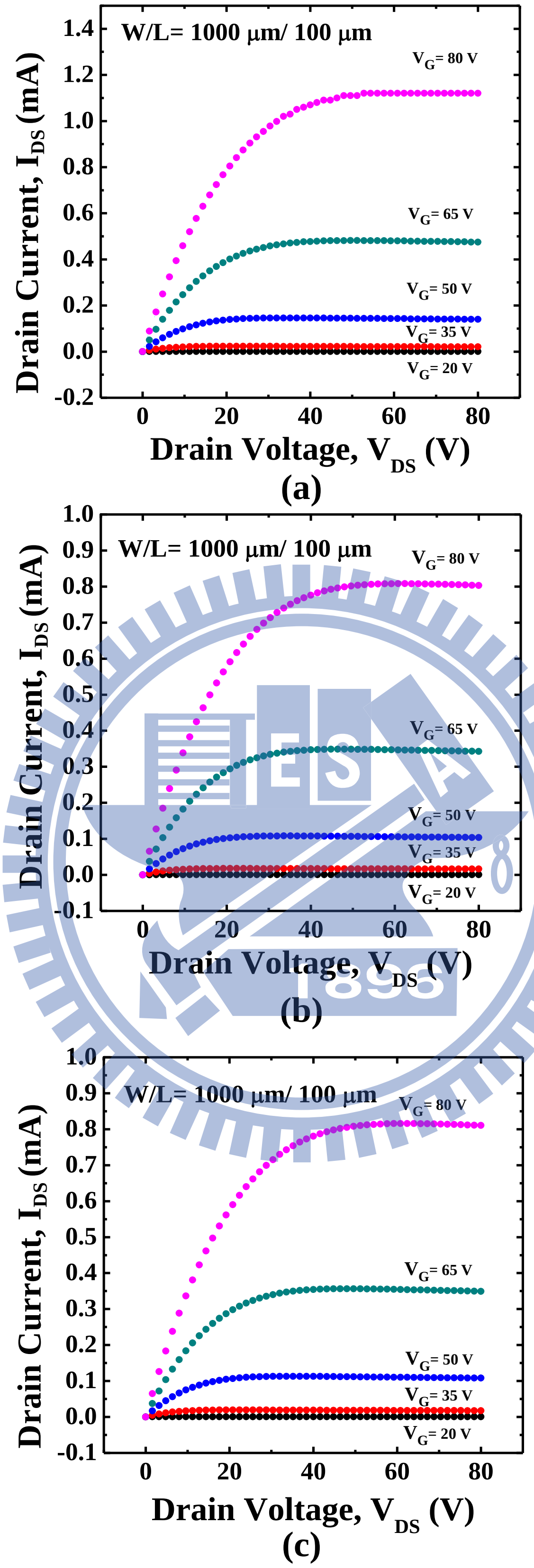

Fig. 4-9 Output characteristics (IDVD) of ZnO TFT with different channel thicknesses (a) 55nm (b) 110nm (c) 165nm.

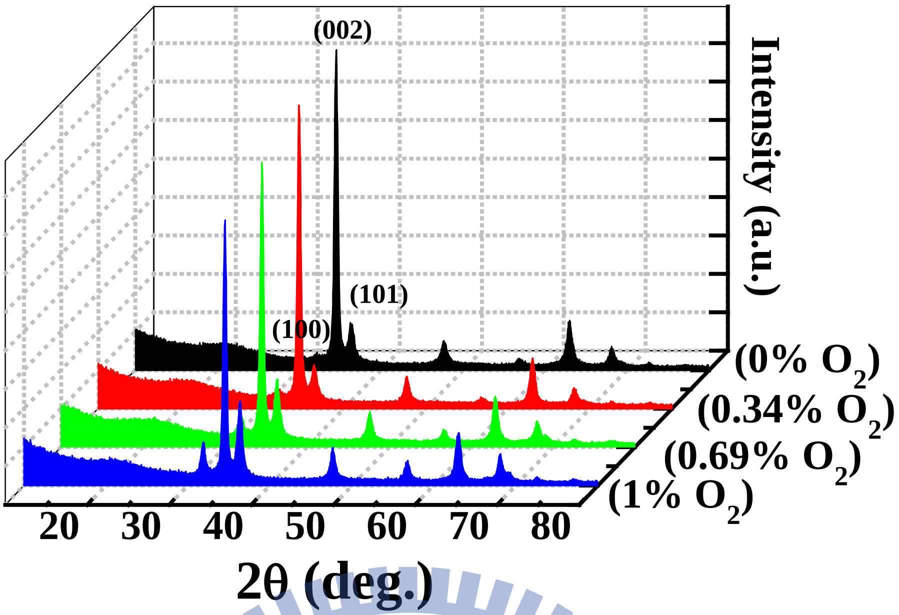

Fig. 4-10 GIXRD spectra of ZnO thin films with different oxygen ratios.

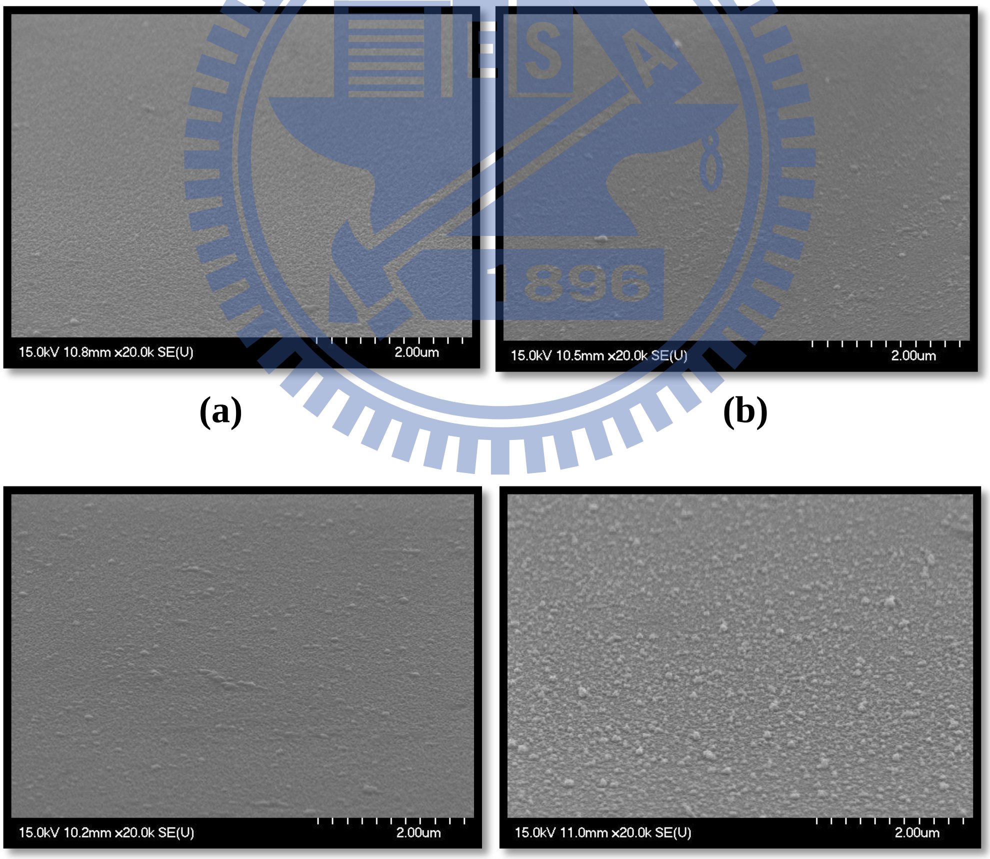

(a) **(b)**

(c) **(d)**

Fig. 4-11 SEM images (tilt angle) of ZnO thin films with different oxygen ratios (a) **(0% O_2)** (b) **(0.34% O_2)** (c) **(0.69% O_2)** (d) **(1% O_2)**.

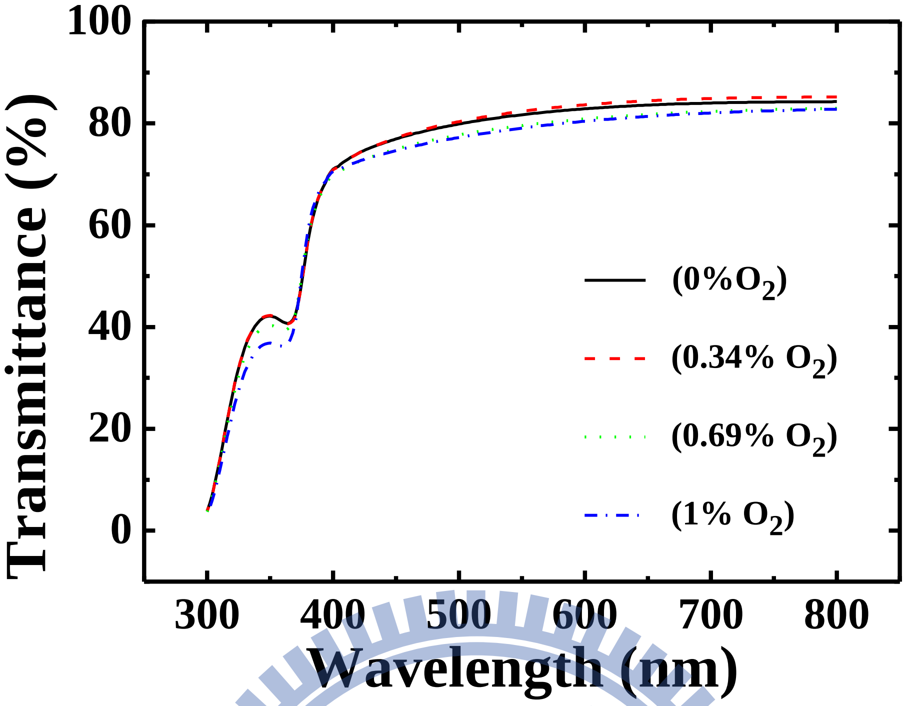

Fig. 4-12 Optical transmission spectra of ZnO thin film with different oxygen ratios deposited on glass.

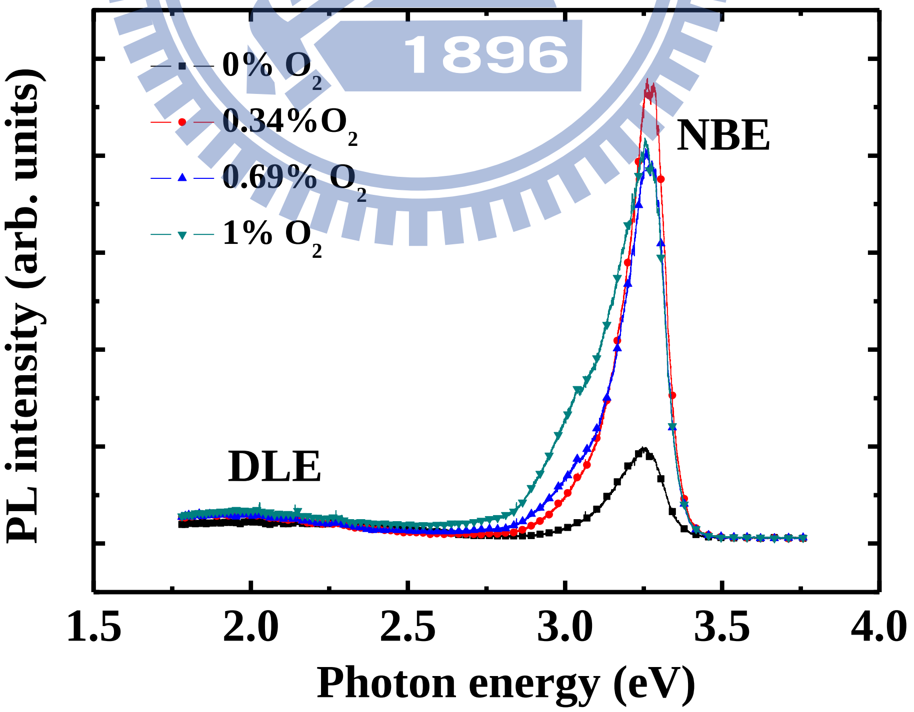

Fig. 4-13 PL spectra for ZnO thin films with different oxygen partial pressures.

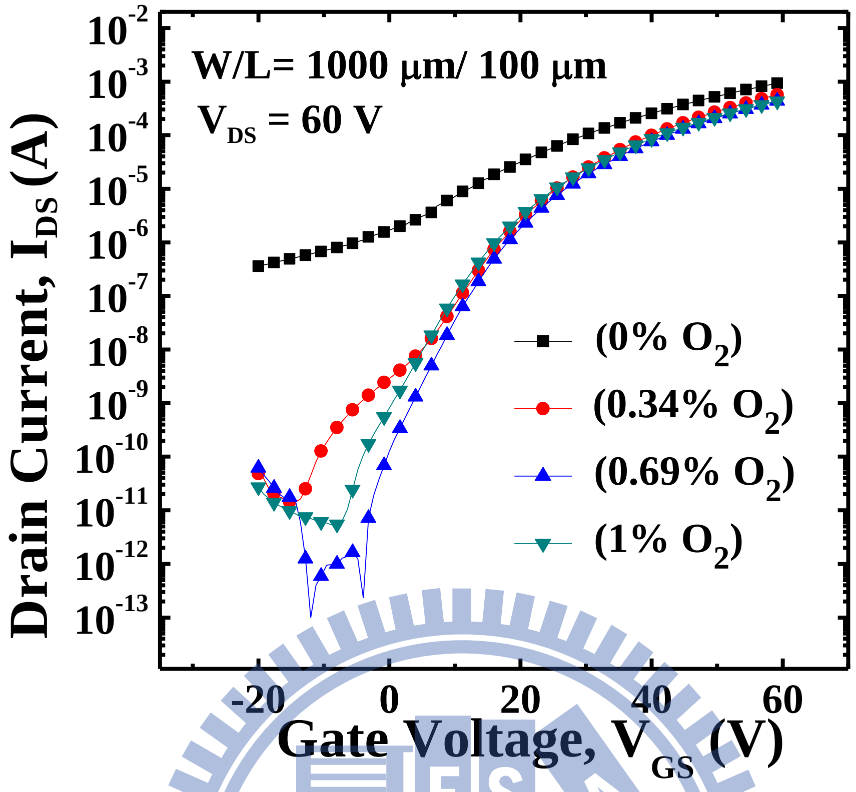

Fig. 4-14 Transfer characteristics of ZnO TFT with different oxygen ratios.

References

[4.1] T. Hirao, M. Furuta, H. Furuta, T. Matsuda, T. Hiramatsu, H. Hokari, M. Yoshida, H. Ishii, and M. Kakegawa, "Novel top-gate zinc oxide thin-film transistors (ZnO TFTs) for AMLCDs," *Journal of the Society for Information Display*, vol. 15, pp. 17-22, 2007.

[4.2] T. Hirao, M. Furuta, T. Hiramatsu, T. Matsuda, L. Chaoyang, H. Furuta, H. Hokari, M. Yoshida, H. Ishii, and M. Kakegawa, "Bottom-Gate Zinc Oxide Thin-Film Transistors (ZnO TFTs) for AM-LCDs," *Electron Devices, IEEE Transactions on*, vol. 55, pp. 3136-3142, 2008.

[4.3] R. Navamathavan, C. K. Choi, E.-J. Yang, J.-H. Lim, D.-K. Hwang, and S.-J. Park, "Fabrication and characterizations of ZnO thin film transistors prepared by using radio frequency magnetron sputtering," *Solid-State Electronics*, vol. 52, pp. 813-816, 2008.

[4.4] K. Song, J. Noh, T. Jun, Y. Jung, H.-Y. Kang, and J. Moon, "Fully Flexible Solution-Deposited ZnO Thin-Film Transistors," *Advanced Materials*, vol. 22, pp. 4308-4312.

[4.5] S.-H. K. Park, C.-S. Hwang, H. Y. Jeong, H. Y. Chu, and K. I. Cho, "Transparent ZnO-TFT Arrays Fabricated by Atomic Layer Deposition," *Electrochemical and Solid-State Letters*, vol. 11, pp. H10-H14, 2008.

[4.6] J. H. Chung, J. Y. Lee, H. S. Kim, N. W. Jang, and J. H. Kim, "Effect of thickness of ZnO active layer on ZnO-TFT's characteristics," *Thin Solid Films*, vol. 516, pp. 5597-5601, 2008.

[4.7] E. M. C. Fortunato, P. M. C. Barquinha, A. C. M. B. G. Pimentel, A. M. F. Goncalves, A. J. S. Marques, R. F. P. Martins, and L. M. N. Pereira, "Wide-bandgap high-mobility ZnO thin-film transistors produced at room temperature," *Applied Physics Letters*, vol. 85, pp. 2541-2543, 2004.

[4.8] B. J. Jin, H. S. Woo, S. Im, S. H. Bae, and S. Y. Lee, "Relationship between photoluminescence and electrical properties of ZnO thin films grown by pulsed laser deposition," *Applied Surface Science*, vol. 169-170, pp. 521-524, 2001.

Chapter 5

The Impacts of Thermal Annealing on the Properties of IGZO TFT Prepared by AP-PECVD

5.1 Introduction

Oxide-based semiconductors, such as ZnO [5.1]-[5.2], ZTO [5.3]-[5.4], IZO [5.5]-[5.6] and IGZO [5.7]-[5.9] have been reported for the active channel layer. These oxide semiconductors offer good electrical properties and high transparency. Among these semiconductors, IGZO TFTs have attracted much attention because of its superior performance compared with conventional Si-based TFTs [5.10]. The conduction band of IGZO is composed of metal s-orbitals and carrier transport is almost not affected by the chemical bond distortion. As a result, IGZO thin film shows a high mobility even in amorphous phase. Furthermore, several prototype displays using IGZO TFT have been demonstrated [5.11]. To deposit IGZO thin films, there are a variety of deposition methods, such as sputtering [6.7], pulse laser deposition [5.12], spin coating [5.13] and ink-jet printing [5.14]. Atmospheric-pressure plasma processing has high potential in several industrial applications due to low cost, high processing speed and simple system [5.15]. Atmospheric pressure plasma jet (APPJ) is an emerging technique for thin film coating. APPJ system is a non-vacuum and simple system.

The purpose of this work is to demonstrate the possibility to fabricate IGZO TFT by using atmospheric pressure plasma jet. We investigated the effect of annealing temperature on the properties of IGZO TFT. The electrical properties of IGZO TFT were improved effectively by post annealing and the devices exhibited good switching properties.

5.2 Experimental procedure

The high doping silicon wafer was used as gate electrode and thermally grown SiO_2 (130nm) on the silicon substrate was used as gate insulator. Indium nitrate ($In(NO_3)_2$), gallium nitrate ($Ga(NO_3)_2$) and zinc nitrate ($Zn(NO_3)_2$) dissolved in deionized water were used as the precursor. The concentration of IGZO solution was 0.2 M with an atomic ratio of In:Ga:Zn=1:1:1. Next, 40nm-thick IGZO thin films were deposited on SiO_2/Si by APPJ at 200^{o}C and then annealed from 200^{o}C to 500^{o}C in N_2 ambient for 30min. IGZO thin films were also deposited on the glass substrate. The pattern on IGZO thin film was obtained by conventional photolithography and wet etching using the $HCl:H_2O$ (1:200). Finally, 100nm thick Al source/drain (S/D) layers were patterned by lift-off technique. The channel width (W) and length (L) of IGZO TFT were 200 μm and 20 μm, respectively. A schematic cross view of the fabricated TFT is shown in Fig. 5-1.

5.3 Results and discussion

Figure 5-2 shows GIXRD spectra of IGZO thin film annealed from 200°C to 500°C in N_2 ambient for 30min. All the samples show a weak broad peak and no obvious sharp peak. The microstructure of 500°C sample using high resolution TEM reveals a low density nanoparticle about 5nm, as shown in Fig. 5-3. The low density and small size of these nanocrystals result in a weak broad peak and exhibit an amorphous-like phase. Figure 5-4 shows the top-view SEM images of IGZO thin films annealing at different temperatures. After the post annealing, the IGZO thin films exhibit a more smooth surface and dense structure. The dense structure could offer the better carrier transport path. Figure 5-5 shows the AFM images of IGZO thin films annealing at different temperatures. Table 5-1 shows the root-mean-square (RMS) roughness of IGZO thin films annealed at different temperatures. As shown in Table 5-1, the surface roughness is significantly different between as-deposited and annealed films. The as-deposited sample shows a roughness of 15.48nm. On the other hand, the surface roughness is reduced after the post annealing and 500°C sample shows a RMS of 6.67nm. The smooth surface also corresponds to the dense structure. Figure 5-6 shows the optical transmission spectra of IGZO. The 500°C sample exhibits a slightly lager transmittance than as-deposited sample. This can be attributed to reduction of the defects by thermal annealing. The average transmittance in the visible range is larger than 80%.

Figure 5-7 depicts transfer characteristics of IGZO TFTs annealing at different temperatures. The as-deposited sample shows poor switching properties, but after post annealing in higher than 300 ^{o}C, the devices show clear switching properties. The threshold voltage (V_T) shifting more positive after post annealing means that free electron carriers are reduced. The free carriers maybe result from oxygen vacancy or H-related species, and the carrier concentration was reduced effectively by post annealing. As a result, the switching behavior was improved. The IGZO TFTs operate in enhancement mode when the annealing temperature is high than 400^{o}C. After 500^{o}C post annealing, good electrical characteristics were achieved, including a V_T of 6.74V, a subthreshold swing (SS) of 1.54 V/dec, a mobility of 10.31 cm^2/V-s and a large I_{on}/I_{off} ratio of 3.28×10^8. Table II summarizes the electrical properties of IGZO TFT annealed at different temperatures. Annealing at high temperature showing a higher mobility indicates the IGZO thin film quality was improved, and intrinsic defects were be repaired. The interface properties between gate insulator and IGZO were also improved, since the subthreshold swing also was reduced by post annealing. Figures 5-8(a) and 5-8(b) show the output characteristics of IGZO TFT. As-deposited sample shows a depletion mode property and the current increases with drain voltage. It indicates that the bulk have external current path due to high carrier concentration.

As a result, saturation region is not obvious. After post annealing at 500^{o}C, the IGZO TFT exhibits excellent linear/saturation behavior and shows an enhancement mode property.

5.4 Conclusion

In summary, IGZO TFTs were successfully fabricated by APPJ system. After post annealing in higher than 300^{o}C the devices show clear switching properties. The defects can be repaired effectively by post annealing. IGZO thin film annealed at 500^{o}C shows an amorphous-like phase and the average transmittance is more than 80% in the visible range. IGZO TFT annealed at 500^{o}C shows excellent electrical characteristics including a V_T of 6.74 V, a subthreshold swing of 1.54V/dec, a high mobility of 10.31cm^2/V-s and a large I_{on}/I_{off} ratio of 3.28×10^8.

Table 5-1 The electrical properties of IGZO TFT annealed at different temperatures.

Annealing	**As-deposited**	**200^{o}C**	**300^{o}C**	**400^{o}C**	**500^{o}C**
V_T	**-**	**-**	**-0.571**	**0.938**	**6.74**
SS (V/dec.)	**-**	**-**	**1.6**	**1.69**	**1.54**
Mobility (cm^2/V-s)	**0.27**	**0.75**	**2.6**	**3.43**	**10.31**
I_{on}/I_{off} ratio	**8.99×10^1**	**9.53×10^3**	**1.88×10^8**	**7.63×10^7**	**3.28×10^8**

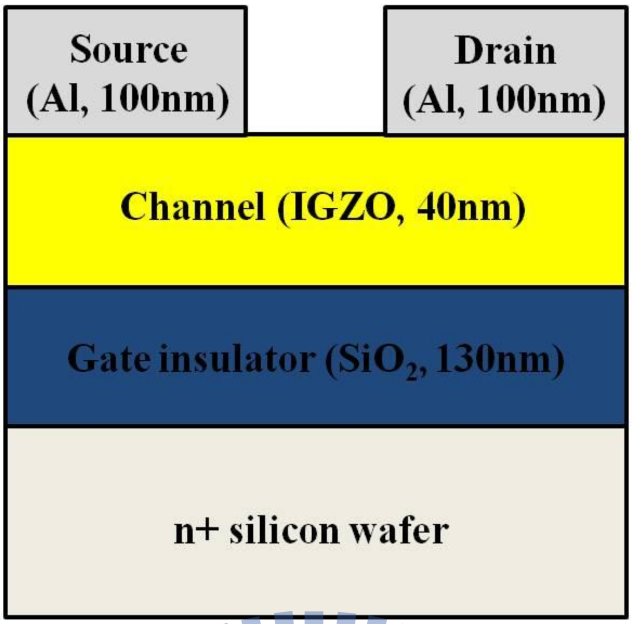

Fig. 5-1 Schematic structure of the bottom-gate TFT test structure.

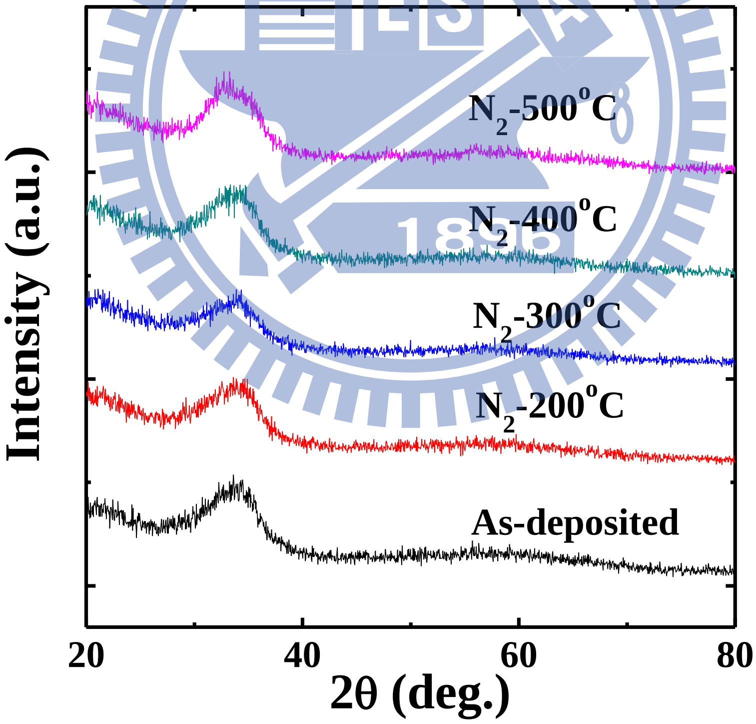

Fig. 5-2 GIXRD spectra of IGZO thin film annealed from 200°C to 500°C in N_2 ambient for 30min.

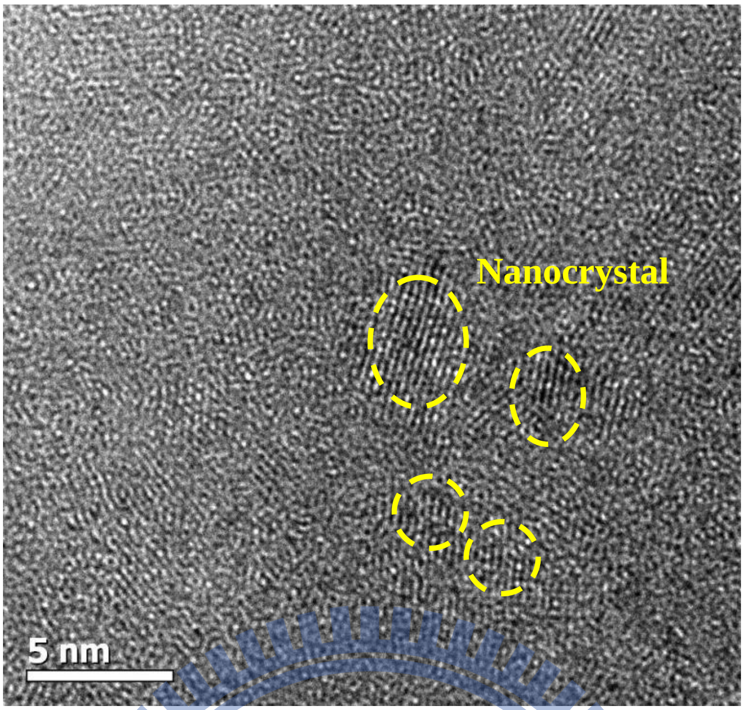

Fig. 5-3 High-resolution TEM cross-section image of IGZO thin film annealed at 500 ^{o}C for 30min.

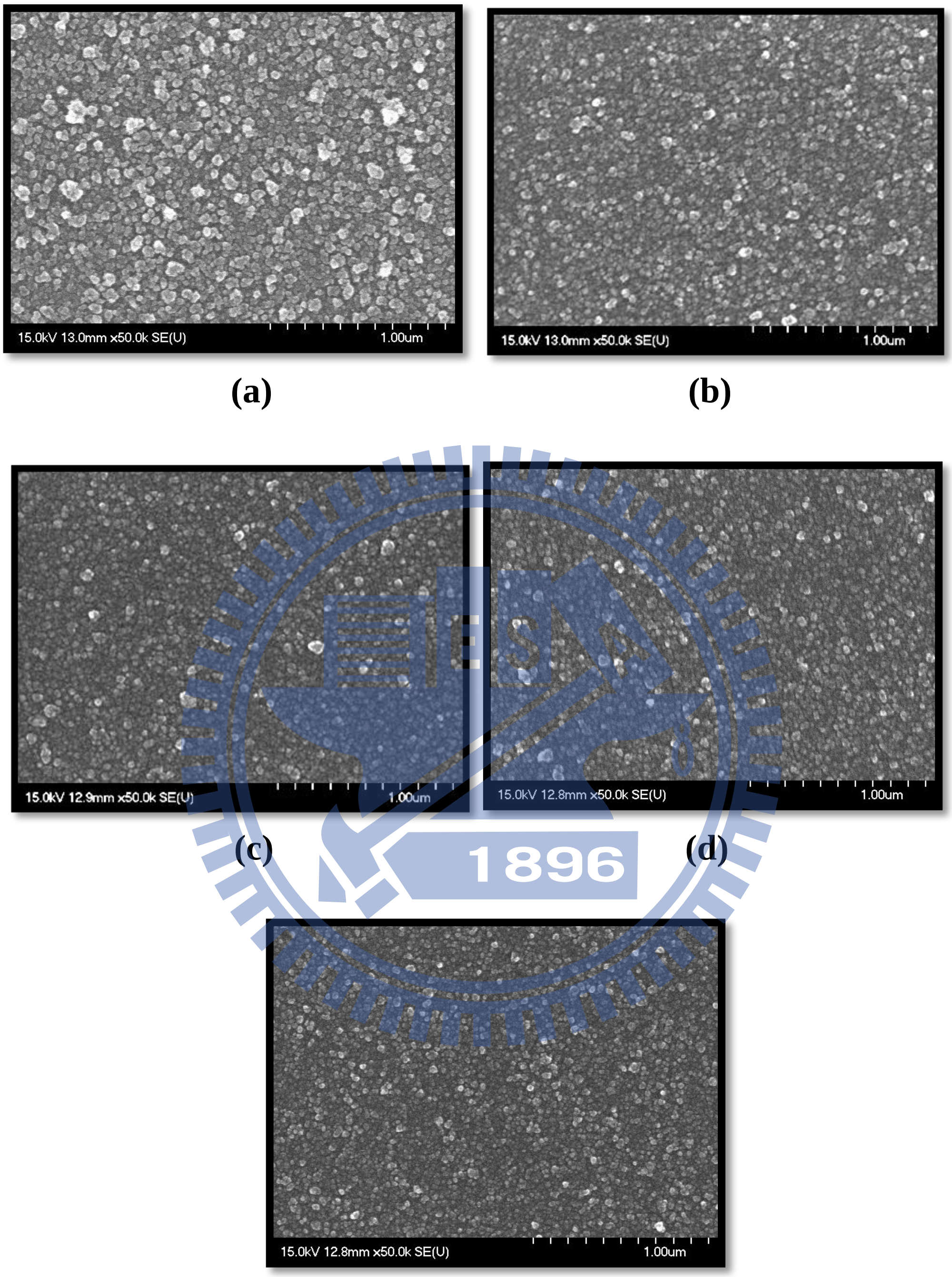

(a) **(b)**

(c) **(d)**

(e)

Fig. 5-4 Top-view SEM images of IGZO thin films (a) as-deposited (b) 200°C (c) 300°C (d) 400°C (e) 500°C.

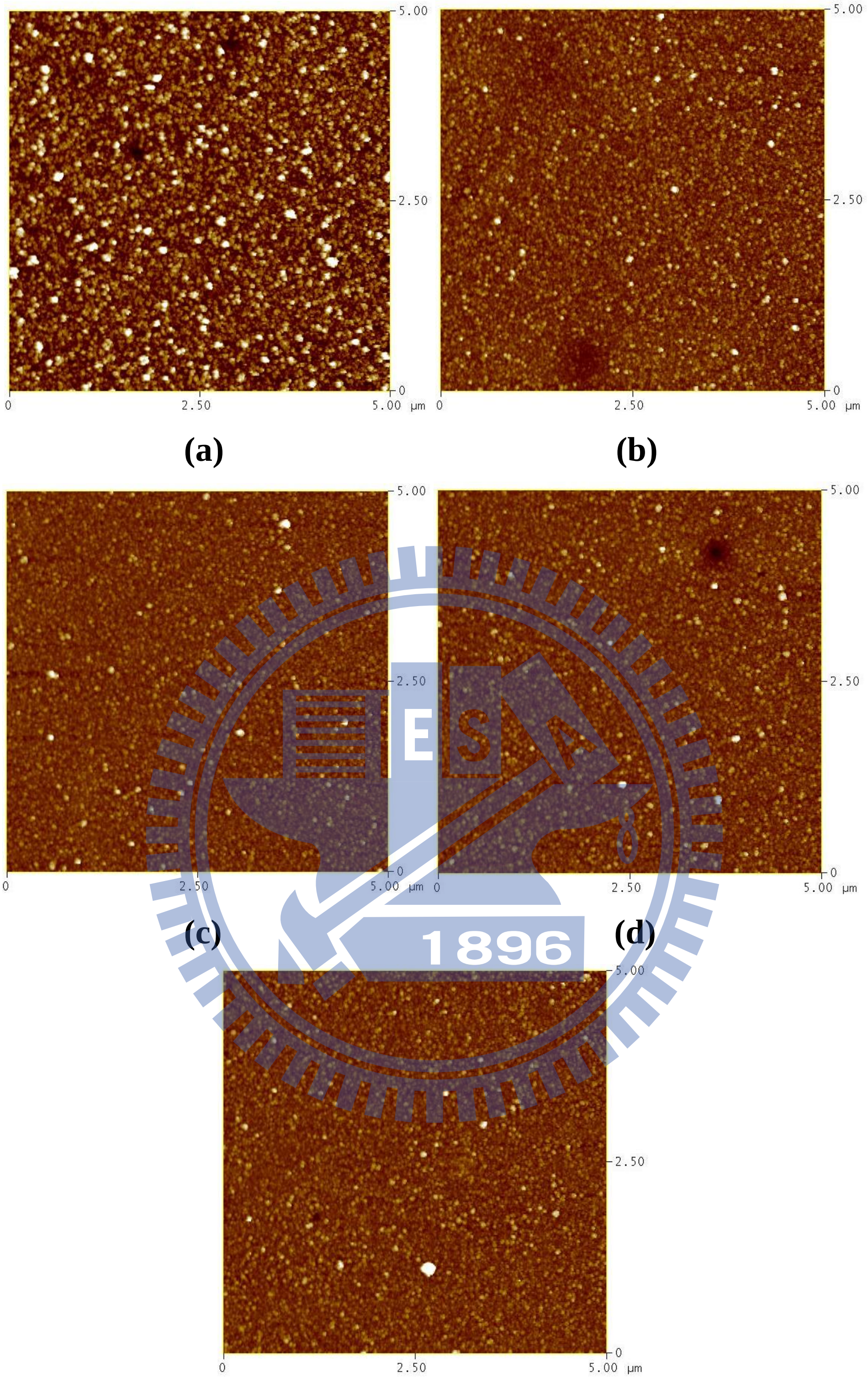

(a)

(b)

(c)

(d)

(e)

Fig. 5-5 AFM images of IGZO thin films (a) as-deposited (Rms=15.48nm) (b) 200°C (Rms=8.37nm) (c) 300°C (Rms=6.18nm) (d) 400°C (Rms=6.74nm) (e) 500°C (Rms=6.67nm).

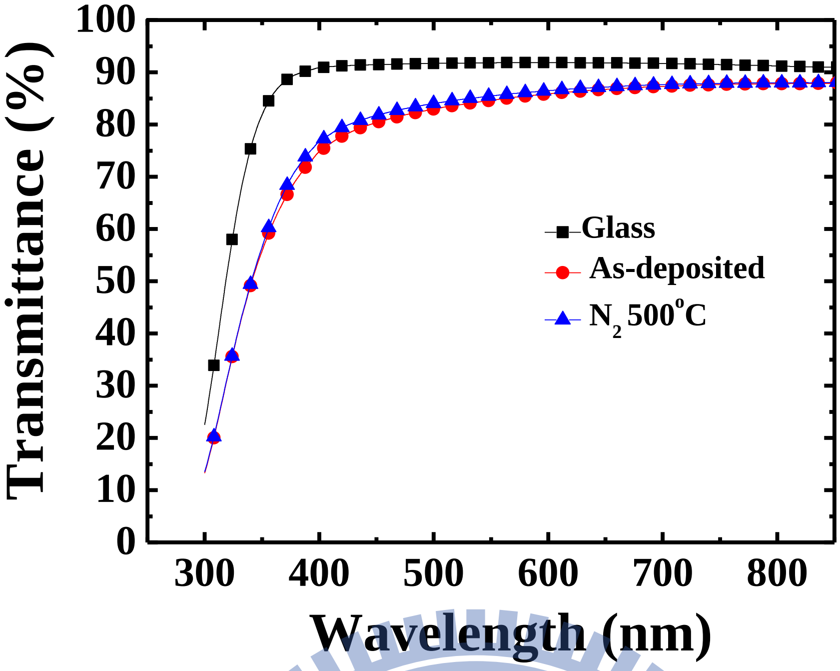

Fig. 5-6 Optical transmission spectra of IGZO thin film deposited on glass.

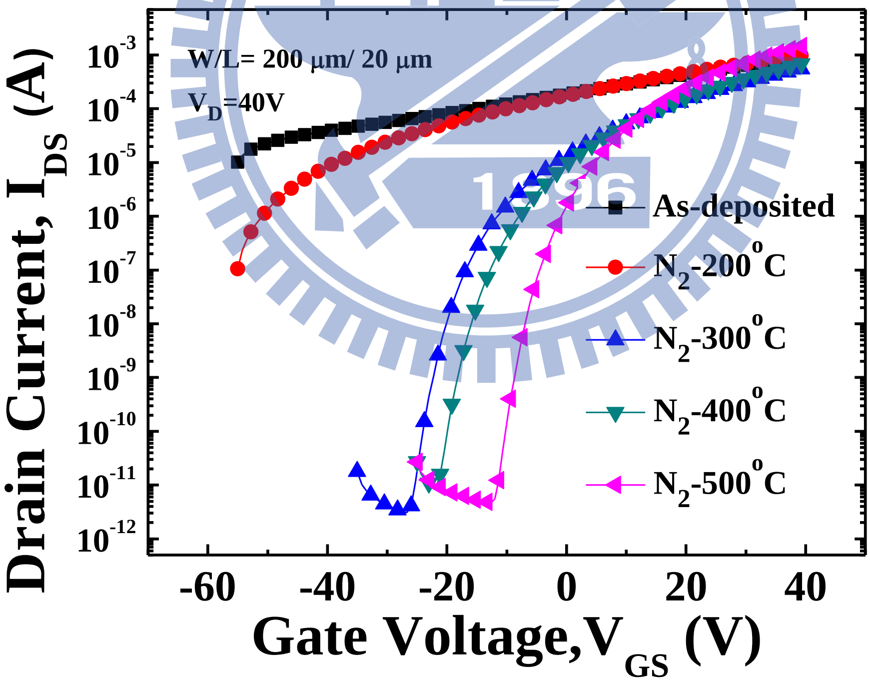

Fig. 5-7 Transfer characteristics of IGZO TFTs annealing at various temperatures.

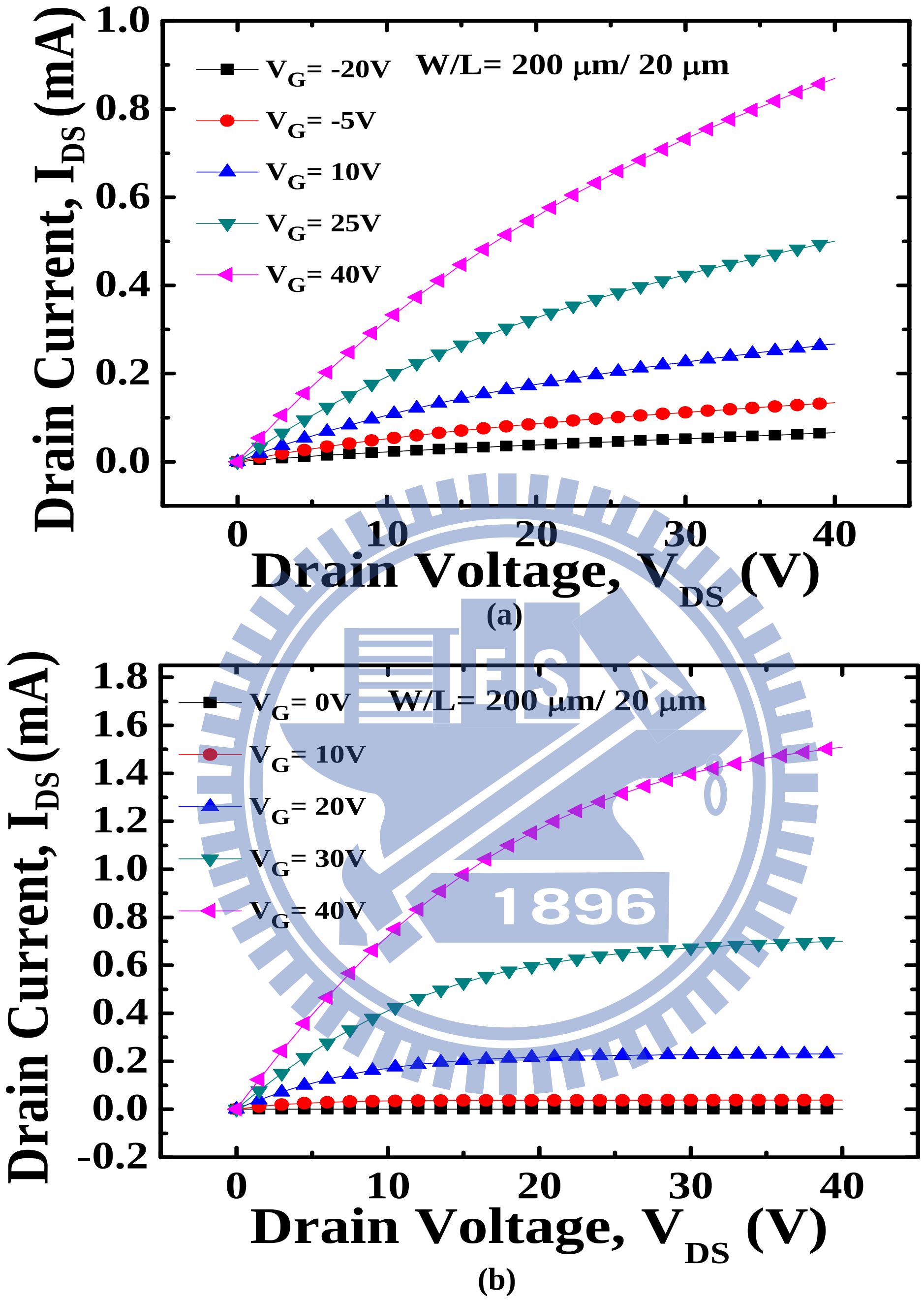

Fig. 5-8 Output characteristics of IGZO TFT (a) as-deposited (b) 500^{o}C.

References

[5.1] G. Adamopoulos, A. Bashir, P. H. Wobkenberg, D. D. C. Bradley, and T. D. Anthopoulos, "Electronic properties of ZnO field-effect transistors fabricated by spray pyrolysis in ambient air," *Applied Physics Letters,* vol. 95, pp. 133507-3, 2009.

[5.2] H.-C. Cheng, C.-F. Chen, and C.-Y. Tsay, "Transparent ZnO thin film transistor fabricated by sol-gel and chemical bath deposition combination method," *Applied Physics Letters,* vol. 90, pp. 012113-3, 2007.

[5.3] C. Avis and J. Jang, "A High Performance Inkjet Printed Zinc Tin Oxide Transparent Thin-Film Transistor Manufactured at the Maximum Process Temperature of 300[degree]C and Its Stability Test," *Electrochemical and Solid-State Letters,* vol. 14, pp. J9-J11.

[5.4] S. K. Park, Y.-H. Kim, H.-S. Kim, and J.-I. Han, "High Performance Solution-Processed and Lithographically Patterned Zinc--Tin Oxide Thin-Film Transistors with Good Operational Stability," *Electrochemical and Solid-State Letters,* vol. 12, pp. H256-H258, 2009.

[5.5] Y.-L. Wang, F. Ren, W. Lim, D. P. Norton, S. J. Pearton, I. I. Kravchenko, and J. M. Zavada, "Room temperature deposited indium zinc oxide thin film transistors," *Applied Physics Letters,* vol. 90, p. 232103, 2007.

[5.6] C. Chang-Ken, H. Hsing-Hung, S. Jing-Jong, and W. Chung-Chih, "The Influence of Channel Compositions on the Electrical Properties of Solution-Processed Indium-Zinc Oxide Thin-Film Transistors," *Display Technology, Journal of,* vol. 5, pp. 509-514, 2009.

[5.7] L. Jae Sang, C. Seongpil, K. Sang-Mo, and L. Sang Yeol, "High-Performance a-IGZO TFT With ZrO2 Gate Dielectric Fabricated at Room Temperature," *Electron Device Letters, IEEE,* vol. 31, pp. 225-227, 2010.

[5.8] C. J. Chiu, S. P. Chang, and S. J. Chang, "High-Performance a-IGZO Thin-Film Transistor Using Ta2O5 Gate Dielectric," *Electron Device Letters, IEEE,* vol. 31, pp. 1245-1247, 2010.

[5.9] L. Linfeng and P. Junbiao, "High-Performance Indium-Gallium-Zinc Oxide Thin-Film Transistors Based on Anodic Aluminum Oxide," *Electron Devices, IEEE Transactions on,* vol. 58, pp. 1452-1455, 2011.

[5.10] K. Nomura, H. Ohta, A. Takagi, T. Kamiya, M. Hirano, and H. Hosono, "Room-temperature fabrication of transparent flexible thin-film transistors using amorphous oxide semiconductors," *Nature,* vol. 432, pp. 488-492, 2004.

[5.11] T. Kamiya, K. Nomura, and H. Hosono, "Present status of amorphous In-Ga-Zn-O thin-film transistors," *Science and Technology of Advanced Materials,* vol. 11, p. 044305, 2010

[5.12] A. Suresh, P. Wellenius, A. Dhawan, and J. Muth, "Room temperature pulsed laser deposited indium gallium zinc oxide channel based transparent thin film transistors," *Applied Physics Letters*, vol. 90, pp. 123512-3, 2007.

[5.13] P. K. Nayak, T. Busani, E. Elamurugu, P. Barquinha, R. Martins, Y. Hong, and E. Fortunato, "Zinc concentration dependence study of solution processed amorphous indium gallium zinc oxide thin film transistors using high-k dielectric," *Applied Physics Letters*, vol. 97, p. 183504.

[5.14] W. Ye, S. Xiao Wei, G. K. L. Goh, H. V. Demir, and Y. Hong Yu, "Influence of Channel Layer Thickness on the Electrical Performances of Inkjet-Printed In-Ga-Zn Oxide Thin-Film Transistors," *Electron Devices, IEEE Transactions on*, vol. 58, pp. 480-485, 2011.

[5.15] K. M. Chang, S. H. Huang, C. J. Wu, W. L. Lin, W. C. Chen, C. W. Chi, J. W. Lin, and C. C. Chang, "Transparent conductive indium-doped zinc oxide films prepared by atmospheric pressure plasma jet," *Thin Solid Films*, vol. 519, pp. 5114-5117, 2011.

Chapter 6

Characterizations of IGZO TFT Prepared by AP-PECVD Using PE-ALD Al_2O_3 Gate Dielectric

6.1 Introduction

Recently, indium-gallium-zinc oxide (IGZO) was widely studied for active-channel material, and exhibited high potential in AMOLED and AMLCD applications [6.1]-[6.2]. The superior properties of IGZO thin films include wide bandgap, high transparency, and high mobility, even in the amorphous phase [6.3]. To prepare IGZO thin films, various deposition methods were developed, including RF/DC magnetron sputtering [6.4], pulsed laser deposition (PLD) [6.5], and solution process [6.6]-[6.7]. Most active-channel layers are fabricated using conventional vacuum techniques because vacuum-processed devices exhibit excellent performance and reliability. However, a non-vacuum process offers competitive advantages, such as low cost, high throughput, and excellent suitability for large-area applications. Atmospheric pressure plasma jet (APPJ) is a recent technology in plasma processing applications [6.8]-[6.9] and is used in several industrial applications, such as surface modification, etching, cleaning, and thin-film coating [6.10]. Considerable progress has been achieved in atmospheric pressure plasma technology for thin-film coating, and several thin-film coatings were demonstrated, including SiO_2 [6.10], ZnO [6.11], and IZO [6.12]. The main benefit of APPJ is the high potential for in-line production without an expensive and complex vacuum system. To our knowledge, this is the first report of IGZO TFT achieved using APPJ. Furthermore, the high-k Al_2O_3 is a promising gate dielectric because of its low leakage current and excellent compatibility with the IGZO thin film [6.13]. The plasma-enhanced ALD (PE-ALD) method was assumed to increase reactivity, reduce impurities, widen the process window, and increase the film density compared with conventional ALD [6.14]. In this study, an environmentally friendly water-based solution precursor was used to deposit the IGZO active layer, and we achieved superior performance of IGZO TFT compared with other non-vacuum process.

6.2 Experimental procedure

Trimethylaluminum (TMA) was used as the precursors, and oxygen plasma reactants were used as the oxidants. The inductively coupled plasma (ICP) source with an operating power of 300 W was used, and the substrate temperature was maintained at 250 ^{o}C during the deposition process. First, the PE-ALD 30-nm-thick Al_2O_3 gate dielectric was directly deposited on heavily doped n-type Si wafers, which served as the gate electrode. Indium nitrate ($In(NO_3)_2$), gallium nitrate ($Ga(NO_3)_2$) and zinc nitrate ($Zn(NO_3)_2$) were used as the precursor, and pure deionized water was used as a solvent. The concentration of the IGZO solution was 0.2 M with an atomic ratio of In:Ga:Zn=1:1:1. Subsequently, the 40-nm-thick IGZO thin films were deposited on the Al_2O_3/n+ Si at a substrate temperature of 200 ℃ by APPJ. In the chapter 5, the optimized condition of post thermal annealing was 500°C. As a result, the as-deposited IGZO films were placed into a furnace and subsequently thermally annealed for 30 min at 500 ℃ in nitrogen ambient to improve the quality of IGZO film. The pattern on IGZO thin film was obtained by conventional photolithography and wet etching by using the HCl:H_2O (1:200). Finally, 100-nm-thick Al source/drain (S/D) layers were patterned by lift-off technique. The channel width (W) and length (L) were 200 μm and 20 μm, respectively. The Al/Al_2O_3/n^+ Si capacitors were also fabricated to analyze the dielectric properties.

6.3 Results and discussion

A schematic cross-view of the bottom-gate/top-contact IGZO TFT is shown in Fig. 6-1. Fig. 6-2 shows the optical transmission spectra of IGZO films deposited on glass. The average transmittance in the visible region is higher than 85%. The optical band gap was estimated by extrapolating the square of absorption coefficient versus the photon energy curve [6.15]. The optical band gap of 3.39 eV indicates that the IGZO thin film is transparent in visible light. The inset graph shows the GIXRD pattern and demonstrates a weak broad (008) peak [6.16], indicating the formation of an amorphous-like phase. High-resolution TEM cross-section image of IGZO/Al_2O_3/n^+ Si is shown in Fig.6-3. Fig 6-3(a) shows 35.87 nm-thick of IGZO as well as 30.48 nm-thick Al_2O_3 thin films, and an interfacial layer is observed between Al_2O_3/n+ Si.

A 1.67nm-thick interfacial layer is shown in Fig. 6-3(b). Fig. 6-3(c) presents low density nanocrystals about 5nm in IGZO thin film. The low density nanocrystals exhibit a broaden peak in GIXRD pattern and show an amorphous-like phase of IGZO thin film. The C-V and J-V characteristics of the Al/Al_2O_3/n+ gate capacitor are shown in Fig. 6-4. The measured capacitance density of 2.15 fF/μm^2 produced a capacitance equivalent thickness (CET) of 16 nm and a high k value of 7.29. The PE-ALD gate dielectric exhibits a low C-V hysteresis of 8 mV and a low leakage current of 1.62×10^{-8} A/cm^2 at 1 MV/cm. Fig. 6-5 shows the transfer characteristics (ID-VG) of the PE-ALD Al_2O_3/IGZO TFT. The field effect mobility (μ_{FE}) and threshold voltage (VT) were extracted from $I_{DS1/2}$ versus V_{GS} Plot. This device exhibited a low SS of 276 mV/dec, a V_T of 0.71 V, an excellent μ_{FE} of 8.39 cm^2/V-s, and an I_{on}/I_{off} as high as 1×10^8. A low V_T and low SS were attributed to the high capacitor density and are suitable for low-voltage operations. Fig. 6-6 shows the output characteristics (IDVD) of IGZO TFT. The IGZO TFT operates in enhancement mode and exhibits excellent linear/saturation behavior. We compared important device parameters of IGZO TFT deposited by non-vacuum process, as shown in Table 6-1. The performance of our IGZO TFT is comparable with that of other devices. Our device exhibited excellent performance compared with the solution-process and may obtain a high quality IGZO thin film deposited by APPJ.

6.4 Conclusion

In summary, we demonstrated IGZO thin films prepared by non-vacuum APPJ and characterized the IGZO TFT by using the PE-ALD Al_2O_3 as the gate dielectric. The IGZO thin films exhibited a high transmittance with a nanocrystalline phase. The PE-ALD Al_2O_3/IGZO TFT demonstrated excellent electrical characteristics, including a low V_T of 0.71 V, small subthreshold swing of 276 mV/dec, a mobility of 8.39 cm^2/V-s, and a large I_{on}/I_{off} ratio of 1×10^8. This device is suitable for low cost and low-operation voltage applications.

Table 6-1 Comparison of IGZO TFTs deposited by non-vacuum process.

Fabrication method	Post treatment	V_T (V)	Mobility ($cm^2/V\text{-}s$)	SS (V/dec.)	I_{on}/I_{off} ratio
APPJ This Work	500 °C for 30min	0.71	8.39	0.276	1×10^8
Spin coating [6.17]	laser annealing	-	7.65	-	$2.88X10^7$
Spin coating [6.7]	500 °C for 1h	2	2	1.5	$>10^7$
Ink-jet printing [6.18]	500 °C for 1 h	1	1.41	0.38	4.3×10^7
Spin coating [6.6]	95 °C for 10min	0.9	2.3	-	$>10^6$

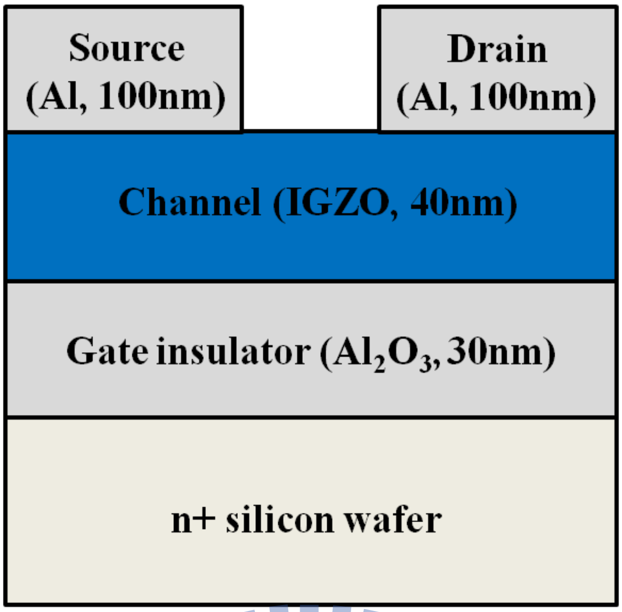

Fig. 6-1 A schematic cross view of the bottom-gate/top-contact IGZO TFT.

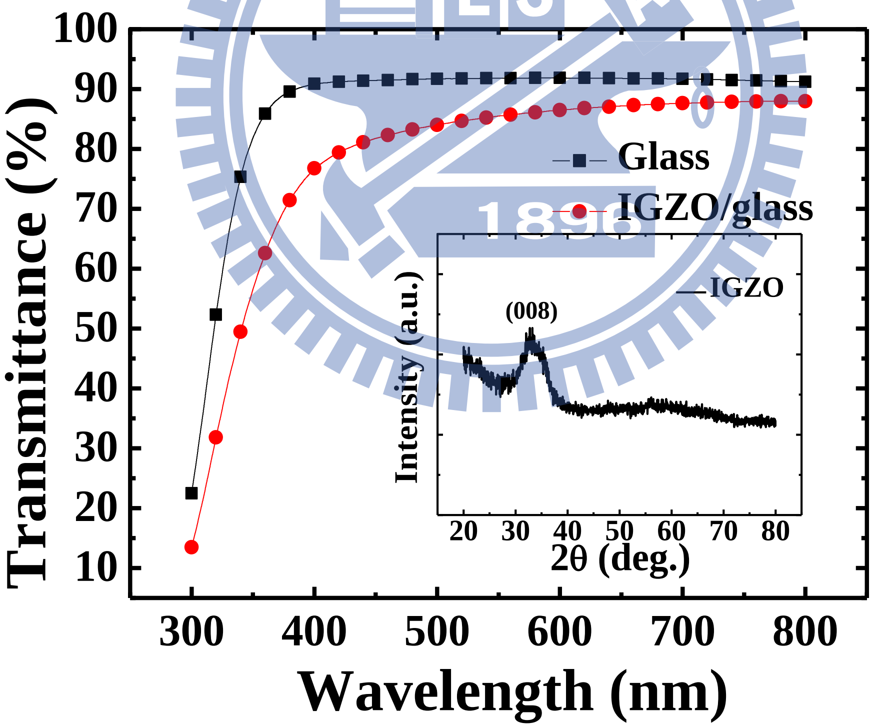

Fig. 6-2 Optical transmission spectra and GIXRD patterns of IGZO films.

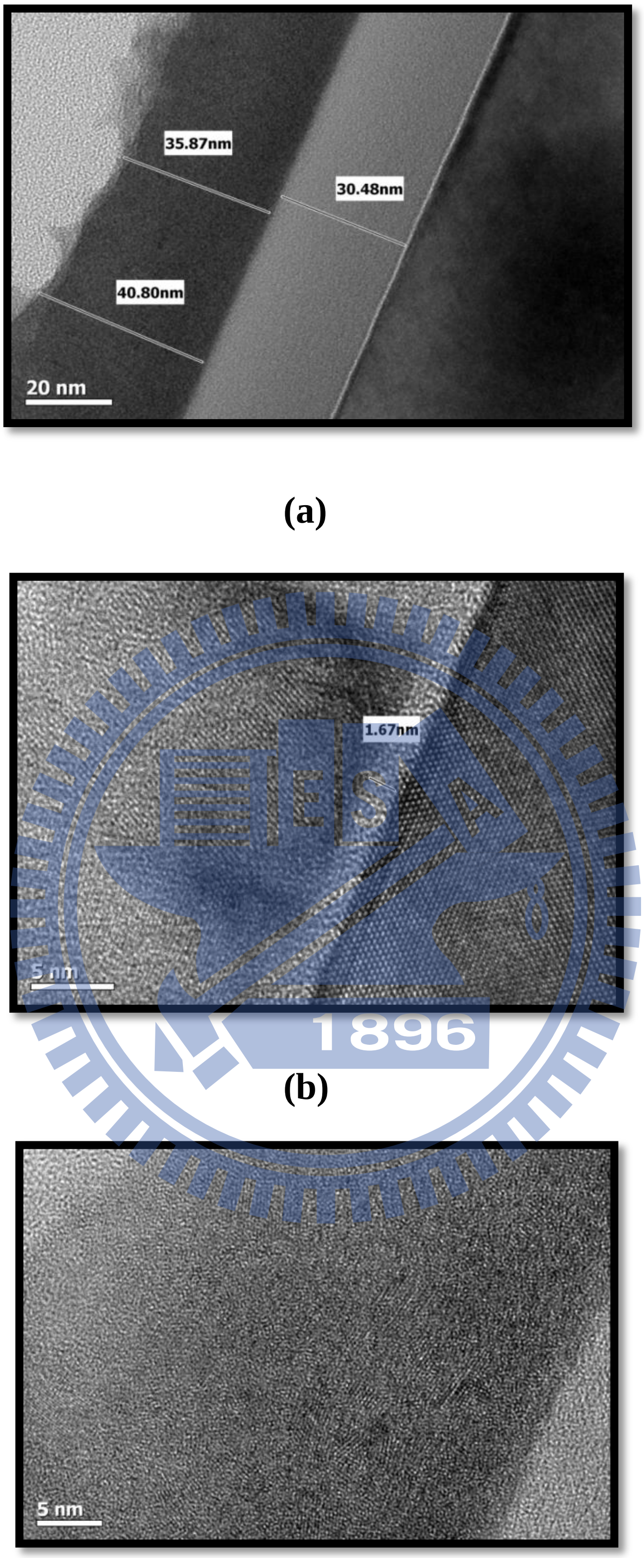

Fig. 6-3 High-resolution TEM cross-section image (a) IGZO/Al_2O_3/n+ Si (b) Al_2O_3/n+ Si (c) IGZO.

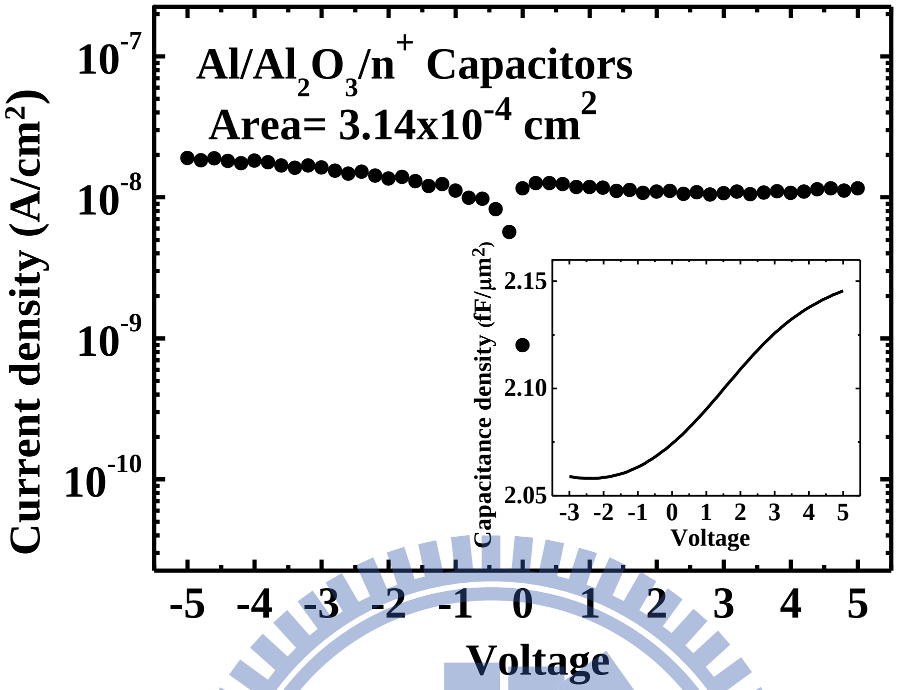

Fig. 6-4 J-V and C-V(inset graph) characteristics of the $Al/Al_2O_3/n+$ capacitors.

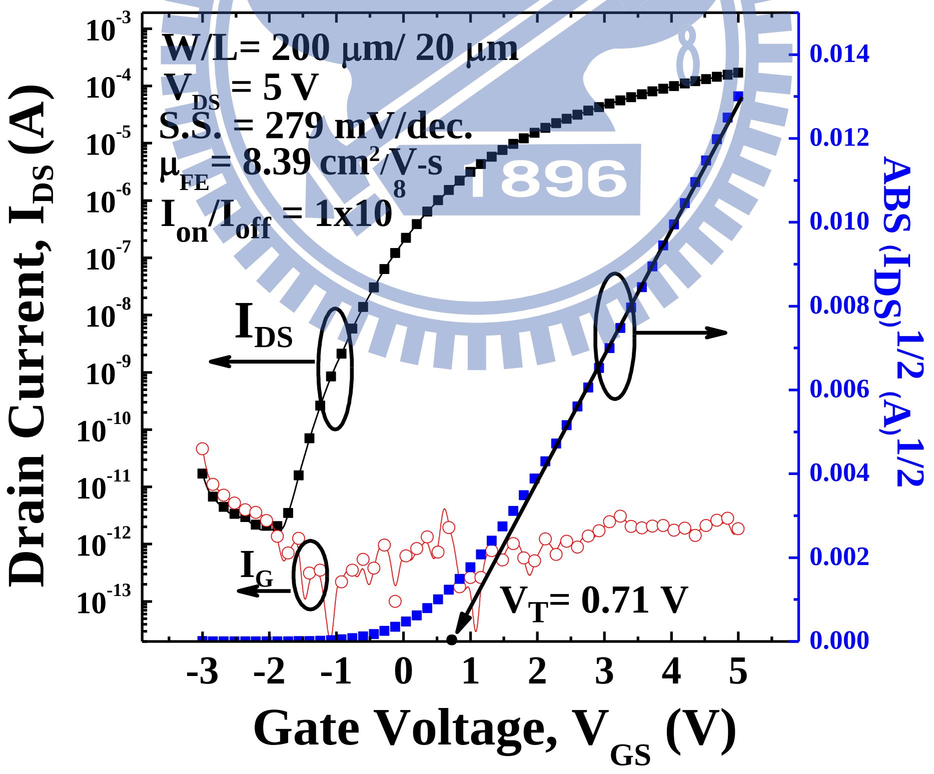

Fig. 6-5 Transfer characteristics (ID-VG) of the IGZO TFT with PE-ALD Al_2O_3 gate dielectric.

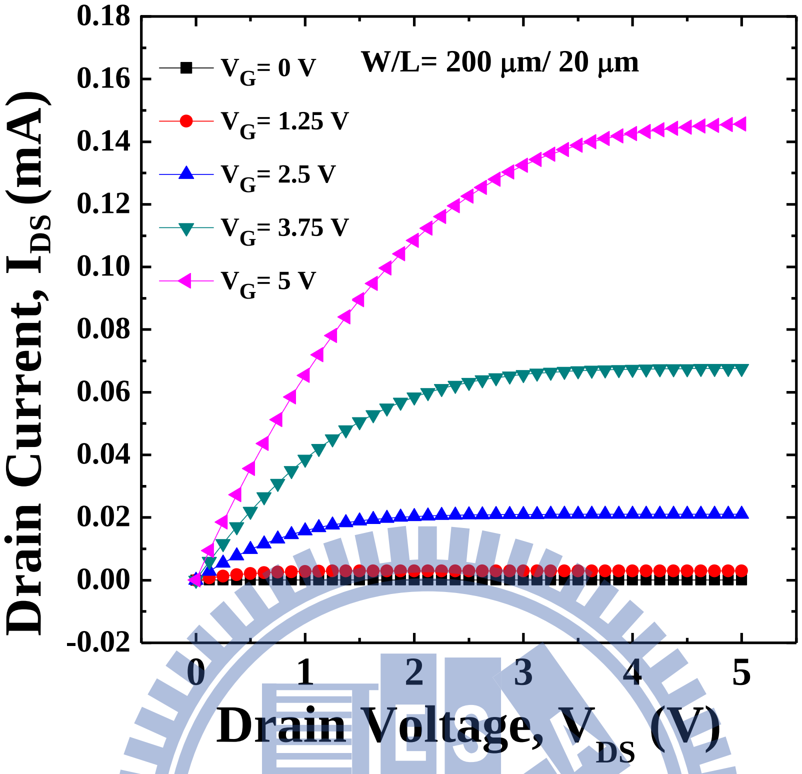

Fig. 6-6 Output characteristics (IDVD) of the IGZO TFT with PE-ALD Al_2O_3 gate dielectric.

References

[6.1] K. Jang Yeon, S. Kyoung Seok, J. Ji Sim, K. Tae Sang, R. Myung Kwan, P. Kyung Bae, Y. Byung Wook, K. Jung Woo, L. Young Gu, P. Kee Chan, L. Sang Yoon, and K. Jong Min, "Bottom-Gate Gallium Indium Zinc Oxide Thin-Film Transistor Array for High-Resolution AMOLED Display," *Electron Device Letters, IEEE,* vol. 29, pp. 1309-1311, 2008.

[6.2] J.-H. Lee, D.-H. Kim, D.-H. Yang, S.-H. Hong, K.-H. Yoon, P.-H. Hong, C.-O. Jeong, H.-S. Park, S. Y. Kim, S. K. Lim, S. S. Kim, K.-S. Son, T.-S. Kim, J.-Y. Kwon, and S.-Y. Lee, "42.2: World's Largest (15-inch) XGA AMLCD Panel Using IGZO Oxide TFT," *SID Symposium Digest of Technical Papers,* vol. 39, pp. 625-628, 2008.

[6.3] K. Nomura, H. Ohta, A. Takagi, T. Kamiya, M. Hirano, and H. Hosono, "Room-temperature fabrication of transparent flexible thin-film transistors using amorphous oxide semiconductors," *Nature,* vol. 432, pp. 488-492, 2004.

[6.4] L. Jae Sang, C. Seongpil, K. Sang-Mo, and L. Sang Yeol, "High-Performance a-IGZO TFT With ZrO_2 Gate Dielectric Fabricated at Room Temperature," *Electron Device Letters, IEEE,* vol. 31, pp. 225-227, 2010.

[6.5] A. Suresh, P. Wellenius, A. Dhawan, and J. Muth, "Room temperature pulsed laser deposited indium gallium zinc oxide channel based transparent thin film transistors," *Applied Physics Letters,* vol. 90, pp. 123512-123512-3, 2007.

[6.6] Y. Ya-Hui, S. S. Yang, K. Chen-Yen, and C. Kan-San, "Chemical and Electrical Properties of Low-Temperature Solution-Processed In-Ga-Zn-O Thin-Film Transistors," *Electron Device Letters, IEEE,* vol. 31, pp. 329-331, 2010.

[6.7] K. Yong-Hoon, H. Min-Koo, H. Jeong-In, and P. Sung Kyu, "Effect of Metallic Composition on Electrical Properties of Solution-Processed Indium-Gallium-Zinc-Oxide Thin-Film Transistors," *Electron Devices, IEEE Transactions on,* vol. 57, pp. 1009-1014, 2010.

[6.8] A. Schutze, J. Y. Jeong, S. E. Babayan, P. Jaeyoung, G. S. Selwyn, and R. F. Hicks, "The atmospheric-pressure plasma jet: a review and comparison to other plasma sources," *Plasma Science, IEEE Transactions on,* vol. 26, pp. 1685-1694, 1998.

[6.9] L. Mounir and A. Tamer, "Arc-Free Atmospheric Pressure Cold Plasma Jets: A Review," *Plasma Processes and Polymers,* 2007.

[6.10] M. H. Han, J. H. Noh, T. I. Lee, J. H. Choi, K. W. Park, H. S. Hwang, K. M. Song, and H. K. Baik, "High-Rate SiO_2 Deposition by Oxygen Cold Arc

Plasma Jet at Atmospheric Pressure," *Plasma Processes and Polymers*, vol. 5, pp. 861-866, 2008.

[6.11] K. Maruyama, I. Tsumagari, M. Kanezawa, Y. Gunji, M. Morita, M. Kogoma, and S. Okazaki, "Preparation of ZnO films from Zn2+ aqueous mist using atmospheric pressure glow plasma," *Journal of Materials Science Letters*, vol. 20, pp. 481-484, 28 February 2001 2001.

[6.12] K. M. Chang, S. H. Huang, C. J. Wu, W. L. Lin, W. C. Chen, C. W. Chi, J. W. Lin, and C. C. Chang, "Transparent conductive indium-doped zinc oxide films prepared by atmospheric pressure plasma jet," *Thin Solid Films*, vol. 519, pp. 5114-5117, 2011.

[6.13] L. Linfeng and P. Junbiao, "High-Performance Indium-Gallium-Zinc Oxide Thin-Film Transistors Based on Anodic Aluminum Oxide," *Electron Devices, IEEE Transactions on*, vol. 58, pp. 1452-1455.

[6.14] Y. Kim, "Characteristics of ZrO2 gate dielectric deposited using Zr t-butoxide and Zr(NEt2)4 precursors by plasma enhanced atomic layer deposition method," *Journal of Applied Physics*, vol. 92, p. 5443, 2002.

[6.15] G. A. Hirata, J. McKittrick, J. Siqueiros, O. A. Lopez, T. Cheeks, O. Contreras, and J. Y. Yi, "High transmittance-low resistivity ZnO:Ga films by laser ablation," *Journal of Vacuum Science & Technology A: Vacuum, Surfaces, and Films*, vol. 14, pp. 791-794, 1996.

[6.16] G. H. Kim, H. S. Kim, H. S. Shin, B. D. Ahn, K. H. Kim, and H. J. Kim, "Inkjet-printed InGaZnO thin film transistor," *Thin Solid Films*, vol. 517, pp. 4007-4010, 2009.

[6.17] Y. Ya-Hui, S. S. Yang, and C. Kan-Sen, "Characteristic Enhancement of Solution-Processed In-Ga-Zn Oxide Thin-Film Transistors by Laser Annealing," *Electron Device Letters, IEEE*, vol. 31, pp. 969-971, 2010.

[6.18] W. Ye, S. Xiao Wei, G. K. L. Goh, H. V. Demir, and Y. Hong Yu, "Influence of Channel Layer Thickness on the Electrical Performances of Inkjet-Printed In-Ga-Zn Oxide Thin-Film Transistors," *Electron Devices, IEEE Transactions on*, vol. 58, pp. 480-485, 2011.

Chapter 7

Conclusions and Future Work

In this dissertation, ZnO-based transparent electrodes and ZnO/IGZO thin film transistors prepared by AP-PECVD were studied. For ZnO-based transparent electrodes, we have successfully fabricated ZnO:Ga/ZnO:In thin films with excellent opto-electrical properties at low-temperature. For ZnO TFT, we have studied the oxygen species and channel thickness on the performance of ZnO TFTs and got excellent performance at low growth temperature. For IGZO TFT, we have studied the impacts of thermal annealing on the properties of IGZO TFTs and also got excellent switching properties with an amorphous-like phase. Finally, we have integrated a high- Al_2O_3 dielectric into IGZO TFTs and achieved excellent TFT performance. Several important results are obtained and summarized as follows:

In chapter 2, we had successfully used APPECVD to fabricate GZO thin films. Gas phase nucleation reaction depends on the process condition of gap distance and carrier flow rate. The concentration of precursor in the plasma region must be well controlled. The abnormal phenomenon of degradation in electrical properties with increasing Ts is attributed to the adsorption of oxygen from air. Since the AP-PECVD operated under air, the effect of environment must be considered when deposited at high substrate temperature. A minimum resistivity was achieved via 8 at% doping.

The GZO thin film presents a resistivity of $7.8\text{x}10^{-4}$ Ω • cm and a transmittance of more than 80 % at a low substrate temperature of 100°C.

In chapter 3, we have demonstrated that indium-doped ZnO films deposited on glass utilizing atmospheric pressure plasma jet. IZO thin film deposited at 100°C shows a lager of structure defect due to the high DLE intensity. IZO thin film deposited at 300°C presents the degradation of electrical properties which can be attributed to the absorption of oxygen. Furthermore, IZO thin films are polycrystalline with a preferred orientation along (002) plane and grain size tend to decrease as doping concentration increases. The films show needlelike geometry from 6at% to 10at% resulting in the rougher surface. The films prepared with 8at% indium-doped zinc oxide show a low resistivity of $1.8\text{x}10^{-3}$ Ω · cm, a carrier concentration of $2.69\text{x}10^{20}$1/cm^{3}, a mobility of 12.86 cm^{2}/V-s, a band gap of 3.51eV and a transmittance of about 80% in the visible range.

In chapter 4, we have studied the effect of channel thickness and oxygen species on the properties of ZnO TFT. During deposition, using CDA as carrier gas can effectively reduce oxygen vacancies and improve the I_{on}/I_{off} current ratio from 1.6×10^{2} to 2.59×10^{5}. Reducing the thickness can increase the channel resistance and reduce the undesired current flow. Using CDA as a carrier gas and reducing the channel thickness to 55nm, a subthreshold swing of 3.75V/decade, a field-effect mobility of 3.49 cm^2/Vs and an I_{on}/I_{off} current ratio of 4.08×10^7 were obtained. With increasing oxygen partial pressure, the gas phase nucleation particle increases and ZnO thin films show a rough surface. PL spectra show that the oxygen vacancies could be repaired effectively by incorporating oxygen into plasma gas. By incorporating 0.69% O_2 into plasma gas, a threshold voltage of 26.7 V, a subthreshold swing of 3.89 V/decade, a field-effect mobility of 2.38 cm^2/Vs and an I_{on}/I_{off} current ratio of $4.63x10^9$ were obtained.

In chapter 5, we have studied the impacts of thermal annealing on the properties of IGZO TFT. As-deposited sample shows a high conductivity and poor switching properties. The high carrier concentration may be due to oxygen vacancies and H species. The post annealing is necessary to repair the defects and reduce the carrier concentration. After 300°C annealing, the IGZO shows an excellent switching properties with depletion-mode operation and the low mobility. On the other hand, 500°C sample operates in enhancement mode, and exhibit higher mobility compared to 300°C sample. IGZO TFT annealed at 500°C shows excellent electrical characteristics including a V_T of 6.74 V, a subthreshold swing of 1.54V/dec, a high mobility of 10.31cm^2/V-s and a large I_{on}/I_{off} ratio of $3.28x10^8$.

In chapter 6, we have integrated PE-ALD Al_2O_3 as a gate dielectric into IGZO TFTs. Good TFT performance was achieved, such as a high drive current, low threshold voltage and sub-threshold slope, as well as an excellent on/off current ratio. The good performance is related to the high gate capacitance density and small EOT provided by the high-k dielectric. The PE-ALD Al_2O_3/IGZO TFT demonstrated excellent electrical characteristics, including a low V_T of 0.71 V, small subthreshold swing of 276 mV/dec, a mobility of 8.39 cm^2/V-s, and a large I_{on}/I_{off} ratio of $1x10^8$. This device is suitable for low cost and low-operation voltage applications.

Although many topics including GZO/IZO transparent electrodes and ZnO/IGZO TFTs have been covered in this study, there are still several works that could be introduced for further study.

At first, for commercial application of TCOs, the high temperature and high humidity test is necessary. Furthermore, the post annealing also can be performed to improve the performance and reliability.

Secondly, for the TFT application, the passivation layer is necessary. Different passivation layers, such as SiNx and SiOx, can be employed and studied.

Third, we can discuss different In:Ga:Zn ratios on the performance of IGZO TFTs since the composition of IGZO affects the TFT properties significantly. The different ratio of IGZO precursor must be discussed.

Finally, previous work in our lab has developed the SiO_2 by APPJ. In this dissertation, we develop the transparent electrodes and oxide-based TFT. We can integrate the result and fabricate the transparent thin film transistor by APPJ.

Vita

姓名：黃菘宏

性別：男

出生年月日：民國 73 年 8 月 30 日

籍貫：宜蘭縣

住址：宜蘭縣礁溪鄉三民村 19 鄰礁溪路三段 89 巷 25 號

學歷：國立宜蘭中學（88 年 9 月~91 年 7 月）
私立長庚大學電子工程學系（91 年 9 月~95 年 7 月）
國立交通大學電子工程研究所碩士班（95 年 9 月~97 年 2 月）
國立交通大學電子工程研究所博士班（97 年 2 月~101 年 6 月）

論文題目：

利用大氣常壓電漿技術開發氧化鋅系透明氧化物半導體於透明電極與薄膜電晶體應用之特性研究

Study on Characterizations of ZnO-Based Transparent Electrodes and ZnO/IGZO Thin-Film Transistors Prepared by AP-PECVD

Publication lists:

(A) International Journal:

[1] Kow-Ming Chang, **Sung-Hung Huang**, Chin-Jyi Wu, Chia-Chiang Chang, Wei-Li Lin, Wei-Chiang Chen, Chia-Wei Chi, Je-Wei Lin, (2011) “Transparent conductive indium-doped zinc oxide films prepared by atmospheric pressure plasma jet”, Thin Solid Films, 519, pp. 5114-5117 (2011)

[2] Kow-Ming Chang, **Sung-Hung Huang**, Chia-Wei Chi, Chin-Jyi Wu, Je-Wei Lin, Chia-Chiang Chang, (2011) “The Effect of Different Carrier Gases and Channel Thicknesses on the Characteristics of ZnO TFTs Prepared by Atmospheric Pressure Plasma Jet”, ECS Transactions, Vol.35, No.6, pp. 199-208 (2011)

[3] Kow-Ming Chang, **Sung-Hung Huang**,Yi-Wen Tseng, (2011) “Performance improvement of pentacene-based organic thin-film transistor with HfO_2 gate dielectrics treated by CF_4 plasma“, ECS Transactions, Vol.35, No.19, 1-9 (2011)

[4] Chien-Hung Wu, Kow-Ming Chang, **Sung-Hung Huang**, I-Chung Deng, Chin-Jyi Wu, Wei-Han Chiang, and Chia-Chiang Chang, (2012) “Characteristics of IGZO TFT Prepared by Atmospheric Pressure Plasma Jet Using PE-ALD Al_2O_3 Gate Dielectric “ IEEE, Electron Device Letter, Vol. 33, No.4, pp. 552-554, (2012)

[5] Chien-Hung Wu, Kow-Ming Chang, **Sung-Hung Huang** , I-Chung Deng, Chin-Jyi Wu, Wei-Han Chiang, Je-Wei Lin and Chia-Chiang Chang, (2012) “ The effect of thermal annealing on the properties of IGZO TFT prepared by atmospheric pressure plasma jet “ECS Transactions, Vol.45, No.7, pp.189-197 (2012)

[6] Chien-Hung Wu, Kow-Ming Chang, **Sung-Hung Huang**, I-Chung Deng, Chia-Wei Chi, Chin-Jyi Wu, and Chia-Chiang Chang, (2012) “ The effect of oxygen species on the ZnO TFT prepared by atmosphere pressure plasma jet “ECS Transactions, Vol.45, No.7, pp.231-237 (2012)

(B) Conferences & Proceeding

[1] Kow-Ming Chang, **Sung-Hung Huang**, Wei-Li Lin, Wei-Chiang Chen, Chia-Wei Chi, Je-Wei Lin, (2010)“Transparent conductive Indium-doped Zinc oxide films prepared by atmospheric pressure plasma jet”, The 5th International Conference on Technological Advances of Thin Films & Surface Coatings, 11-14 July, 2010

[2] Kow-Ming Chang, **Sung-Hung Huang**, Chia-Wei Chi, Chia-Chiang Chang, Chin-Jyi Wu, Je-Wei Lin, (2011) “The effect of different carrier gases and channel thicknesses on the characteristics of ZnO TFTs prepared by atmospheric

pressure plasma jet”, 219th ECS Meeting, Montreal, QC, Canada, May 1-6, 2011

[3] Kow-Ming Chang, **Sung-Hung Huang**, Yi-Wen Tseng, (2011)“Performance improvement of pentacene-based organic thin-film transistor with HfO_2 gate dielectrics treated by CF_4 plasma”, 219th ECS Meeting, Montreal, QC, Canada, May 1-6, 2011

[4] Kow-Ming Chang, Wei-Han Chiang, Wei-Li Lin, Chin-Jyi Wu, Chia-Chiang Chang, Je-Wei Lin, **Sung-Hung Huang**, (2011) “Thermal stability of indium doped zinc oxide thin films prepared by atmosphere pressure plasma jet”, 219th ECS Meeting, Montreal, QC, Canada, May 1-6, (2011)

[5] Kow-Ming Chang, Po-Ching Ho, Chia-Chiang Chang, Chin-Jyi Wu, Wei-Chiang Chen, Je-Wei Lin, **Sung-Hung Huang**, (2011) “The effect of carrier flow rate on the properties of gallium doped zinc oxide thin films by atmosphere pressure plasma jet”, 219th ECS Meeting, Montreal, QC, Canada, May 1-6, (2011)

[6] Kow-Ming Chang, **Sung-Hung Huang**, Wei-Han Chiang, I-Chung Deng, Chin-Jyi Wu, and Chia-Chiang Chang, (2012) ” Low-voltage IGZO TFT Prepared by APPJ Using HfO_2 as a Gate Dielectric”, 221th ECS Meeting, Seattle, WA, U.S., May 6-10.

[7] Kow-Ming Chang, **Sung-Hung Huang**, Wei-Han Chiang, Chin-Jyi Wu, and Chia-Chiang Chang, (2012), “The Effect of Thermal Annealing on the Properties of IGZO TFT Prepared by Atmospheric Pressure Plasma Jet”, 221th ECS Meeting, Seattle, WA, U.S., May 6-10.

[8] Kow-Ming Chang, **Sung-Hung Huang**, Chia-Wei Chi, Chin-Jyi Wu, and Chia-Chiang Chang, (2012) “The Effect of Oxygen Species on the ZnO TFT Prepared by Atmosphere Pressure Plasma Jet”, 221th ECS Meeting, Seattle, WA, U.S., May 6-10.

[9] Kow-Ming Chang, **Sung-Hung Huang**, Yi-Wen Tseng, (2010) “HfO_2 gate dielectrics by CF_4 plasma treatment for pentacene-based organic thin-film transistors”, 第十七屆 奈米元件技術研討會(SNDT 2010)

[10] Kow-Ming Chang, **Sung-Hung Huang**, Chia-Wei Chi, Chin-Jyi Wu, Je-Wei Lin, Chia-Chiang Chang, (2011) “The Improvement in the Performance of ZnO-TFTs by Using CDA as a Carrier Gas and Reducing the Channel Thickness Prepared by Atmospheric Pressure Plasma Jet”, 2011 電子工程技術研討會(ETS 2011)

[11] Chien-Hung Wu, Kow-Ming Chang, **Sung-Hung Huang**, I-Chung Deng, Chin-Jyi Wu, Wei-Han Chiang, Je-Wei Lin and Chia-Chiang Chang, (2012) “Characterization of annealing temperature on the performance of InGaZnO thin film transistors deposited by AP-PECVD” , 2012 電子工程技術研討會(ETS 2012)